

December 2017

Development of Pre-Clinical Assays Based on Tandem Mass Spectrometry to Investigate Gabaa Receptor Modulators

Margaret Laurel Guthrie
University of Wisconsin-Milwaukee

Follow this and additional works at: <https://dc.uwm.edu/etd>

 Part of the [Analytical Chemistry Commons](#)

Recommended Citation

Guthrie, Margaret Laurel, "Development of Pre-Clinical Assays Based on Tandem Mass Spectrometry to Investigate Gabaa Receptor Modulators" (2017). *Theses and Dissertations*. 1631.
<https://dc.uwm.edu/etd/1631>

This Dissertation is brought to you for free and open access by UWM Digital Commons. It has been accepted for inclusion in Theses and Dissertations by an authorized administrator of UWM Digital Commons. For more information, please contact open-access@uwm.edu.

DEVELOPMENT OF PRE-CLINICAL ASSAYS BASED ON TANDEM MASS SPECTROMETRY TO
INVESTIGATE GABA_A RECEPTOR MODULATORS

by

Margaret L. Guthrie

A Dissertation Submitted in
Partial Fulfillment of the
Requirements for the Degree of

Doctor of Philosophy
in Chemistry

at

The University of Wisconsin – Milwaukee

December 2017

ABSTRACT

DEVELOPMENT OF PRE-CLINICAL ASSAYS BASED ON TANDEM MASS SPECTROMETRY TO INVESTIGATE GABA_A RECEPTOR MODULATORS

by

Margaret L. Guthrie

The University of Wisconsin – Milwaukee, 2017
Under the Supervision of Professor Alexander (Leggy) Arnold

Drugs are compounds that interact with a biological system to produce a specific biological response. The goal of drug discovery is to design and synthesize a pharmaceutical agent that will produce a desired biological effect. However, the *in-vivo* effects of a drug molecule cannot be predicted without a variety of test results prior to human clinical trials. In order to designate any drug compound as a leading candidate (or “lead” compound), it needs to show significant pharmacological activity, maintain a desirable metabolic half-life, and display minimal side effects and toxicity. Several *in-vitro* and *in-vivo* pre-clinical assays have been developed to measure metabolic parameters and aim to qualify, or rule out, compounds based on drug distribution within the body. The developments of these assays are presented herein.

First, an assay was developed to estimate metabolic half-life of drug compounds *in vitro* using human and mouse liver microsomes by liquid chromatography-mass spectrometry (LC-MS). Secondly, a method for determination of pharmacokinetic (PK) parameters was developed and optimized using absolute quantitation by LC-MS/MS. Thirdly, metabolic stability was further estimated in cell suspensions and tissue homogenates, specifically using HepG2

cells as a model for hepatocytes, and rat brain as a model for illustrating stereochemical specificity within the brain enzymatic metabolism. Finally, to visualize the spatial distribution of small molecules *in-vivo*, matrix assisted laser desorption ionization tandem mass spectrometry (MALDI-MS/MS) was employed to image the distribution of drug compounds in whole tissue slices. By employing a variety of mass spectrometric techniques, we have been able to both assess the viability and follow the distribution of lead compounds from *in-vitro* sub-cellular fractions to whole cells through whole tissues and carry out *in-vivo* studies.

© Copyright by Margaret L. Guthrie, 2017
All Rights Reserved

TABLE OF CONTENTS

CHAPTER 1.	INTRODUCTION	1
1.1	<i>Introduction to Drug Discovery</i>	1
1.2	<i>Drug Target: GABA_A Receptor</i>	5
1.3	<i>Instrumental Techniques</i>	7
1.3.1	High Performance Liquid Chromatography	8
1.3.2	Mass Spectrometry	13
1.4	<i>Conclusions</i>	24
CHAPTER 2.	Liver Microsome Stability Assay	25
2.1	<i>Introduction</i>	25
2.2	<i>Materials & Methods</i>	31
2.3	<i>Results and Discussion</i>	36
CHAPTER 3.	Primary Human Hepatocyte Assay	42
3.1	<i>Introduction</i>	42
3.2	<i>Materials & Methods</i>	44
3.3	<i>Results & Discussion</i>	45
CHAPTER 4.	<i>In vitro</i> Brain Metabolism Assay	52
4.1	<i>Introduction</i>	52
4.2	<i>Materials & Methods</i>	55
4.3	<i>Results</i>	56
4.4	<i>Discussion</i>	58
CHAPTER 5.	Quantification of GABA with a novel HILIC based method	60
5.1	<i>Introduction</i>	60
5.2	<i>Materials & Methods</i>	64
5.3	<i>Results</i>	65
CHAPTER 6.	Pharmacokinetic Studies	69
6.1	<i>Introduction</i>	69
6.2	<i>Experimental Procedure</i>	75
6.3	<i>Results</i>	80
6.4	<i>Conclusions</i>	95

CHAPTER 7. MALDI imaging mass spectrometry (MALDI IMS)	97
7.1 Introduction.....	97
7.2 Materials and Methods.....	103
7.2.1 MALDI IMS	103
7.2.2 H&E stain	104
7.2.3 Immunohistochemistry:.....	105
7.3 Results & Discussion.....	107
7.3.1 MALDI IMS results using MS/MS mode	109
7.3.2 MALDI results in MS1 mode	121
7.3.3 Immunohistochemistry results	123
7.4 Conclusions.....	131
Appendix A: MRM parameters for $\alpha_5\beta_3\gamma_2$ selective ligands.....	138
Appendix B: MRM parameters for $\alpha_4\beta_3\gamma_2$ selective ligands.....	140
Appendix C: MRMs for non-benzodiazepine compounds	142
Curriculum Vitae	144

LIST OF FIGURES

Figure 1. General outline of the drug discovery process from target inception to market.....	2
Figure 2. Criteria for optimization of lead compounds in drug development.....	4
Figure 3. GABA _A receptor.....	6
Figure 4. Structures of benzodiazepines.....	7
Figure 5. Visual representation of the components of the van Deempter equation, a plot which aids in describing theoretical plate height.....	11
Figure 6. Basic schematic of HPLC.....	12
Figure 7. Block diagram of features of a typical mass spectrometer.....	13
Figure 8. Schematic diagram of a mass spectrometer with HPLC as the sample introduction system.....	14
Figure 9. Schematic representation of ESI.....	15
Figure 10. Positive ion generation mechanism by ESI.....	16
Figure 11. Positive ion generation mechanism by atmospheric pressure chemical ionization.....	17
Figure 12. Cartoon representation of MALDI.....	18
Figure 13. A quadrupole mass analyzer.....	19
Figure 14. Schematic of triple quadrupole (replace this Skoog image with a Shimadzu image).....	20
Figure 15. General schematic of a TOF mass analyzer.....	21
Figure 16. Ion detection system.....	23
Figure 17. Cascading effect generated when the ion beam is focused onto the conversion dynode, which emits electrons in direct proportion to the number of ions bombarding the dynode.....	24
Figure 18. The two phases of drug metabolism and how they generate resulting metabolites.....	26
Figure 19. Illustration of benzodiazepine metabolism.....	27
Figure 20. Isolation of microsomes from liver tissue, typically acquired through organ procurement organizations. Image: BD Biosciences.....	28
Figure 21. Crystal structure of the midazolam-bound CYP3A4.....	30
Figure 22. HPLC-UV chromatogram of drug compound degradation by human liver microsomes.....	35
Figure 23. Chromatogram from the triple quadrupole LC-MS 8040.....	36
Figure 24. Explanation of calculations performed for liver microsome assays.....	37
Figure 25. Percentage plot of human liver microsome results for $\alpha_5\beta_3\gamma_2$ and $\alpha_4\beta_3\gamma_2$ GABA _A R selective ligands.....	37
Figure 26. Structures correlating with the results for several imidazobenzodiazepine compounds.....	38
Figure 27. $\alpha_4\beta_3\gamma_2$ selective ligands, natural log plot.....	38
Figure 28 $\alpha_5\beta_3\gamma_2$ selective ligands, natural log plot.....	39
Figure 29 Scheme of the metabolism of MP II 069 by hydroxylation.....	40
Figure 30 Structures for $\alpha_5\beta_3\gamma_2$ GABA _A R selective ligands.....	45
Figure 31. Results for $\alpha_5\beta_3\gamma_2$ GABA _A R selective ligands in HepG2 cell stability assay, presented as percent compound remaining over the course of two hours.....	46
Figure 32. Comparison of CL values for five benzodiazepine compounds as estimated in human liver microsomes, human cryopreserved hepatocytes, and fresh human hepatocytes.....	47
Figure 33. Structures of $\alpha_4\beta_3\gamma_2$ GABA _A R selective ligands.....	48

Figure 34. Results for four $\alpha_4\beta_3\gamma_2$ GABA _A R selective ligands in HepG2 cells.....	48
Figure 35. Xhe III 74 and its deuterated analog shown with the 95% confidence interval.	50
Figure 36. Xhe III 74 Ethyl Ester and its deuterated analog shown with the 95% confidence interval.	50
Figure 37. The S and R isomers of Thalidomide, which are effective, and dangerous, respectively.....	53
Figure 38. Structures of chiral $\alpha_5\beta_3\gamma_2$ selective GABA _A R ligands and a proposed metabolite of both isomers identified <i>in vivo</i>	54
Figure 39. Known cytochrome enzymes and their identified substrates.	54
Figure 40. Pharmacokinetic profiles of the R and S isomers of the SH-053-2'F-R/S-CH3 compound.	56
Figure 41. Results of the brain homogenate assay displayed as a percentage remaining as well as the linear regression (and the 95% confidence interval).	57
Figure 42. Cartoon image of the coexisting GABA, GABA _A receptor, glutamic acid decarboxylase (GAD), and the GABA transporter 1 (GAT).	61
Figure 43. Cartoon representation of the polar stationary phase, the adsorbed water layer, and the partitioning mechanism of retention seen in HILIC separations (Image: Waters).	64
Figure 44. Calcium assay response of the lead asthma compound Xhe-III-74 acid in the presence of Jurkat cells illustrating the similarity of results with or without the addition of [1 mM] GABA.	66
Figure 45. Results from the IL-2 ELISA assay from Jurkat cell extract showed a reduction of IL-2 in the presence of GABA and in XHE-III-74 acid and XHE-III-74 EE.	67
Figure 46. Calibration curve for GABA determined by HILIC/MSMS. R square = 0.9902.	68
Figure 47. General representation of a pharmacokinetic curve.....	69
Figure 48. General image of a pharmacokinetic curve resulting from oral or i.p. dosing schedule.	73
Figure 49. Schematic of the on-line solid phase extraction and UHPLC system, featuring four pumps, three degassing units, two rotation valves, and an autosampler.....	80
Figure 50. Results of initial compound extraction study.	82
Figure 51. Diazepam and its active metabolite, nordiazepam.	83
Figure 52. Modified graph including the quantification of diazepam and nordiazepam (denoted DzNz for both compounds together).....	83
Figure 53. Pharmacokinetic analysis of Xhe-III-74 Ethyl Ester.	85
Figure 54. Conversion of Xhe-III-74 Ethyl Ester to the Xhe-III-74 Acid by hydrolysis <i>in vivo</i>	86
Figure 55. Pharmacokinetic curve for the Xhe-III-74 Acid in brain, lung, and blood samples. The animals were originally dosed with the Xhe-III-74 Ethyl Ester, therefore this acid compound is a metabolite.....	86
Figure 56. Pharmacokinetic study for the Xhe-III-74 acid analog, dosed in the same manner as the Xhe-III-74 Ethyl Ester.	87
Figure 57. Brain extractions using the BeadBug tool. Figure 58. Lung extractions using the BeadBug. .	88
Figure 59. Homogenization methods overall comparison.....	89
Figure 60. Structure for MRS-01-66, the dimethyl amide analog to Xhe-III-74.....	90
Figure 61. SPE vs. LLE data for blood samples, from the PK study of MRS-01-66. The variances seen are not statistically different. The means are only statistically different at the end time points (60, 90, 240 minutes), which are at quantities <LLOQ.....	90
Figure 62. PK graph for the dimethyl amide compound.....	92
Figure 63. Transition of pBBG compound into the diacid analog, proposed to occur <i>in vivo</i>	94
Figure 64. PK graphs for pBBG diacid and MeGFN in the brain.	94

Figure 65. Shimadzu 7090 MALDI-TOF/TOF instrument schematic.	98
Figure 66. H&E stain of mouse lung, showing the airway morphology.....	101
Figure 67. Cartoon of the reaction of horseradish peroxidase and DAB substrate to produce brown coloration in tissue stains.	102
Figure 68. Dyes used for immunofluorescence. FITC shows excitation and emission at 495 nm and 519 nm, respectively, and Cy5 Ex: 650nm, Em: 667nm.....	102
Figure 69. 4,6-Diamidino-2-phenylindole DAPI Ex: 358 nm, Em: 461 nm.	103
Figure 70. MALDI IMS workflow. Images presented in this chapter were generated from a compound synthesized by Guanguan Li of the Cook research group. Pharmacokinetic study was performed previously by Revathi Kodali and Nick Zahn, as published previously.....	109
Figure 71. MALDI-MS/MS spectrum of the SH-053-2'F-R-CH ₃ acid spotted with DHB as the matrix.....	110
Figure 72. Lung section imaged for the 360>316 transition in MALDI-MS/MS. MSI import 200-400 bin size 3, 5905 data points, 54.1843 MB, 62x74x51500 dpi and H&E stained serial tissue section.	110
Figure 73. Comparison of unwashed vs. washed lung tissue sections in MALDI IMS using the 360>316 transition.....	111
Figure 74. Images of two lung tissue sections of SH-053-2'F-R-CH ₃ acid dosed mice at 360>283 m/z and 360>301 m/z transition, respectively.	112
Figure 75. Comparison of lung tissue from vehicle and SH-053-2'F-R-CH ₃ acid dosed mice. These sections were taken using the same MS/MS method 360>283 m/z. Both samples were prepared on the same day with the same matrix solution and application.	113
Figure 76. [M+1] ion image for the lead compound (SH-053-2'F-R-CH ₃ acid) in reflectron mode and fragmentation 360>282.932 m/z in reflectron MS/MS mode.....	114
Figure 77. Tuning settings for the linear, reflectron, and reflectron MSMS modes of the MALDI-7090.	115
Figure 78. Light microscope image of lung tissue stained with H&E (4x magnification) and MALDI IMS image of the daughter ion in a serial tissue section (transition 360>282.930).	116
Figure 79. Two separate lung tissue sections imaged for GL-II-93 in reflectron MSMS mode, for the transition of the parent 416>357.....	117
Figure 80. Structure of GL-II-93 and SH-053-2'F-R-CH ₃ acid.	117
Figure 81. Images for GL-II-93 with dihydroxybenzoic acid (416>237), and with dihydroxyacetophenone (416 parent viewed in MSMS mode) as the matrix, respectively.....	118
Figure 82. Fragment images for GL-II-93 for 416>331 and 416>370 transitions.....	119
Figure 83. Proposed fragmentation pattern for the GL II 93 compound.....	119
Figure 84. GL-II-93 parent compound (416 m/z) at 50 micron resolution, for two lobes of lung tissue..	120
Figure 85. Samples imaged at 70 micron and 80 micron spatial resolution, respectively, with the laser diameter held at 100 micron. Left image is GL-II-93 416>373, right image is SH-053-2'F-R-CH ₃ acid 360>283. H&E stain is also pictured at zero magnification, which correlates with the SH section.	121
Figure 86. The GL-II-93+Na ⁺ imaged in a lung tissue section.....	122
Figure 87. Unknown metabolite at m/z 203. The top sections show the lung without and with washing to remove salt interferences.....	123
Figure 88. HRP stain of lung tissue section, with brown and blue colors.....	124
Figure 91. Mouse lung airways stained with the Cy5 probe at the alpha 5 receptor (positive staining and negative control).	127

Figure 92. DAPI stain of lung tissue, showing two airways.....	128
Figure 93. Serial section of lung tissue imaged for the SH-053-2'F-R-CH ₃ acid.	128
Figure 94. Mouse brain sections stained for alpha 5 GABA _A R subunit.....	129
Figure 95. Mouse lung serial sections including overall ion density map, correlating H&E stain at 10x magnification, and Cy5 IHC at 200x magnification.	130

LIST OF TABLES

Table 1. Metabolic parameters for seven imidazobenzodiazepine compounds.	38
Table 2. Stability parameters for $\alpha_5\beta_3\gamma_2$ GABA _A R selective ligands.	46
Table 3 Stability parameters for $\alpha_4\beta_3\gamma_2$ GABA _A R selective ligands.	49
Table 4. Estimated metabolic parameters for the R and S isomers in brain tissue homogenates.	57
Table 5. Pharmacokinetic parameters of interest for the PK study of the Xhe-III-74 Ethyl Ester.	85
Table 6. Pharmacokinetic data for the acid metabolite of the Xhe-III-74 Ethyl Ester.	86
Table 7. Results for MRS-01-66.....	92
Table 8. GLO1 inhibitor PK parameters.	94

LIST OF ABBREVIATIONS

AC	Alternating current
ADME	Absorption, distribution, metabolism, and excretion
ADMET	Absorption, distribution, metabolism, excretion, and toxicity
APCI	Atmospheric pressure chemical ionization
ASDF	Axial spatial distribution focusing
CL _{int}	Intrinsic clearance
CYP	Cytochrome P450 enzymes
DC	Direct current
DMSO	Dimethylsulfoxide
ESI	Electrospray ionization
GABA	Gamma-aminobutyric acid
HETP	Height equivalent to theoretical plate
HPLC	High performance liquid chromatography
LC-MS	Liquid chromatography- mass spectrometry
MALDI	Matrix-assisted laser desorption ionization
MRM	Multiple reaction monitoring
MS	Mass spectrometry
MWCO	Molecular weight cutoff
NIH	National Institutes of Health
PBS	Phosphate buffered saline
PK	Pharmacokinetics
RF	Radiofrequency
SD	Standard deviation
SIM	Selected ion monitoring
TOF	Time-of-Flight
UV	Ultra violet

CHAPTER 1. INTRODUCTION

1.1 Introduction to Drug Discovery

The successful introduction of a new therapeutic treatment into the marketplace is a time consuming and expensive endeavor, one which is estimated to take more than 8 years and \$500 million dollars.² Before a novel treatment can reach clinical trials, it must withstand a myriad of pre-clinical assays, and show efficacy to treat the disease, display selectivity to the intended target molecule or target organ, and yield limited adverse side effects. The ability to exclude underperforming lead compounds in a high throughput and cost effective manner is crucial to the field of drug discovery. The development of a new pharmaceutical product occurs in several stages. Some general stages include target identification, drug compound discovery, investigational new drug application, clinical trials, and commercialization. Firstly, the biological target mediating the disease must be verified. This can be a protein target, such as an enzyme or receptor, or a nucleic acid target, such as DNA. The drug discovery process then moves to the identification of an initial lead compound, which has been identified as a promising candidate to treat the disease by way of acting at the established drug target. Usually this strategy involves a high throughput screening method or rational drug design. Typically, the initial lead compound will require structural modifications to improve binding, reduce adverse side effects, and to produce the maximum desired pharmacological effect. Changes in the structure of a drug compound, as well as changes to the method of administration (oral dosing, inhalation, or injection), will impact the biological effects to the test subject. The assays presented herein are designed to aid in the drug discovery process after an initial lead has been identified, by measuring parameters that impact important drug properties. A general outline for the drug discovery and development process is presented in Figure 1.

The study of how a drug is absorbed, distributed, metabolized and excreted (generally abbreviated as ADME) is a vast field in drug discovery as it characterizes important drug-like properties of a lead compound.¹ The term ‘ADMET’ is often used as well to describe toxicity in addition to the other terms, which is an important consideration because drugs that are not undeniably safe will not become commercial drugs. It is important to understand the movement of a drug within the body and how the body processes a drug. In this work, assays are presented using mice to ascertain such information. However, before a compound can advance to *in vivo* experiments with animals, it should be characterized by inexpensive, rapid, efficient and high-throughput *in vitro* assays. These assays are presented first and foremost in the upcoming chapters.



Figure 1. General outline of the drug discovery process from target inception to market.³

Both *in vitro* and *in vivo* assays have been developed by the Arnold Group embedded in the Milwaukee Institute for Drug Discovery to characterize synthesized drug candidates at UWM and in collaboration with other universities and companies. The goal of these collaborative projects is to move a lead compound forward into clinical trials, ideally creating a novel treatment for a selected disease target (such as asthma, cancer, neuropathic pain, depression, and many others). The assays assist medicinal chemists within the MIDD to determine if structural modifications can be made to lead compounds to increase desirable drug-like properties of the molecule. These properties include bioavailability, metabolic stability, and absence of toxicity. Figure 2 illustrates characteristics of drug compounds that should be optimized, as well as characteristics that should be avoided when designing a new drug. The assays developed herein have kept these properties in mind and aim to answer questions regarding these characteristics.

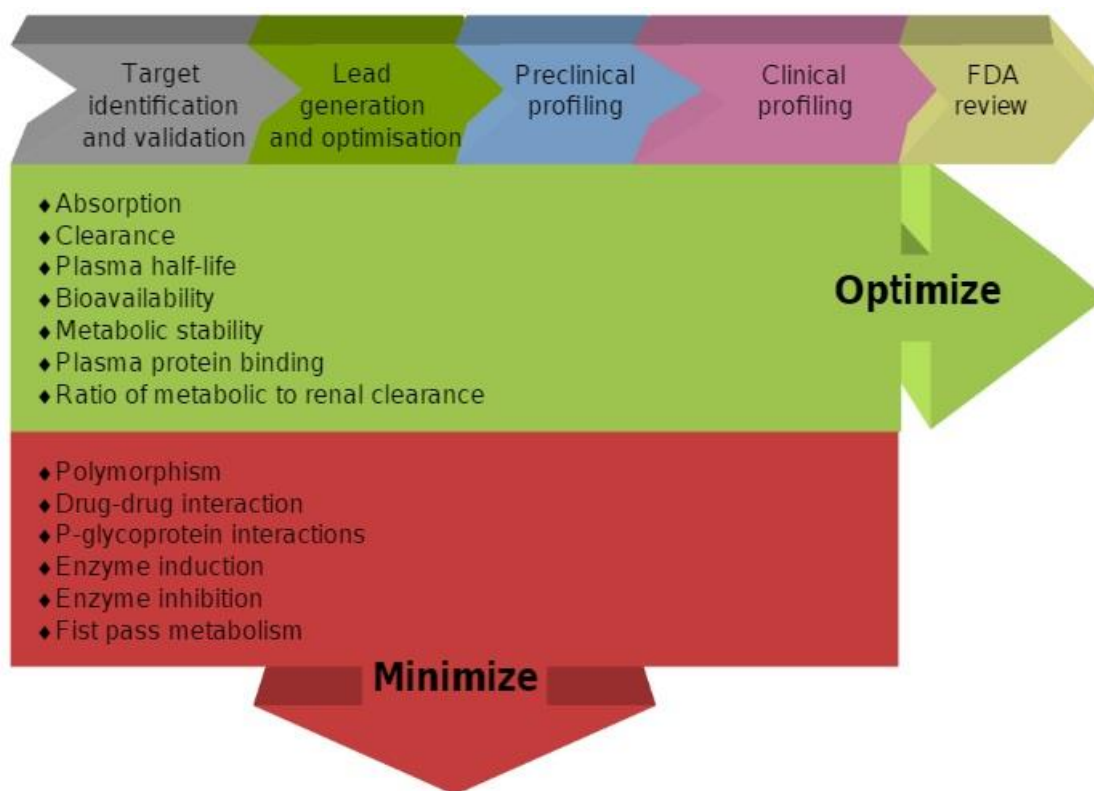


Figure 2. Criteria for optimization of lead compounds in drug development.⁴

There are some general guidelines that medicinal chemists follow to aid in improving a drug candidate with regard to the above criteria. One such guideline is Lipinski's Rules of Five.⁵ These rules include avoiding molecules with more than five hydrogen bond donors, molecular weights over 500, octanol-water partition coefficients ($\log P_{o/w}$) greater than five, or a sum of nitrogen and oxygen atoms (within the molecule) above ten. Typically molecules that do not obey these general rules will display poor ADME properties.⁵⁻⁶ It is important for a drug candidate to display optimum ADME characteristics, as compounds that are not stable in the body (whether they are excreted too quickly or readily metabolized into other compounds) may not have the desired pharmaceutical effects. Not only must a compound be stable upon entering the body, it also must be relocated to its target tissue after absorption into the

bloodstream. For example, in our pursuit to treat asthma, it is important to verify that the compound reaches the lung, as it is the target organ. Drug distribution refers to the relocation of the drug from blood to the various tissues in the body, and the rate at which it occurs is an important ADME property.⁷

Once the drug has been distributed to the target location, the body will clear the drug by two general pathways; metabolism and excretion. Understanding the metabolism of highly lipophilic molecules is important, because these molecules will typically undergo biotransformation into a readily excreted polar metabolite.⁸ Many xenobiotics, or compounds that are exogenous to the body, are cleared this way. Large lipophilic molecules will be converted to more water-soluble products before renal elimination. The liver will also participate in the excretion process via the bile duct.⁷ *In vitro* assays can be conducted to estimate the uptake of a compound into cells (for example, in hepatic cells), but this does not necessarily equate directly to excretion, as there are many processes that occur after a drug has been taken up into a cell.⁹ Therefore, renal and fecal excretions are studied *in vivo* because *in vitro* assays do not emulate these processes well.⁶ For this reason, the excretion portion of ADME has not been extensively studied in this work.

1.2 Drug Target: GABA_A Receptor

The molecular target that has been identified for all lead compounds tested herein is the GABA_A receptor (GABA_AR). GABA (1,4-aminobutanoic acid, or γ -aminobutyric acid) is the major inhibitory neurotransmitter in the brain that influences neurons via a large number of receptors, which are grouped based on their pharmacology (A, B, or C). The GABA_A and GABA_C receptors are ligand-gated ion channels, whereas the GABA_B receptor is a G-coupled protein

receptor. The target for the following studies is the GABA_AR. In particular, the GABA_AR has been extensively studied due to the variety of modulators that act on this receptor, including benzodiazepines, ethanol, general anesthetics, and barbiturates.¹⁰

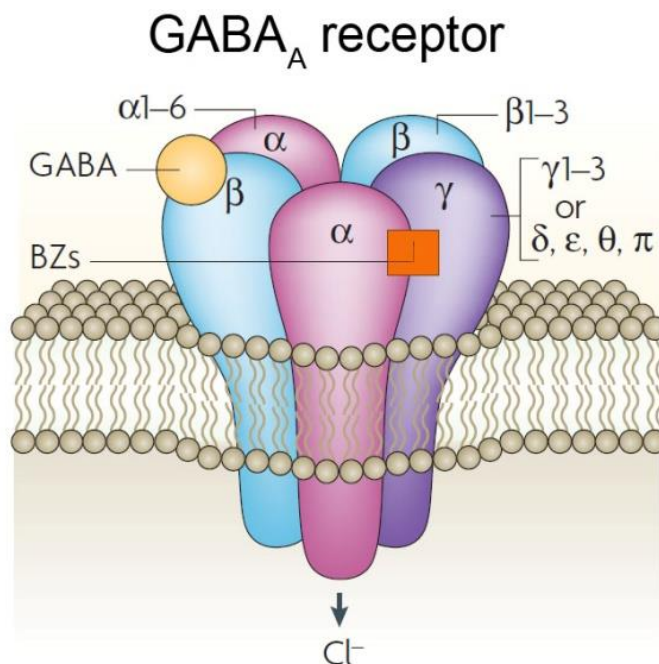


Figure 3. GABA_A receptor.¹¹

The majority of the compounds investigated herein are novel GABA_AR subtype-selective imidazobenzodiazepine scaffold as displayed in Figure 4. Both, non-selective benzodiazepines and selective imidazobenzodiazepine are allosteric modulators, which bind at a topographically distinct site from the endogenous ligand GABA and potentiate or inhibit the activity of that ligand (e.g. binding or signaling).¹²

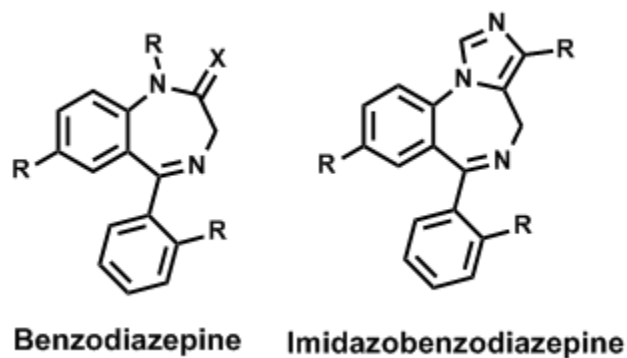


Figure 4. Structures of benzodiazepines.

During the development of selective GABA_AR modulators, these compounds have been crucial to identify the pharmacology of different GABA_AR subtypes. The subtype selectivity of ligands was achieved by changing their substitution patterns. Most of the imidazobenzodiazepines obey Lipinski's Rules of Five and have good ADME properties. In addition, they contain many heteroatoms that make them well suited for analysis by mass spectrometry.

1.3 Instrumental Techniques

A mass spectrometer is an analytical instrument used to identify and quantify analytes based on their mass-to-charge ratio (m/z). In combination with our assays, these instruments enable accurate, rapid, and reproducible ADME results. The analytical methods presented herein are designed for inexpensive, high-throughput analyses to gain a lot of ADME information in a short period of time. Mass spectrometry is both sensitive and selective, making it an ideal method by which to analyze compounds in complex biological matrixes. Tandem mass spectrometry (MS/MS) refers to ion selection, fragmentation, and detection, and employs multiple mass analyzers within one instrument. MS/MS allows for the absolute

quantification of analytes in these complex sample types. In addition, high resolution mass spectrometry can determine the exact mass of compounds that enable exact molecular formula determination. This is especially important for metabolite identification. Although this work does not focus heavily on metabolomics, strategies for doing such shall be discussed. Lastly, imaging mass spectrometry enables the visualization of the analyte spatially within whole tissue slices retrieved from animals dosed *in vivo*. This cutting-edge technology is gaining prominence in modern drug discovery and clinical settings. The instrument-based assays outlined herein determine the drug-like properties of analytes from the sub-cellular and cellular *in vitro* level to tissues and overall characteristics *in vivo*.

1.3.1 High Performance Liquid Chromatography

The first analytical technique employed in our analyses is high-performance liquid chromatography (HPLC). HPLC is a versatile and widely used separation technique employed in drug analysis to ascertain purity, quantify amounts of compound in biological samples, separate components of complex biological matrixes and a myriad of other applications. The sample, as a mixture of solutes, is contained in a liquid solvent and separated on a stationary phase via one of several possible retention mechanisms, including partitioning, adsorption, ion-exchange, size-exclusion, affinity, or chiral chromatography.¹³ The separations achieved with HPLC for this work were generally achieved by either partitioning mechanisms or adsorption. HPLC is often coupled to mass spectrometry to form a combination technique known as LC-MS, separating the analytes first by chromatography and then using the mass spectrometer as detection system. LC-MS is a core technique used in chemical analysis within the drug discovery arena, as well as many other fields. For drug discovery, many drug compounds are hydrophobic and

therefore well retained and may be separated by common stationary phases with HPLC. Similarly, many drug compounds have functional groups, such as amines, that can aid in the detection by mass spectrometry. Drug molecules in large part are inherently amenable to LC-MS analysis based on the physical properties of their chemical structure.

The history of chromatography dates back to Mikhail Tswett, a Russian botanist. Tswett fathered the idea of adsorption chromatography by postulating that chlorophyll was retained by some molecular forces on the leaf (yielding the green color) and that is why he struggled to extract the compound with petroleum ether. He developed a technique to separate plant pigments, such as chlorophylls and xanthophylls, by using a calcium carbonate stationary phase and a diethyl ether mobile phase. He published this work in 1906 in *Berichte der Deutschen Botanischen Gesellschaft*, 24, 384.¹⁴ Tswett separated these plant pigment species as colored bands and coined the term 'chromatogram' as a junction of the Greek 'chroma', meaning color, and 'graphein', meaning writing.¹³

Decades later, in 1952, Martin and Synge further defined the separation mechanisms at work in chromatography (and, invented gas chromatography) with the idea of theoretical plates.¹⁵ In this theory, which in part won them the Nobel Prize, the chromatographic column is envisioned as a series of many layers. These hypothetical layers exist orthogonally to the direction in which the analyte is moving, thereby playing a role in separation of the analytes as they "migrate through" the layers. According to this theory, with every theoretical plate, equilibration of the solute between the stationary and mobile phase occurs (however, in reality, a true 'equilibrium' is never reached between the stationary phase and the mobile phase). The

thickness of each of these layers is called the height equivalent to the theoretical plate (HETP, H). The number of theoretical plates (N) is equivalent to the ratio of the column length (L) to the plate height ($N = L/H$), and varies with any given column. This theory within chromatography describes the separation of analytes as being improved by increasing the number of theoretical plates.¹⁶ The height of the theoretical plate can be described by Equation 1, the van Deemter equation.

$$H = A + \frac{B}{\bar{u}} + C \bar{u} \quad \text{Equation 1.}$$

The van Deemter equation is a well-known model to chromatographers as a way to estimate the number of theoretical plates and to understand sources of band broadening.¹⁷ Each variable in this equation impacts the chromatography, and can be used to illustrate challenges in chromatographic separations. The 'A' variable refers to eddy diffusion, which describes movement through a non-ideal packing material for the solid phase. Particularly in the early days of chromatography, stationary phases were quite roughly prepared and the particles packed within the column were far from uniform. The 'B' term refers to longitudinal diffusion, or how particles elute in the lengthwise direction of the column. The 'C' term describes the resistance of the analyte to mass transfer between the mobile phase and the stationary phase. The interaction between the analyte with respect to both phases is a key aspect of chromatographic separations, however that does not mean that these interactions are without flaws. The 'u' term refers to the linear velocity.^{16a} The average of these plots shown as plate height vs. flow velocity can be seen in Figure 5.

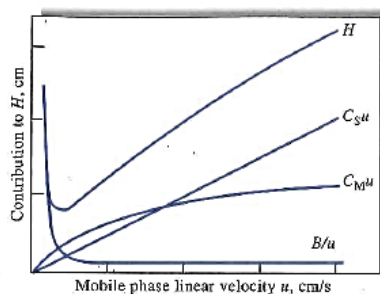


Figure 5. Visual representation of the components of the Van Deemter equation, a plot which aids in describing theoretical plate height.

The basic components of an HPLC system are shown in Figure 6. The main components include a solvent reservoir (typically 1L glass bottles), binary pump system, an injector (which can be automated or manual), an analytical column, and the detector. The detector for many HPLC systems is a molecular absorption spectrometer, such as a photodiode array (PDA). Many compounds are detectable in the ultraviolet range. Although the analytes that can be detected by UV are vast, the limits of detection are typically much lower for MS, therefore this work did not utilize UV detection systems. Other minor components include an inlet and in-line solvent filters, sample filters, pre-column filters (or “guard columns”), and a back-pressure regulator.¹⁸ In recent years, ultra-high pressure HPLC (or UHPLC) has become much more common, allowing for much higher pressures and less of a need to regulate the pressure to a lower value. This is advantageous for greater peak resolution, shorter analysis times, and the ability to separate complex mixtures. The LC-MS analyses presented herein were all performed using UHPLC, which is desirable for drug discovery applications because of the short analysis time.

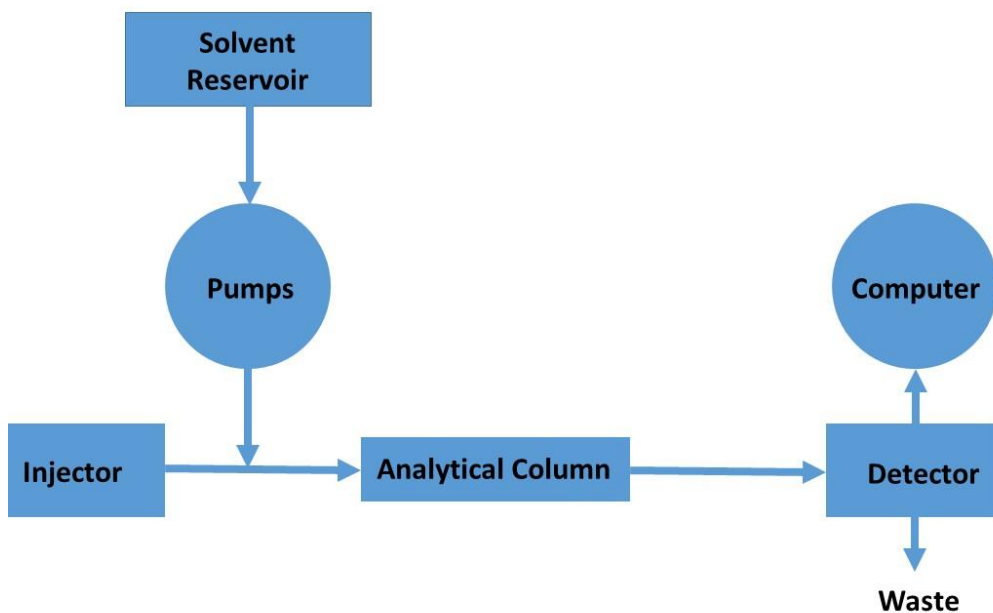


Figure 6. Basic schematic of HPLC.

As illustrated in the Figure 6 above, the HPLC system begins with solvents from a reservoir, which are filtered with an inlet solvent filter to remove particulates. The solvents are pumped to the analytical column, and on the way the flow passes an injection valve.¹⁸ The injection valve is equipped with a sample loop (50 μ L) and either a manual valve or, more commonly, an autosampler, which is preferred for high-throughput analyses. The sample loop allows for the repeatable introduction of sample into the flow path. The sample is then separated on the analytical column based on the attraction of the sample components between the solvent (i.e., the mobile phase) and the packing material (i.e., the stationary phase) within the column.¹⁸

1.3.2 Mass Spectrometry

Mass spectrometry (MS) is a technique used to study molecules or fragments of molecules, which are separated and analyzed based on their mass-to-charge (m/z) ratio. Current techniques in MS involve the creation of ions in the gas phase, generally from more condensed phases (although not always, as is the case for gas chromatography mass spectrometry, GC-MS). A general scheme of the components of a mass spectrometer is presented in Figure 7. First developed by Francis W. Aston in 1919, it was originally employed to separate isotopes of neon onto a photographic plate and contributed to his award of the Nobel Prize in 1922.¹⁹

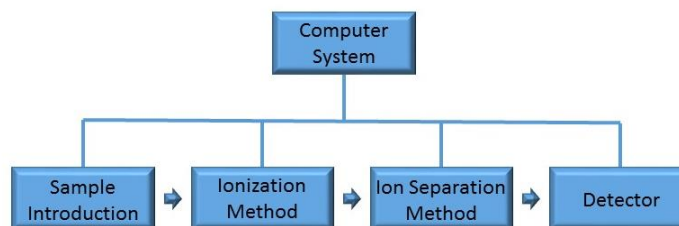


Figure 7. Block diagram of features of a typical mass spectrometer.²⁰

MS is often used as a detector following chromatography and can garner both qualitative and quantitative information with a high level of sensitivity and selectivity. As described in the HPLC section above, the sample is injected and pumps are used to migrate the sample through separation on the analytical column. When MS is used in conjunction with HPLC, the pumps then pump the eluate from the analytical column to the ionization source. Ions are generated in the gas phase and are then separated by m/z ratio via the mass analyzer. There are several ionization methods for LC-MS, the most common of these being electrospray ionization (ESI) and atmospheric pressure chemical ionization (APCI). Mass analyzers used to

separate ions by mass include the very commonly used quadrupole, ion trap, and time-of-flight mass analyzer. Finally, a detector is employed such as an electron multiplier tube, and the information generated is processed and stored on a computer. A general schematic of LC-MS instrumentation is shown in Figure 8.

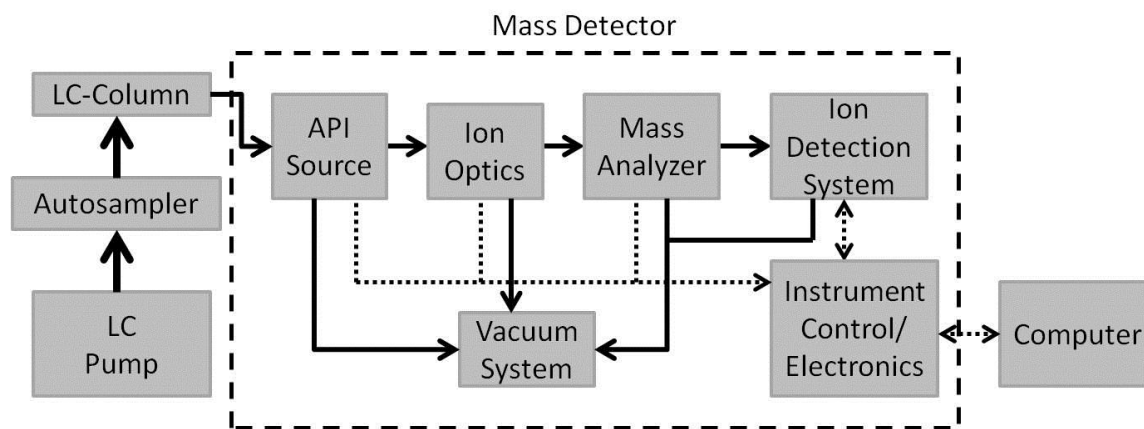


Figure 8. Schematic diagram of a mass spectrometer with HPLC as the sample introduction system.²¹

There are many other ionization methods available to generate gas phase ions for mass spectrometry, such as electron impact (EI) and chemical ionization (CI), which are the oldest methods and employ a gas phase sample introduction. This work has utilized exclusively ionization methods compatible with more condensed phases, namely evaporative ionization methods (ESI, APCI), and also desorption from solid phase samples by matrix-assisted laser desorption ionization (MALDI). Schematic representations of these methods are illustrated in Figure 10, Figure 11, and Figure 12, respectively.

3.2.1 Ionization Methods

ESI as an ionization method for mass spectrometry was first published by John B. Fenn in 1988.²² A high voltage is applied to the capillary wire, while the eluent is pumped through the capillary, creating a very fine mist. Droplets become highly charged, and the positive charge of the droplets is repelled from the positive charge of the capillary.¹⁹ As the electrostatic repulsion exceeds the surface tension, a coulombic explosion occurs releasing ions into the gas phase. Meanwhile, the charge density at the surface of the droplets increases as the solvent is heated and evaporated (this occurs at the critical point, known as the Rayleigh stability limit). The instrument is operated under high vacuum and so ions and neutral molecules in the gas phase are drawn through the entrance cone and toward the mass analyzer.²¹ ESI can yield sample ions with multiple charges, which can be advantageous when working with larger molecules, in order to yield a mass-to-charge ratio (m/z) within the detection range of the mass analyzer.

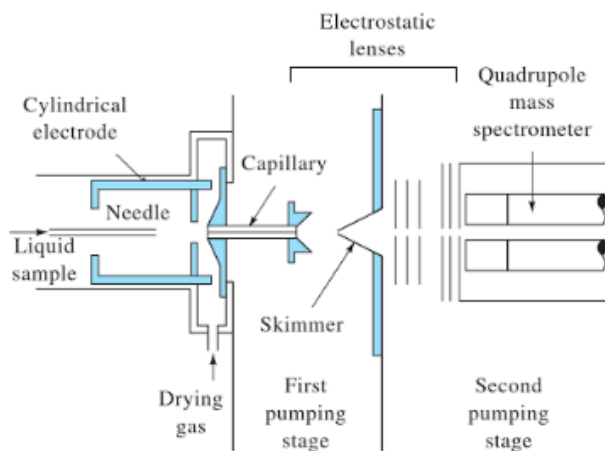


Figure 9. Schematic representation of ESI.¹³

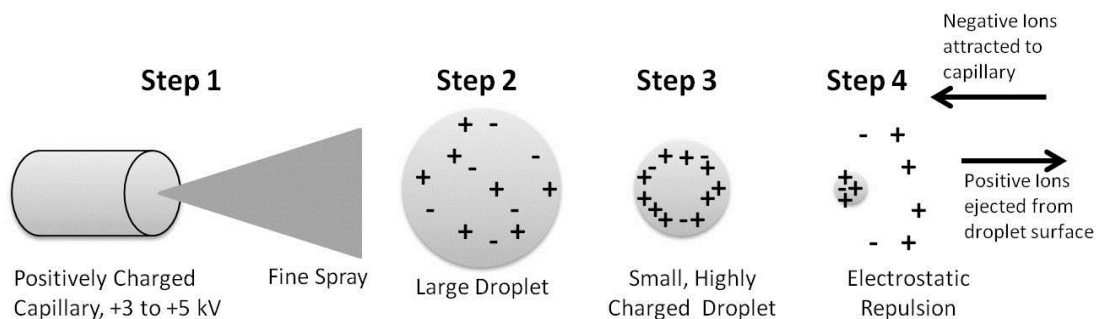


Figure 10. Positive ion generation mechanism by ESI.²¹

APCI also contains a heated vaporizer, which facilitates the rapid desolvation and vaporization off the droplets that are sprayed from the capillary. Reagent ions are generated from this solvent vapor by a corona needle discharge, which is created with a constant current between 2 and 10 μA leading to the formation of ions. The energized electrons produced by the corona discharge ionize the flowing nitrogen gas by primary ion formation. Ionized nitrogen reacts with solvent molecules, forming solvent ions through secondary ion formation. Solvent ions react via a proton transfer with the sample molecules to form sample ions $[\text{M}+\text{H}]^+$. Chemical ionization is an efficient method due to the numerous ion-molecule collisions. As with other ionization methods, charged ions and neutral molecules in the gas phase are drawn through the entrance cone by vacuum and travel to the mass analyzer.²¹ APCI yields singly-charged sample ions and is therefore limited to molecules with masses up to about 2000 atomic mass units (amu). However, APCI can allow for the ionization of less polar compounds, and can sometimes be a more efficient method of ionization than ESI depending on the analyte. In addition, on some instruments (including the Shimadzu LC-MS instruments employed in this work), APCI can be used in conjunction with ESI (known as DUIS mode).

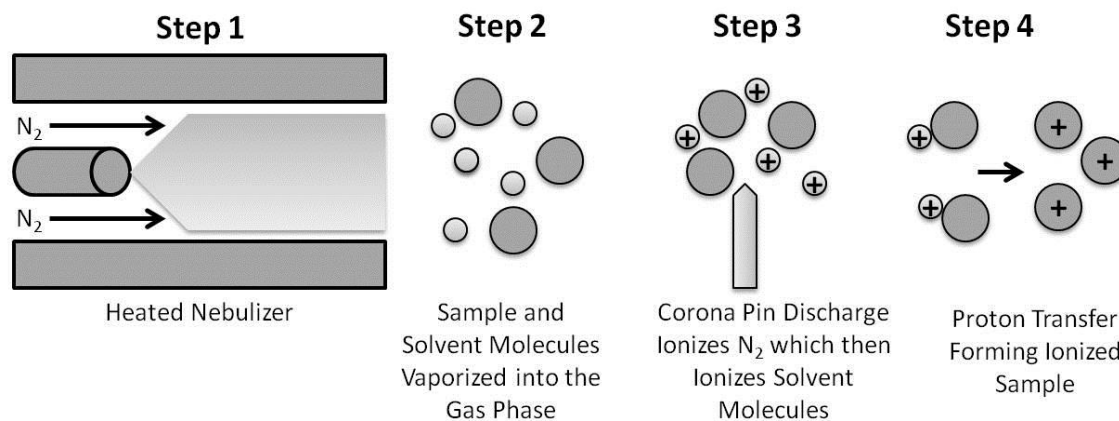


Figure 11. Positive ion generation mechanism by atmospheric pressure chemical ionization.²¹

Although ESI and APCI are the most common soft ionization techniques seen in LC-MS, these ionization methods are only appropriate for samples in the liquid state. Samples in the solid state require another ionization technique, and one such example is matrix-assisted laser desorption ionization, or MALDI. To create ions by MALDI, analytes are dried on a solid conductive surface, usually a metal plate, and coated with a matrix, which will then co-crystallize with the analyte. A laser is fired at the sample surface and the matrix absorbs the energy that enables both analyte and matrix to desorb from the surface creating an ion plume. The exact mechanism of the formation of this ion plume is not completely understood, but it is thought that the matrix absorbs energy from the laser and transfers that energy to the analyte. It is also believed that the analyte is desorbed as a neutral molecule and ionized by proton transfer from protonated matrix ions. MALDI is the method of choice for larger molecules such as proteins and peptides, and is employed to ionize dry solid samples into the gas phase.

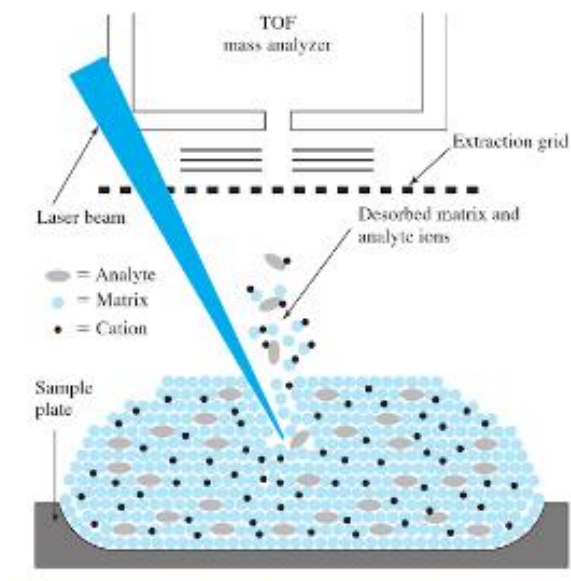


Figure 12. Cartoon representation of MALDI.¹³

3.2.2. Mass Analyzers

In addition to the variety of ionization methods employed in this work, there are also several different types of mass analyzers employed based on the type of analysis performed. The mass analyzers used predominantly in this work are the quadrupole and time-of-flight mass analyzers. The most common type of mass analyzer seen is the quadrupole mass analyzer. This mass analyzer is an inexpensive mass filter consisting of four cylindrical rods. A constant DC voltage is applied to the rods modified by a radio frequency. The four rods create a “tunnel” where the ions are introduced, and only ions with a certain m/z possess the stable trajectory necessary to pass through the quadrupole to the detector (as shown in Figure 13).¹³

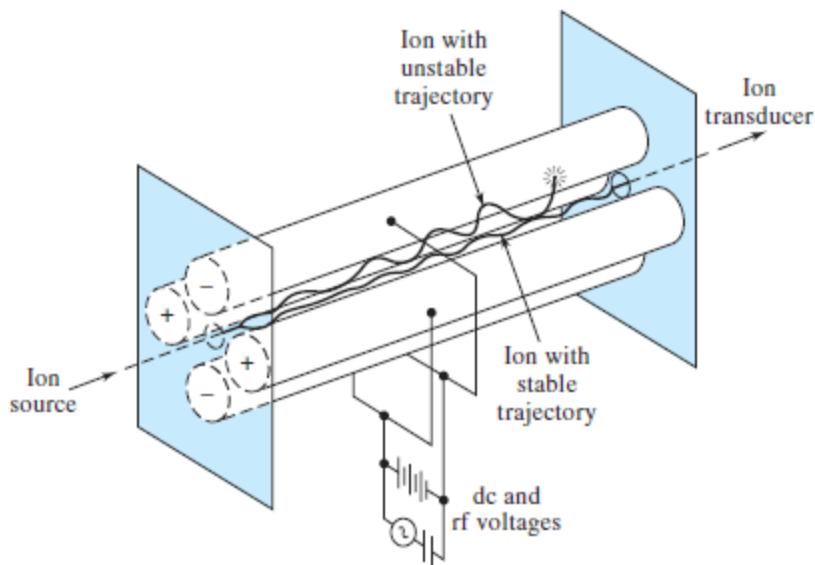


Figure 13. A quadrupole mass analyzer.

It is possible to utilize more than one mass analyzer for analysis, a technique known as tandem mass spectrometry (MS/MS). One prevalent example is the triple quadrupole, wherein two quadrupole mass analyzers sandwich a collision cell, which may or may not be a quadrupole. So the name 'triple quad' can actually be a misnomer. The MS/MS instrument can be used to select for a specific ion (the "parent ion"), fragment this ion, and then select or scan for the various fragments (the "daughter ions"). Tuning the voltages of the collision cell allows the triple quadrupole to reproducibly create fragments for a specific analyte. Not only is the mass of the fragments identical each time but they are also produced in the same ratio each time the parent ion enters the collision cell. Therefore, the triple quad generates what are called "reference ion ratios", meaning that the daughter ions seen are in a specific ratio to each other and to the parent ion. This relationship allows analytes to be detected at high sensitivity (low picomolar range), as they are identified not only by the LC retention time but also by the reference ion ratio spectra. Tandem mass spectrometry provides a high level of specificity to

the samples, which is advantageous when working with low concentrations of analytes in complex mixtures.

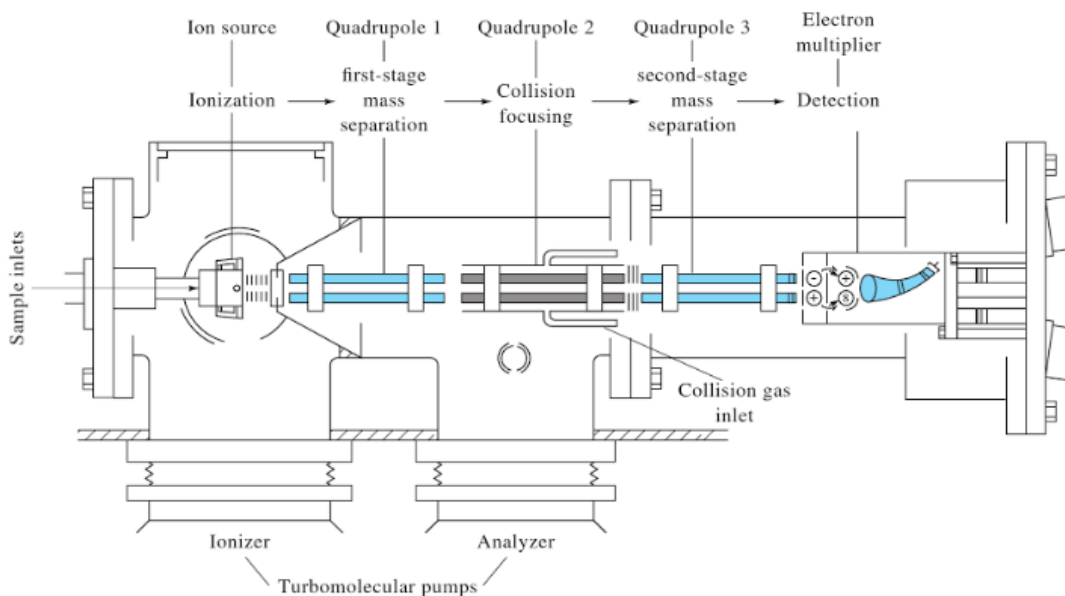


Figure 14. Schematic of a triple quadrupole mass analyzer.

The time-of-flight (TOF) mass analyzer works in a different manner than the quadrupole. In TOF, ions are accelerated through a potential, so they are starting with the same kinetic energy. Ions are then sent down a drift tube, after which they arrive at the detector at different times. If all ions have the same energy to start, then ions of different mass will have different velocities by $v=(2zeV/m)^{1/2}$ and therefore arrive at the detector at different times. The flight tube has a known length, therefore the arrival time can be used by the instrument to calculate the mass: $t=(L^2m/wzeV)^{1/2}$. TOF based mass spectrometers are often used with pulsed ionization techniques (as is the case with the laser employed in MALDI-TOF) because the start time and position must be known.¹³

The instrument used for MS imaging studies presented herein is a TOF/TOF instrument, again employing tandem mass spectrometry to increase the specificity by which the instrument can detect analytes within complex biological matrices. The instrument has two detection modes, linear mode and reflectron mode. This instrument has two detectors available regardless of the mode chosen. In linear mode, analytes are sent through the flight tube to the detector without any fragmentation. This mode is typically used for very large biomolecules, which have larger masses that are able to be resolved by one pass through the flight tube. In reflectron mode, the ions are reflected to travel a longer path, which changes the ion arrival time and therefore enhances the resolution. This is important for smaller analytes because it is more challenging for the instrument to distinguish between small masses with very similar arrival times.¹³

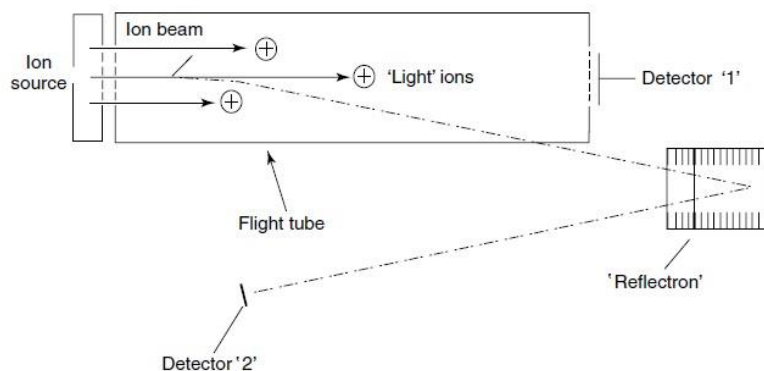


Figure 15. General schematic of a TOF mass analyzer.²³

The MALDI-TOF instrument employed for imaging experiments has a 2 kHz solid state UV laser for acquisition at a wavelength of 355 nm. The diameter of the laser beam is adjustable from 10 to 200 micrometers. Axial spatial distribution focusing (ASDF) is a technology designed to address issues with the curved field reflectron, where mass resolution

can decrease as the instrument changes from MS to MS/MS mode.²⁴ This mass resolution drop is produced by the increased spatial distribution of the ions as they leave the sample surface. ASDF aims to refocus this spatial distribution to keep the mass resolution independent of the laser power. The mass resolution should also be independent of sample thickness and topography. In the curved field reflectron, ions leave the MALDI source and are introduced into the TOF analyzer with 20 kV of kinetic energy. The ions maintain this energy as they enter the collision cell. The instrument employs high energy collision induced dissociation (CID), to generate fragments for TOF/TOF analyses. The ASDF technology is just before the reflectron and acts as a focusing lens for the fragment ions. The Shimadzu 7090 is designed to allow for mass resolution up to 10,000. Ions which are chosen to be fragmented are allowed through an ion gate combined with a collision gas which bombards the analytes and generates fragments. The fragments are then detected by passing through the flight tube completing the TOF/TOF analysis.

Tandem mass spectrometry is important to achieve high specificity. Thus, tandem mass spectrometry provides low limits of detection (for example, 1 pg/mL sensitivity on the triple quadrupole instrument). This low detection limit is possible due to reference ions that are created and optimized for each analyte. Because LC-MS/MS analysis is specific to the fragments generated, analytes do not need to be baseline resolved chromatographically. When working with complex biological samples that are difficult to purify, the ability to select masses for fragmentation and use those fragments to identify analytes is important.

3.2.3. The Detection System

After ions have been separated by the mass analyzer, they are detected, typically by an electron multiplier as illustrated in Figure 16. The electron multiplier tube contains a conversion dynode, with a concave piece of metal angle that can angle the ion beam. The off-axis orientation greatly reduces the noise by limiting the probability that a neutral molecule will strike the conversion dynode. A high voltage is used to increase the conversion efficiency and thus increase the signal (Figure 17). There is also typically a shield to protect the vacuum manifold from the electric field produced by the conversion dynode.²¹

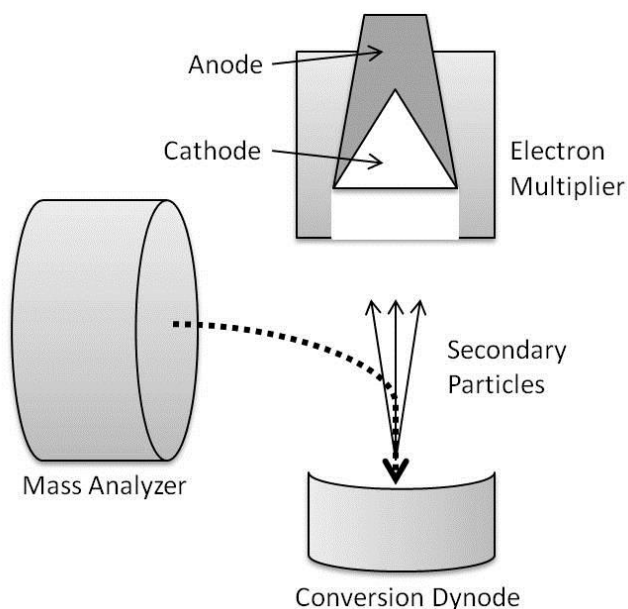


Figure 16. Ion detection system.²¹

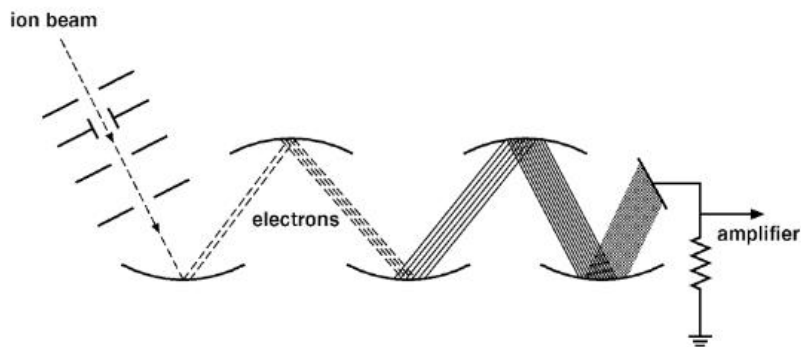


Figure 17. Amplification created when the ion beam is focused onto the conversion dynode, which emits electrons in direct proportion to the number of ions bombarding the dynode. These electrons are accelerated and focused onto another dynode, thereby creating a cascading effect from dynode to dynode.²⁵

1.4 Conclusions

In summary, the Arnold research group is interested in compounds that bind to the GABA_A receptor. This work illustrates the method development for several assays to characterize drug-like properties of lead molecules. Several different mass spectrometers were implemented to make these assays possible. The analytical accuracy of mass spectrometry is important and is therefore utilized frequently in the drug discovery arena. The work presented in the subsequent chapters shows how such a powerful technology can be employed to create information.

CHAPTER 2. Liver Microsome Stability Assay

2.1 Introduction

In-vitro assays used for the evaluation of ADMET (absorption, distribution, metabolism, excretion, and toxicity) properties are an essential part of drug discovery programs. *In-vitro* studies are generally performed to individually study these compound properties. Assays of this nature are extensively performed early-on to assess drug-like properties of lead molecules, ideally in a high-throughput and inexpensive fashion. It is important to quickly gain information regarding these drug-like properties when investigating a lead compound. These types of studies inform medicinal chemists if a drug candidate might have desirable therapeutic effects *in vivo*. With regard to metabolism within the ADMET field, optimum drug performance is determined largely by xenobiotic liver metabolism, because drugs taken orally are absorbed from the gastrointestinal tract and must pass through the liver in order to reach the circulatory system. Once in the circulatory system, the drug can be transported to its target organ to elicit a therapeutic response. However, it is rare for 100% of a dosed drug to reach the disease target location. A fraction of the drug is lost by xenobiotic metabolism and excretion, which is referred to as first-pass metabolism. A flow chart of how a xenobiotic is processed is illustrated in Figure 18. *In vitro* metabolic assays can be predictive tools for first-pass metabolism, as these predictions are based on the metabolism of a compound in a known enzyme system. For example, enzymes known to exist in the liver and in other locations in the body are cytochrome P450 enzymes. Approximately 60% of all marketed drugs are cleared from the body by hepatic cytochrome P450 metabolism.²⁶ Although both phase I and phase II metabolic processes are important for the metabolic processing of both exogenous and endogenous compounds,

typically the interactions seen in phase I metabolism are initially considered for *in vitro* metabolic studies. However, the study of metabolites generated by glucuronosyltransferase enzymes are commonly seen as well, and these UGT enzymes are also present in liver microsomes.²⁷

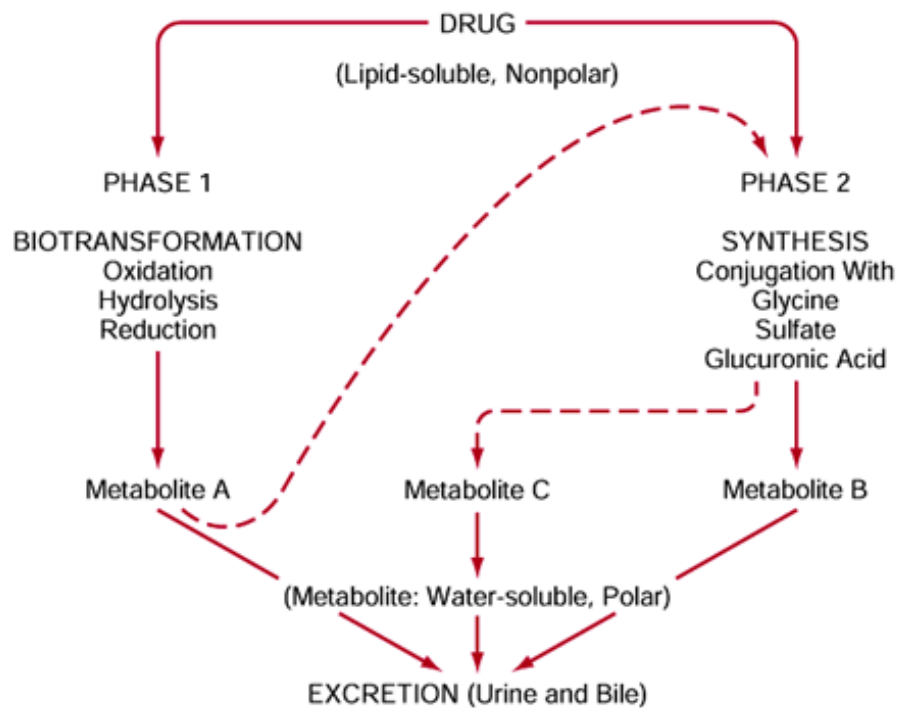


Figure 18. The two phases of drug metabolism and how they generate resulting metabolites.¹

The imidazobenzodiazepines investigated in this work are expected to undergo hepatic metabolism and generate metabolites similar to those frequently seen for benzodiazepine drug compounds, including hydroxylation products and benzophenone products. Figure 19 shows the core benzodiazepine ring featuring a pendant phenyl ring, which is a functionality seen in several of the lead compounds in this work. There are several prominent metabolic transformations that are known to occur in the liver, such as oxygenation, reduction, and hydrolysis, which are all dependent on the structure of the initial compound.

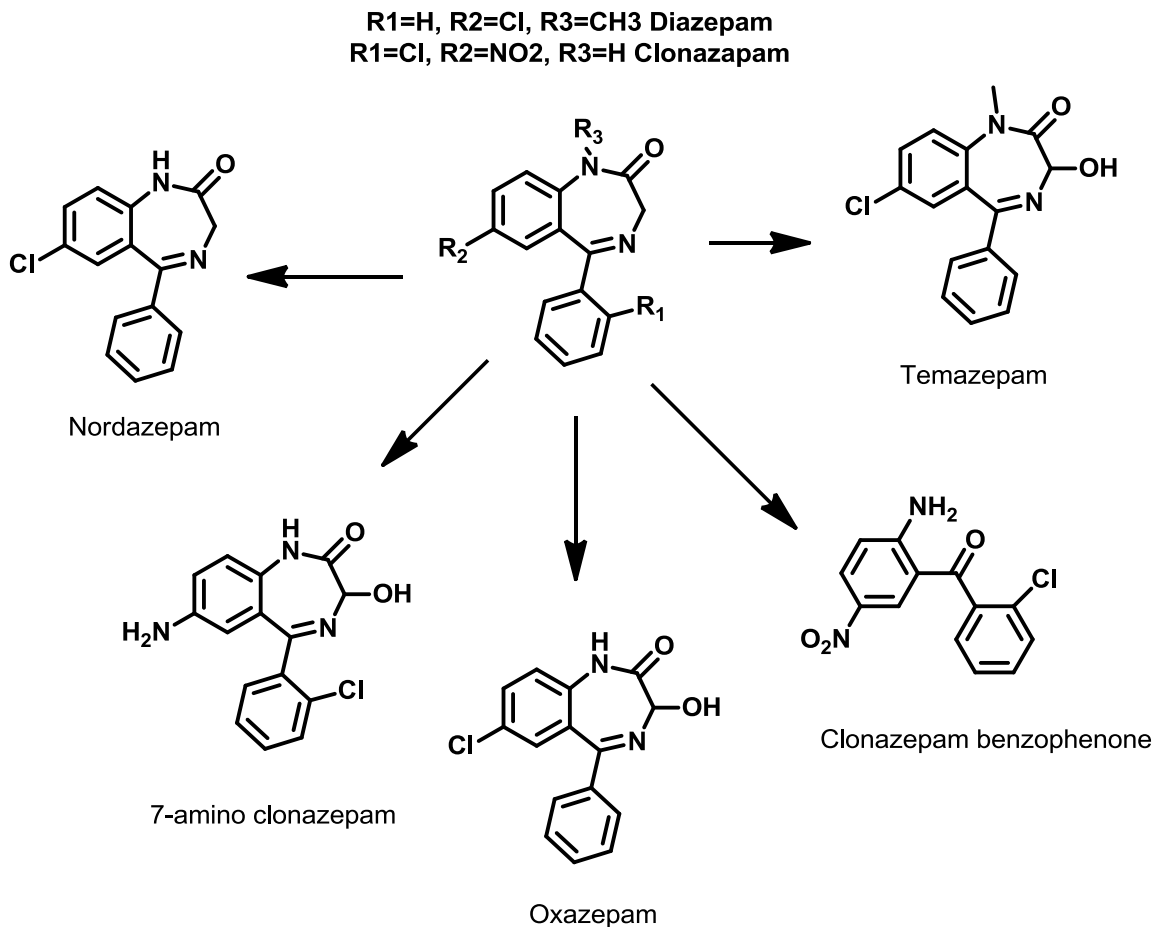
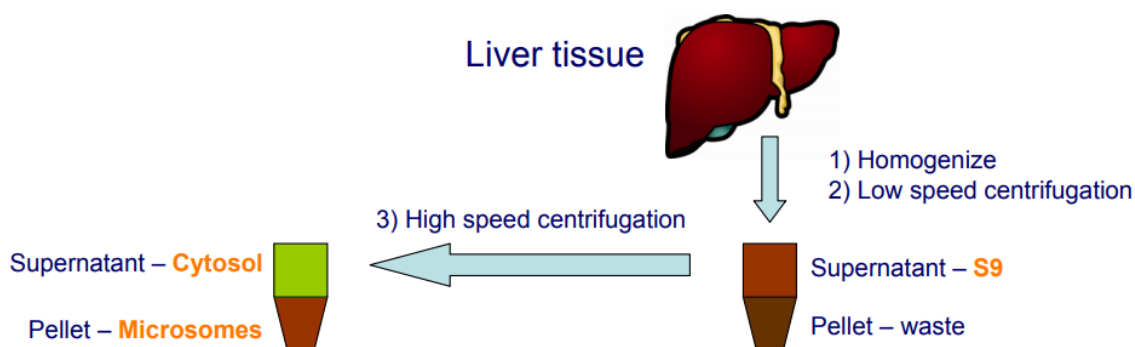


Figure 19. Illustration of benzodiazepine metabolism.²⁸

In order to test the metabolic stability of drug compounds *in vitro*, an inexpensive assay which can be conducted in a high throughput manner is required to efficiently screen as many analogs as possible. Therefore, a “mix-and-go” assay featuring commercially available reagents was optimized to meet this research need. Liver microsomes were chosen to provide the enzyme system necessary to degrade drug candidates and generate metabolites *in vitro*. Liver microsomes are subcellular fractions of liver cells, which are commercially available and have a reasonable cost and shelf life. Microsomes have been shown to contain drug metabolizing enzymes of interest such as the aforementioned cytochrome P450 enzymes (e.g. the

monooxygenase CYP3A4) which play a significant role in metabolizing drug compounds in the liver. Figure 20 shows the simple process of isolating microsomes from fresh liver tissue. Typically, this tissue is purchased from organ procurement sources when deemed unsuitable for human transplantation. The microsomes are the final product of the isolation scheme shown below, however assays can also be conducted using the cytosol, as well as the S9 fraction (which is the cytosol and microsomes together).



S9 = Both cytosol and microsomes = Phase I and II enzymes

Cytosol = Soluble proteins (phase II enzymes) = NAT, GST, SULT

Microsomes = membrane proteins (phase I enzymes) = P450

Figure 20. Isolation of microsomes from liver tissue, typically acquired through organ procurement organizations. Image: BD Biosciences

Due to the fact that these enzymes are known to play such a large role in the Phase I metabolism in the liver, within the context of pre-clinical drug development this is one of the first studies performed and published when investigating new drug compounds. Compounds that do not display good metabolic stability may potentially be discounted from the list of lead options, which is typically a lengthy list of compounds created by medicinal chemists. Generally, unless a compound is a pro-drug, quickly cleared compounds are considered to be unfavorable.

In-vitro metabolic assays can also be used to investigate reactive metabolites, drug-drug interactions, phenotyping, and *de novo* metabolite identification. Predictions can be made regarding how drugs will be metabolized in the liver based on known enzymatic transformations and previously published compounds with similar functionalities. Ultimately, these predictions need to be verified and this type of *in-vitro* assay can be used to accomplish that goal early-on in the drug development process. With regard to processing a xenobiotic, the body's metabolism is usually attempting to clear any xenobiotics. Often metabolic enzymes will make compounds more polar to aid in excretion. Therefore, liver microsome assays performed *in vitro* can also be used to enzymatically synthesize and identify metabolites that would be excreted as well. It is very difficult to replicate an excretion system *in vitro*, therefore the liver microsome assay is currently the best option for seeking to gain excretion info *ex vivo*.

Cytochrome P450 enzymes are heme-protein molecules. The heme group (protoporphyrin IX) contains coordinated iron. It has been proposed that the substrate binds to the active site followed by a reduction of the iron III of cytochrome P450 to the iron II state, by a one electron transfer catalyzed by P450 reductase. Subsequently, molecular oxygen binds to the iron II and is converted to an activated oxygen species.²⁹ This system can be non-specific and will oxidize a variety of substrates. Non-selective enzymes such as CYP3A4 metabolize a large number of drugs including our current analytes of interest, imidazobenzodiazepines.

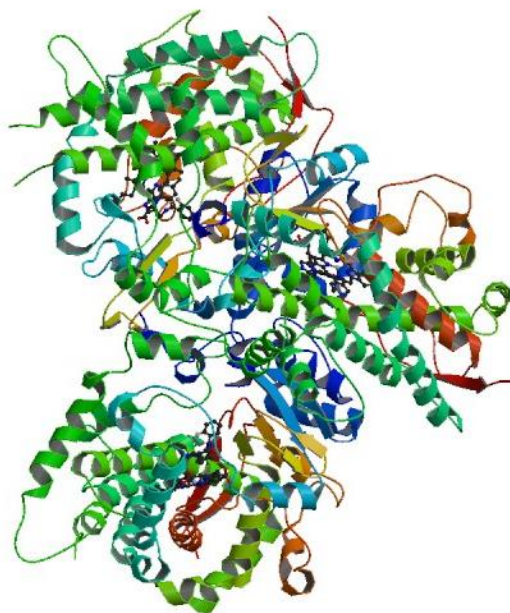


Figure 21. Crystal structure of the midazolam-bound CYP3A4.³⁰

In addition to identifying potential metabolites utilizing CYP450 enzymes, several numeric parameters can be estimated from the *in-vitro* degradation of compounds by liver microsomes. The assay presented herein estimates the rate of metabolism based on the free intrinsic clearance, which is a description of metabolism due to enzyme activity alone (other factors such as blood flow through the liver or drug binding percentages are not accounted for in the calculation of intrinsic clearance).³¹ The values calculated for the clearance are based on the Michaelis-Menten kinetic model in biochemistry, which is outlined in Equation 2. Under linear conditions, as is the case with the liver microsome assay, the concentration at the enzyme site is 10% or less of the K_m , and equation 2 is reduced to form Equation 3.

Equation 2. Rate of metabolism = $V_{max} * C_E / K_m + C_E$

Equation 3. Rate of metabolism = $V_{max} * C_E / K_m$

The rate of metabolism is equal to the product of the intrinsic clearance and the concentration of drug, and is expressed as $\mu\text{L}/\text{min}/\text{mg}$ microsomal protein. The analogy extended to an *in vivo* situation would be the volume of blood that is cleared of a drug per unit time. Based on the same kinetic model, the metabolic half-life of the drug can also be calculated (the time taken for the concentration of a drug to be eliminated to half of its original value). This procedure has been optimized using both human and mouse liver microsomes to identify any metabolic differences between species, as most pre-clinical assays are conducted in mice. Drugs can behave differently in certain animal species, therefore it is necessary to conduct this assay with both human and mouse liver microsomes to illustrate the metabolic behavior in animal and human.

2.2 Materials & Methods

Four μL of 1 mM test compound (XHE-III-74 ethyl ester or XHE-III-74-Acid at a final concentration of 10 μM) in DMSO were preincubated at 37°C for 5 minutes on a digital heating shaking dry bath (Fischer scientific, Pittsburgh, PA) in a mixture containing 282 μL of water, 80 μL of phosphate buffer (0.5 M, pH 7.4) 20 μL of NADPH Regenerating System Solution A (BD Bioscience, San Jose, CA) and 4 μL of NADPH Regenerating System Solution B (BD Bioscience, San Jose, CA) in a total volume of 391.2 μL . Following preincubation, the reaction was initiated by addition of 8.8 μL of either human liver microsomes (BD Gentest, San Jose, CA), or mouse liver microsomes (Life technologies, Rockford, IL at a protein concentration of 0.5 mg/mL. Aliquots of 50 μL were taken at time intervals of 0 (without microsomes), 10, 20, 30, 40, 50 and 60 minutes. Each aliquot was added to 100 μL of cold acetonitrile solution containing 1 μM of verapamil HCL as internal standard. This was followed by sonication for 10 seconds and

centrifugation at 10,000 rpm for 5 minutes. 100 μ L of the supernatant was transferred into Spin-X HPLC filter tubes (Corning Incorporated, NY) and centrifuged at 13,000 rpm for 5 minutes. The filtrate was diluted 100 fold and subsequently analyzed by LC-MS/MS with Shimadzu LCMS 8040, (Shimadzu Scientific Instruments, Columbia, MD). The ratio of the peak areas of the internal standard and test compound was calculated for every time point and the natural log of the ratio were plotted against time to determine the linear slope (k). The metabolic rate ($k \cdot C_0/C$), half-life ($0.693/k$), volume of distribution ($V_d = \text{volume of the assay } (\mu\text{L})$ divided by the protein of the incubation in mg (2000 $\mu\text{L}/\text{mg}$ in our assay)), and intrinsic clearance ($V_d \cdot \ln 2/t_{1/2}$) were calculated, where C_0 is the initial concentration of test compound, C is the concentration of microsomal protein. All time points were repeated in triplicate. Human and mouse liver microsomes were purchased as a 50 donor pool to ensure sufficient diversity for reproducible assay results. NADPH is a necessary co-factors for enzymatic activity, therefore when this fuel for the enzymes has been used up in its entirety, the enzymes can no longer metabolize xenobiotics and the conversion will stop. HyClone phosphate buffered saline was purchased from Fisher Scientific (Waltham, MA). The initial development of this assay was performed on a Thermo HPLC with a PDA detector. Further optimization and metabolite identification was performed on a Shimadzu 8040 triple quadrupole UHPLC-MS/MS system as it became available. Optima LC/MS grade methanol, acetonitrile, formic acid and water were purchased from Fisher Scientific. Separation was performed on a Restek C18 column (25 mm x 2.1 mm, 3 μ m particle size). Uracil was purchased at Sigma Aldrich (Milwaukee, WI) and used to measure the instrument void time. Test compounds were synthesized as published previously³² and received as pure powder, which was weighed and dissolved in DMSO to create original

stock solutions at [10mM]. Stock solutions were diluted to a working concentration of 1 mM, also in DMSO, as described above. Microsomes were stored at -80°C prior to use and thawed over wet ice. All solutions purchased (NADPH and microsomes) were aliquot into smaller volumes to minimize the number of freeze/thaw cycles. Solutions A contains NADP⁺ and solution B contain glucose-6-phosphate dehydrogenase to create NADPH when combined. The initial assay solutions consisted of a mixture of 200 µL total, 10 µL of solution A, 2 µL of solution B, 2 µL of 1 mM stock in DMSO were added to 181 µL of PBS. However this volume was increased over time to allow for additional replicates. This mixture was pre-incubated for 5 minutes to reach physiological temperature, followed by the addition of 5 µL microsomes (20 mg/ml protein concentration). Initially, 30 µL of the microsomal assay mixture was taken out at time points 0, 5, 10, 15, 30 and 60 minutes and immediately added to 1 equivalent volume of cold acetonitrile containing a pre-chosen internal standard. However, these time points were altered to be every ten minutes, to generate more consistent plots. The acetonitrile used to precipitate the protein was upgraded from standard reagent grade to LC-MS grade when the methods were to be run on the LC-MS/MS instrument. In the original development of this assay, the quenched mixture was spun down at 10,000 rpm for 5 minutes, the supernatant withdrawn from atop the protein pellet, transferred to a 384 well plate and placed directly onto the HPLC-UV instrument. However, additional filtration steps were later added prior to LC-MS analysis, using 0.22 µm nylon spin filter vials. Although all particulates and large proteins should be removed from the acetonitrile by precipitation and centrifugation, it was determined that additional filtration was necessary to generate clean, consistent data on the LC-MS 8040. This

procedure was developed in duplicate and increased to triplicate repeats for more reliable results and lower standard deviation values.

Initial method development and analyses were performed on a Thermo LTQ HPLC-UV instrument. However, shortly after this assay was developed the method was transferred to the triple quadrupole UHPLC-MS/MS instrument (Shimadzu 8040). The initial analysis conditions performed on the now decommissioned HPLC-UV system were under isocratic conditions, 30% acetonitrile and 70% water. The flow rate was 150 $\mu\text{L}/\text{min}$, with a column oven temperature of 50°C and a pressure of 75 bar. This instrumental method was problematic due to a consistent yet sloping baseline, as pictured in the chromatogram below. Although the peak shape is sufficiently symmetrical and the signal to noise ratio is calculated as infinite, it is not ideal to have such a baseline. HPLC-UV also shows a large solvent front, which is not seen on the LC-MS/MS instrument, as MS/MS methods are specific to the masses of interest. Although the HPLC-UV chromatogram shows sufficient baseline separation for each peak, as well as sufficient signal to noise, the peak shape does illustrate some tailing, and the proximity of the first peak to the solvent front is somewhat concerning. Typically this issue can be remedied with modifications to the mobile phase conditions, such as switching from acetonitrile to methanol, decreasing the flow rate, or increasing the water content in the mobile phase. However, these typical troubleshooting strategies were not sufficient for the analysis initially because the C18 column was well past retirement. Column care is exceptionally important for the lifetime of the column in liquid chromatography, if the column is stored uncapped or not handled carefully, it will dry out the stationary phase and deteriorate the column's ability to sufficiently retain analytes.

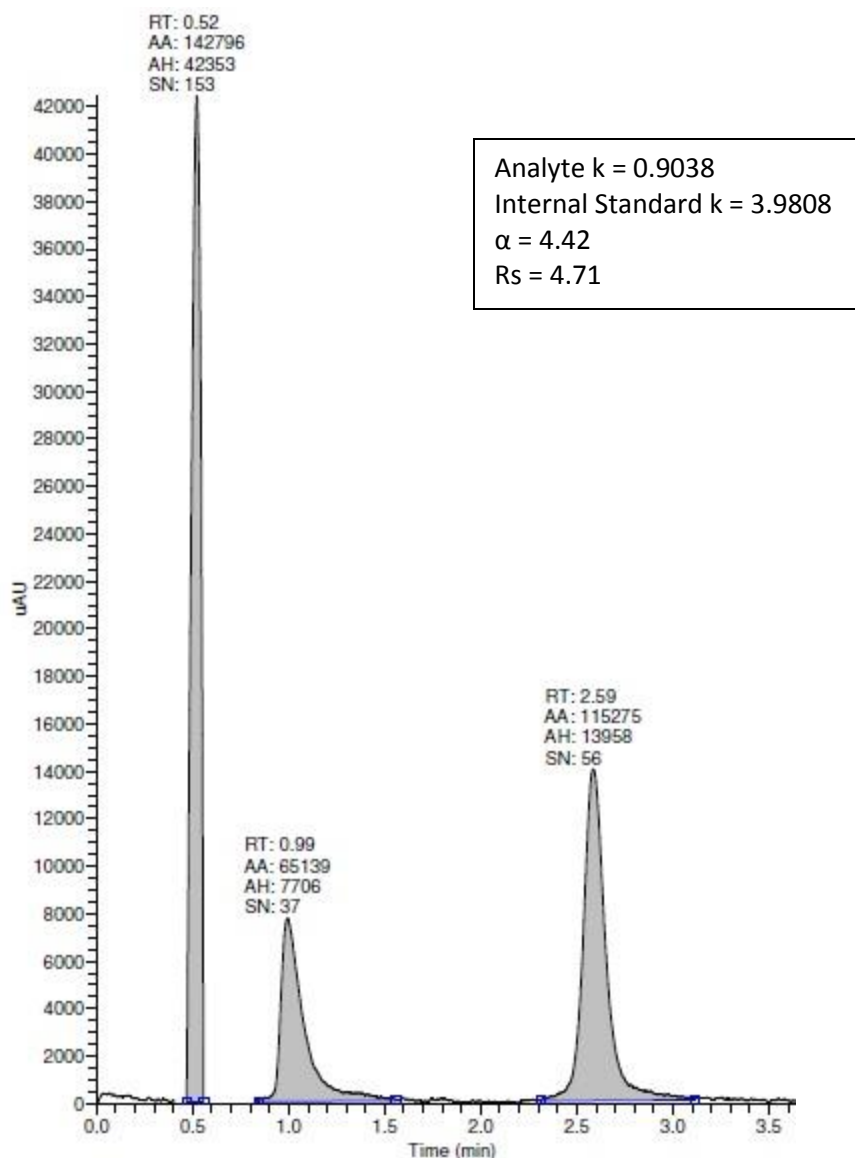


Figure 22. HPLC-UV analysis of drug compound degradation by human liver microsomes. The peaks shown are the solvent front (t_r : 0.52 min), the analyte (t_r : 0.99 min), and the internal standard (t_r : 2.59 min). RT is retention time, AA is the area of the peak, AH is the peak height, and SN is the signal to noise ratio.

Upon implementation of the triple quadrupole instrument, a new C18 column was purchased for microsomal assay analysis. Analytes were optimized individually by testing collision energies from -15 to -40 V in positive mode, tested in increments of 5. Proposed fragmentation patterns for analytes are listed in Appendix A. Masses and voltages used for

reference ion ratios are listed in Appendix B. All fragmentation patterns were optimized with pure compounds dissolved from powder into mobile phase.

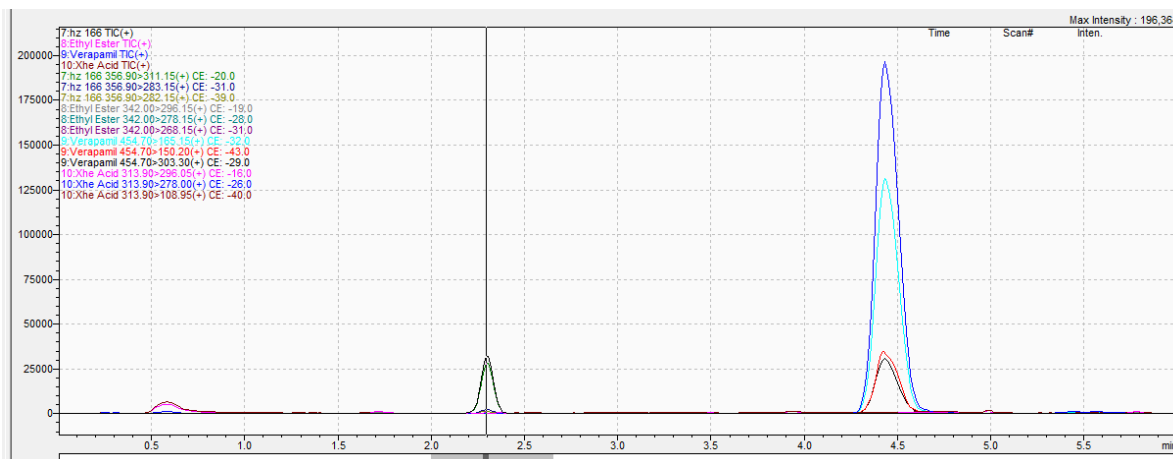


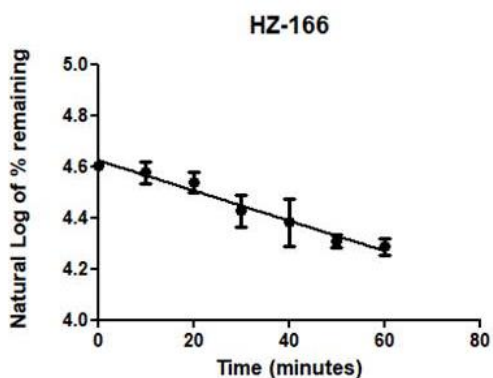
Figure 23. Chromatogram from the triple quadrupole LC-MS 8040. Each peak represents the total ion chromatogram followed by each ion in the reference ion ratio (underlying peaks). For example, the peak at RT 4.4 minutes is for verapamil. The largest peak in blue is a sum of all the ions for that compound. The second largest peak in light blue is for most abundant of the reference ions, followed by smaller peaks in red and black for the less abundant reference ions for verapamil.

2.3 Results and Discussion

Peak areas were integrated by LabSolutions software and the analyte area was divided by the area of the internal standard, to create a ratio. This ratio was converted to a percentage by taking the zero time point as 100% and scaling the ratio values to that assumed zero. Then, to compute pharmacokinetic parameters, the natural log of the percentage was plotted and fit with a linear regression (as illustrated in Figure 24). The metabolic half-life was calculated by taking the natural log of 2 divided by the slope of the regression line. The volume of distribution for our assay was 2000 $\mu\text{L}/\text{mg}$. That volume of distribution was multiplied by the $\ln(2)$ and divided by the previously calculated metabolic half-life to yield the internal clearance. The

metabolic rate is determined by the slope of the regression line multiplied by the concentration of compound (10000 nM) and divided by the concentration of protein (500 mg/l).

Linear Regression Plot



Slope of regression line = 0.005904

Half-life: $\ln(2)/\text{slope}$

$0.693/0.0059 = 117.5$ minutes

Clearance: $V_d * \ln(2) / \text{half-life}$

$2000 \mu\text{L} * 0.693 / 117.5 = 11.8$
 $\mu\text{L}/\text{min}/\text{mg}$ protein

**Metabolic Rate: Slope *
 [compound]/[protein]**

$0.0059 * (10\,000 \text{ nM}/\text{l}) / (500 \text{ mg}/\text{L}) =$
 $0.118 \text{ nmol}/\text{min}/\text{mg}$

Figure 24. Example of calculations performed for liver microsome assays.

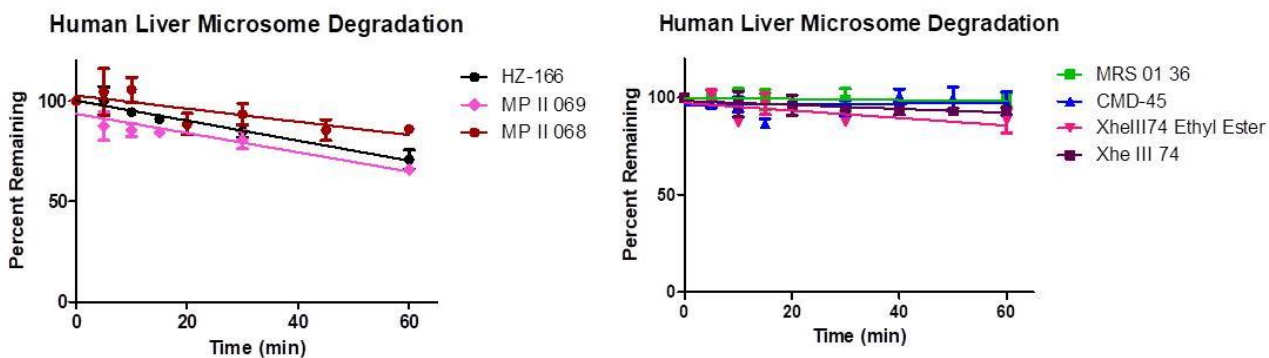


Figure 25. Percentage plot of human liver microsome results for $\alpha_5\beta_3\gamma_2$ and $\alpha_4\beta_3\gamma_2$ GABA_AR selective ligands.

Table 1. Metabolic parameters for seven imidazobenzodiazepine compounds.

Compound	HZ-166	MP-II-069	MP-II-068	Xhe-III-74	Xhe-III-74 EE	MRS-I-36	CMD-45
Metabolic Half Life, minutes	117.46	116.20	200.58	663.79	334.94	2252.93	4129.92
Intrinsic Clearance, uL/min/mg	11.8	11.9	6.9	2.1	4.1	0.6	0.3
Metabolic rate, nM/min/mg	0.118	0.119	0.069	0.021	0.041	0.006	0.003

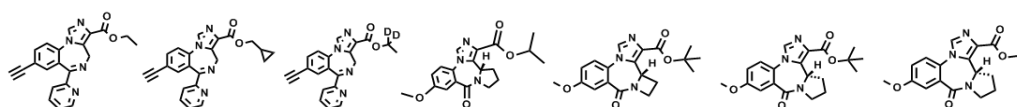


Figure 26. Structures correlating with the results for several imidazobenzodiazepine compounds.

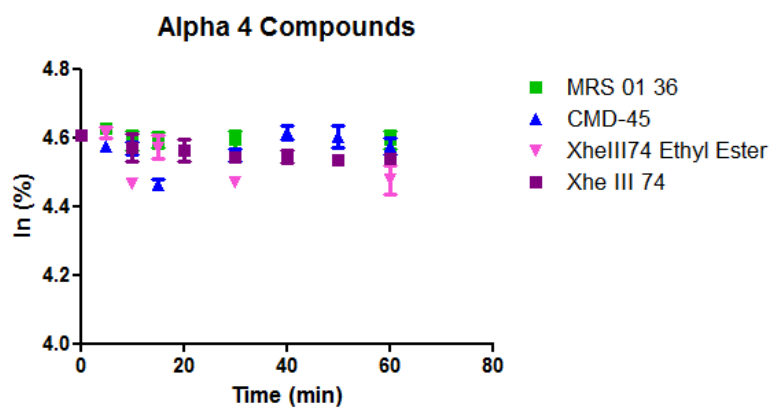


Figure 27. $\alpha_4\beta_3\gamma_2$ selective ligands, natural log plot.

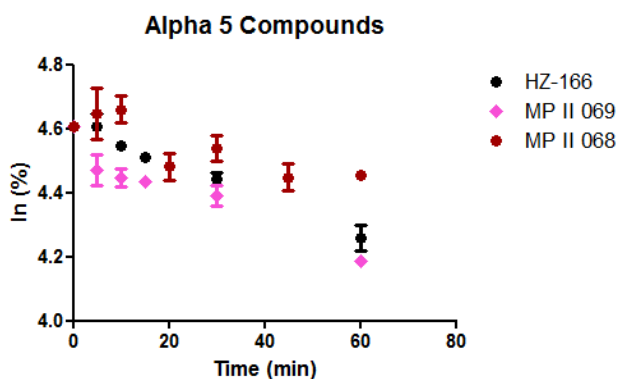


Figure 28 $\alpha_5\beta_3\gamma_2$ selective ligands, natural log plot.

The results for this assay show a distinct difference in metabolic stability between the $\alpha_4\beta_3\gamma_2$ selective GABA_AR ligands and the $\alpha_5\beta_3\gamma_2$ selective GABA_AR ligands alpha 5 receptor ligands. The compounds that are selective for the alpha 4 receptor have an extra ring attached directly to the core structure, in a rigid position that will prevent metabolism at the 4 position of the seven membered ring. The alpha 5 receptor ligands, however, do not have a ring in this position, they have a pendant phenyl ring that is designed to fit into the binding pocket (as shown in the structures in Figure 26). These structural differences lead to subtype selectivity, but also have an impact on the *in vitro* stability of these compounds.

This assay can also be used to identify metabolites that are generated by CYP450 enzymes. Although the quantitation is done in MRM mode, which identifies a specific mass and subsequently fragments of that mass, the assay samples can also be scanned over a mass range in an attempt to identify metabolites. General scans can be performed on a quadrupole instrument, but for more detailed analysis and formula prediction, the high resolution IT-TOF

presents the opportunity to research in depth metabolomics. One such example of a newly discovered metabolite generated through the microsome assay is presented in Figure 29. The hydroxylation product for the MP II 069 compound was identified in scan mode on the LC-MS 8040 at the 60 minute time point. As this time point, which is at the end of the assay, enzymatic transformations have occurred and therefore metabolites are present in the solution.

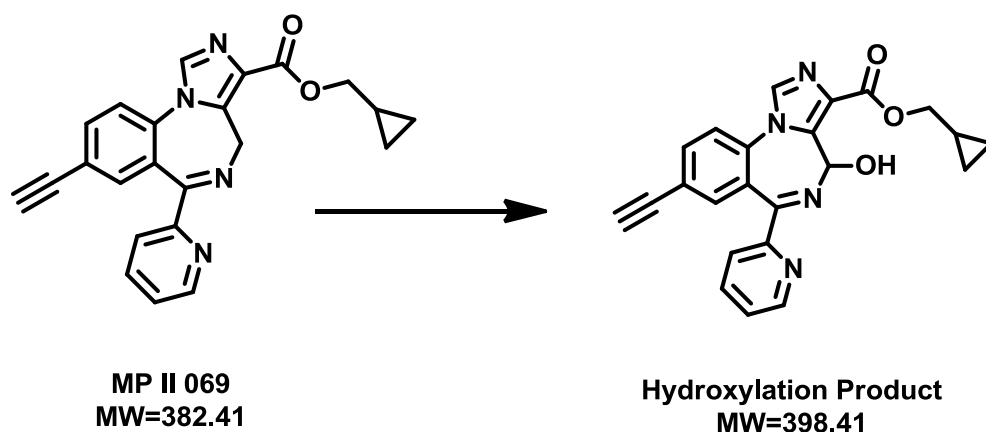


Figure 29 Scheme of the metabolism of MP II 069 by hydroxylation.

Metabolomics is in and of itself a vast research area within the field of drug discovery. With the resources available to the MIDD, this is a promising future direction that the medicinal chemists at UWM will be able to pursue to further understand the pharmacological promise of lead compounds.

This assay has been successfully developed to investigate the metabolic stability of various lead compounds under *in vitro* conditions. This procedure has been implemented to study not only imidobenzodiazepines synthesized by the Cook group, but other compound types as well for a variety of projects. Prior to the development of this assay, medicinal chemists at UWM would be required to utilize external contract research organizations for

metabolic stability studies. One such example is the compound HZ-166, which was investigated by a contract research organization as published previously.³³ The assay presented above shows good correlation with the CRO results (indicating this compound to have 66% of the parent remaining after one hour), further illustrating the effectiveness of the method presented.

In conclusion, this assay is a commonly used screening tool that has been implemented in the MIDD to screen over 100 compounds to date. This assay provides a sufficiently high-throughput approach to the assessment of metabolic stability.

CHAPTER 3. Primary Human Hepatocyte Assay

3.1 Introduction

Assays which employ human liver microsomes to illustrate analyte degradation give medicinal chemists valuable information regarding *in-vitro* stability of lead compounds because they contain important drug-metabolizing enzymes such as CYP450 enzymes. However, microsomes do not contain the full complement of enzymes that a drug will encounter during metabolism in the liver.²⁶ Although the liver microsome assay is rapid, inexpensive, and therefore useful in high-throughput screening, it can be necessary to carry out additional metabolic stability assays using cell culture. To gain insight into the metabolism a drug will encounter in the liver, it is obvious to use a liver cells for *in-vitro* screening. These so called hepatocytes can be harvested directly from liver tissue and can be cultured for a limited period of time. An alternative is the use of immortalized or carcinogenic liver cells that can be propagated unlimited in cell culture. Freshly isolated liver cells are called primary human hepatocytes, which have become the “gold standard” for looking at hepatic clearance as well as identifying drug metabolites *in-vitro*. It is important to mention that liver microsome contain less enzymes than the hepatocytes they are derived from. One example are transport proteins that may play a role in the performance of a drug compound.³⁴ Typically, primary human hepatocytes are isolated from livers deemed unsuitable for transplantation and are relative expensive. They can be plated and cultured, however the maximum time that they will typically live is a few days. Therefore, the use of primary human hepatocytes, while it is the best case scenario for gaining insight into the hepatic clearance of a drug in Phase I metabolism, is far too expensive to employ for a high throughput preclinical assays. For that reason, it is typical

practice to use liver microsomes to screen a large number of compounds, and only the most promising lead compounds are investigated with a hepatocyte based metabolism assay.

In addition to the high cost and limited life span of freshly isolated primary human hepatocytes, they are also phenotypically unstable and exhibit large variations between donors when mixed.³⁵ Commercially available human liver microsomes are typically pooled from 50 donors in order to eliminate large variations. This is not an option for primary hepatocytes. Alternatively, utilizing a hepatoma cell line (derived from cancer cells) has become a more cost effective research option. Several cell lines currently exist as options, and are employed for this purpose. These include HepG2, Hep3B, Huh7, HBG, HepRG and PLC/PRFs.³⁵ In general, cell lines derived from cancer cells easy proliferate. HepG2 cells have lost some functionality since their initial establishment as a hepatoma cell line, however, drug-metabolizing potentials can still be characterized for each cell line and are shown to be of use in drug discovery programs. Typically, suppliers of these cell lines will characterize pertinent proteins (such as cytochromes) expressed by these cells. With regard to xenobiotic metabolism, these cells generate some of the metabolites that would be formed *in vivo*, although the quantitative amounts are different. This makes sense because the human body has many different organs responsible for metabolism and therefore the number and quantity of enzymes available to process a drug are clearly very different from cell culture. The quantity of parent compound and metabolites varies based on the chemical composition, amount of compound, number of cells, media and temperature. Both Phase I and Phase II metabolizing enzymes can be transcriptionally induced in cell culture and will change with the culture conditions. Primary cells from different donors inherently have very high batch variability but represent the different metabolism by patients

taking these drugs eventually. However, this variability is a disadvantage when it comes to reproducible quantification of generated metabolites and parent drug degradation. Hepatoma cells don't change their genetic makeup in culture thus metabolic stability assay results are more uniform. Therefore, HepG2 are a useful substitute for assay development and have been employed in the studies listed herein.

3.2 Materials & Methods

HepG2 cells were purchased from ATCC (Manassas, VA) and were stored in liquid nitrogen prior to use. Cells were quickly thawed at room temperature and added to 20 mL of Minimum Essential Medium (Hyclone, #SH3024301) media in a culture flask to which non-essential amino acids (Hyclone, #SH30238.01), 5×10^6 units of penicillin and streptomycin (Hyclone, #SV30010) and 10% of heat inactivated fetal bovine serum (Gibco, #10082147) were added. The cells were grown for 3 days at 37° C with 5% CO₂, trypsinized with 0.25% Trypsin (Hyclone, #SH3004201) for 5 minutes to detach from the cell culture flask and were then added to 20 mL fresh MEM media. Cells were spun down in conical tubes at 1000 rpm for 3 minutes, resuspended in a smaller volume of MEM media and counted with a hemocytometer at 4.2 million cells per mL. Cells were diluted 2x with additional MEM media and aliquots of 100 µL were dispensed into wells of a sterile 96 well plate (Nunc #12-566-71). 0.5 µL of compound (2 mM in DMSO) at different concentrations was dispensed into each well of the 96 well plate for a final incubation concentration of 10 µM (0.5% DMSO). The plate was incubated for 24 hours at 37° C with 5% CO₂. 65 µL of media was aspirated and combined with 130 µL of cold acetonitrile solution containing 1 µM of verapamil HCL as internal standard. This was followed

by sonication for 10 seconds and centrifugation at 10,000 rpm for 5 minutes. 100 μ L of the supernatant was transferred into Spin-X HPLC filter tubes (Corning Incorporated, NY) and centrifuged at 13,000 rpm for 5 minutes. The filtrate was diluted 100 fold and subsequently analyzed by LC-MS/MS with Shimadzu LCMS 8040, (Shimadzu Scientific Instruments, Columbia, MD). The ratio of the peak areas of the internal standard and test compound was calculated for every time point and the natural log of the ratio were plotted against time to determine the linear slope (k). The half-life ($0.693/k$) was calculated.

3.3 Results & Discussion

Several compounds were screened using the HepG2 cell based assay. Initially, the first compound chosen was MP III 024 (Figure 30), which was incubated for 90 minutes with HepG2 cells. Unlike for the liver microsome assay, no notable change in the concentration of MP III 24 was observed for a period of 90 minutes. Therefore, after this initial run it was decided to extend the timeline of this assay to two hours (Figure 31).

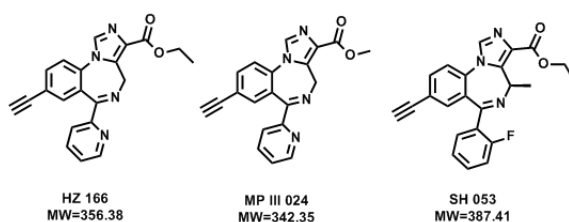


Figure 30 Structures for $\alpha_5\beta_3\gamma_2$ GABA_AR selective ligands.

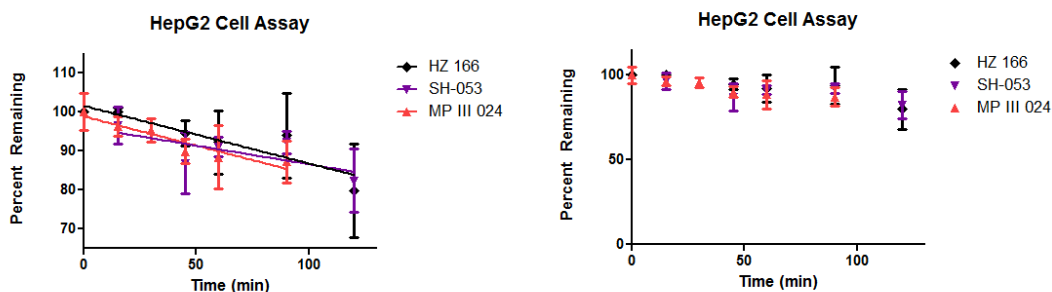


Figure 31. Results for $\alpha_5\beta_3\gamma_2$ GABA_AR selective ligands in HepG2 cell stability assay, presented as percent compound remaining over the course of two hours. The left plot shows the linear regression from 65 to 100%, the right plot shows the percent scale from zero to 100%.

We observed that all three compounds were relative stable in the presence of HepG2 cells. In comparison the half-lives in the presence of liver microsomes were 167 minutes SH-053, 209 minutes MP-III-024 and 158 minutes Hz-166. The calculated stability parameters for HepG2 cells are presented in Table 2.

Table 2. Stability parameters for $\alpha_5\beta_3\gamma_2$ GABA_AR selective ligands.

Compound	Half Life, min	R square	Sy.x	Deviation from linearity
MP-III-024	432.1366	0.9069	0.01862	Not significant
SH 053	647.1962	0.5197	0.04819	Not significant
HZ 166	423.9432	0.7924	0.04225	Not significant

The half-lives of $\alpha_5\beta_3\gamma_2$ GABA_AR selective ligands were lower than those determined with the liver microsome stability assay. It is generally known that microsome stability assays actually overestimate the internal clearance for a compound, as illustrated in Figure 32. The clearance of these FDA approved GABA_AR ligands is significantly faster in microsomes than in the presence of fresh hepatocytes. The data seen in this work is thus consistent with the trend published in the literature.

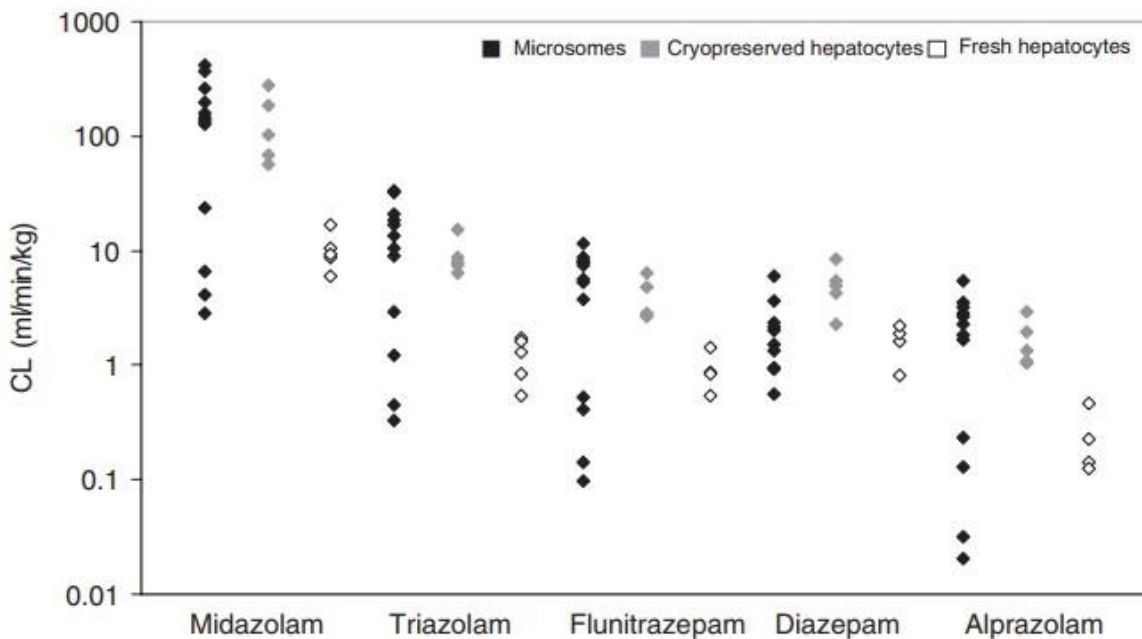


Figure 32. Comparison of CL values for five benzodiazepine compounds as estimated in human liver microsomes, human cryopreserved hepatocytes, and fresh human hepatocytes.³⁶

The assay described herein involves a living cell system, therefore many factors contribute to the repeatability of this assay. HepG2 cells are an adhesion cell line thus they grow on the flask bottom. A substance called matrigel is often used to assist in adhering cells to plastic surfaces during cell culture. This assay was tested both with and without matrigel. However, it was determined that the addition of this material to the assay plate did not have any noticeable effect the results of this assay.

During the time this assay was being developed, the Cook group synthesized many deuterated analogs in an effort to exploit the kinetic isotope effect for metabolic stability. A carbon-deuterium bond is more difficult to break than is a carbon-hydrogen bond, thus it is expected that the deuterated analogs would display better stability in both the human liver microsome assay as well as the hepatocyte assay. The kinetic isotope effect is a commonly studied phenomenon in the field of drug development and was therefore a logical strategy for

the medicinal chemists synthesizing compounds for this work to increase metabolic stability.

The compounds investigated were $\alpha_4\beta_3\gamma_2$ GABA_AR selective ligands (Figure 33).

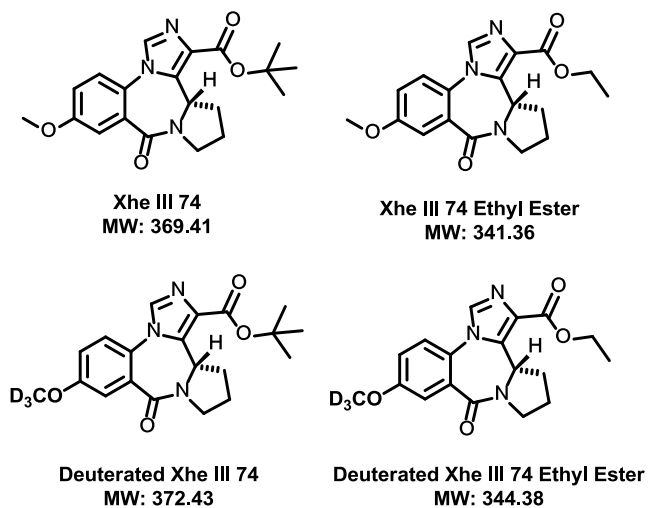


Figure 33. Structures of $\alpha_4\beta_3\gamma_2$ GABA_AR selective ligands .

Also these compounds were investigated with the developed HepG2 cell stability assay and the results are summarized in Figure 34.

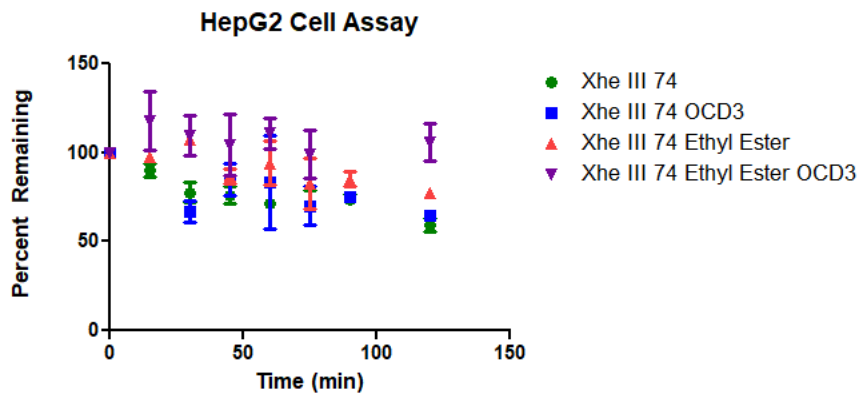


Figure 34. Results for four $\alpha_4\beta_3\gamma_2$ GABA_AR selective ligands in HepG2 cells.

We observed that the four compounds displayed different stabilities in the presence of HepG2 cells. In comparison the percentage left after 60 minutes in the presence of liver microsomes was 59% XHE-III-74, 65% XHE-III-74 OCD₃, 77% XHE-III-74 ethyl ester, and 99% XHE-III-74 ethyl ester OCD₃. The calculated stability parameters are presented in Table 3.

Table 3. Stability parameters for $\alpha_4\beta_3\gamma_2$ GABA_AR selective ligands.

Compound	Half Life, min	R square	Sy.x	Deviation from linearity
Xhe III 74	184.2007	0.8708	0.0627	Not significant
Xhe III 74 OCD ₃	255.3969	0.4782	0.1233	Not significant
Xhe III 74 EE	293.4577	0.7313	0.0619	Not significant
Xhe III 74 EE OCD ₃	2690.7887	0.0287	0.0662	Not significant

Figure 34 showed that little variation in hepatocyte stability between the OCH₃ and OCD₃ analogs for the original Xhe III 74. However, for the Xhe III 74 Ethyl Ester compound, the substitution of the OCH₃ to the OCD₃ did appear to increase the metabolic stability in the cell-based assay based upon this plot. However, upon closer evaluation at the 95% confidence interval, the data can be assessed for a slope that deviates significantly from zero. Due to the larger error bars for the Xhe III 74 OCD₃ compound (shown in blue) this statistical test does show that for both the OCD₃ analogs, the slope does not deviate significantly from zero, whereas the original lead compounds without deuterium do significantly deviate from zero. These preliminary assay results do indicate that the substitution from OCH₃ to OCD₃ does in fact increase the metabolic stability of the compound.

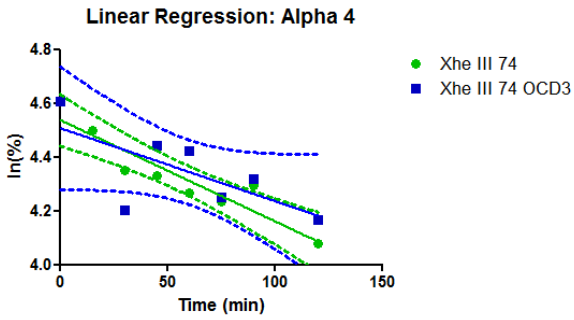


Figure 35. Xhe III 74 and its deuterated analog shown with the 95% confidence interval.

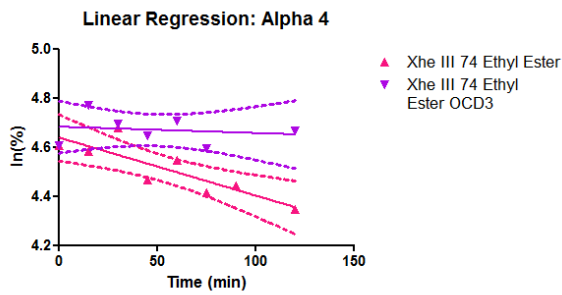


Figure 36. Xhe III 74 Ethyl Ester and its deuterated analog shown with the 95% confidence interval.

The linear regression results for the $\alpha_4\beta_3\gamma_2$ GABA_AR selective ligands presented in Figure 35 and in Figure 36 as shown for the deuterated and non-deuterated version of each compound, with the error bars bracketed for the slope of the linear regression at the 95% confidence interval (shown in dashed lines).

The intrinsic clearance estimated by *in vitro* metabolic assays such as the liver microsome stability assay and the hepatocyte cell-based assay provide useful information regarding both Phase I and Phase II metabolism of drugs in the liver. We have successfully established a cell-based metabolic assay for the assessment of compound stability *in vitro*. The

assay can be carried out with the inexpensive HepG2 cells. In the future, this assay can be adapted with slight modifications to test compounds in fresh or cryopreserved human hepatocytes.

CHAPTER 4. *In vitro* Brain Metabolism Assay

4.1 Introduction

Stereochemistry is an important consideration in drug development. Stereoisomers are compounds with the same molecular formula and bonds, but different three dimensional structures. Stereoisomers are divided into subcategories of enantiomers (mirror-images) and diastereoisomers (non-mirror images).³⁷ It is important to consider the spatial arrangement of the atoms within a drug compound because the three-dimensional orientation of the functional groups must fit into the three-dimensional binding pocket of the target receptor. Therefore, the drug-like properties of a molecule can be greatly impacted by variations in stereochemistry. Approximately 25% of drugs currently on the market are comprised of a mixture of stereoisomers, however the biological activity may be predominantly or wholly induced by one stereoisomer in the mixture. One simple example is ibuprofen, in which the R conformation is inactive but the S isomer displays the therapeutic effect.¹⁻² This drug is sold as a racemic mixture. While some components of a racemic mixture may display no effects, enantiomers can also display different physicochemical properties resulting in adverse effects or toxicity.³⁷ Proteins are composed of amino acids, which are chiral molecules, thus differing stereoisomers may interact differently with a particular protein. The classic example of the dangers of stereoisomerism lies in the story of thalidomide.² This compound was prescribed as an anti-nausea medication to pregnant women and the alleviation of the symptoms of nausea was a result of the R enantiomer of this drug. However, the S enantiomer caused birth defects. For this reason, this drug cannot be sold as a racemic mixture. Furthermore, even if this drug was synthesized and marketed as a single enantiomer, the R enantiomer alone, the body actually

creates a racemic mixture. Thalidomide (Immunorin or Contergan) caused limb deformities in many children in the 1960's, as a result of restricted blood flow to developing limbs.³⁸ Serendipitously, thalidomide is investigated as a potential anti-cancer drug, for types of tumors that require an ample blood supply to grow.^{2,39}

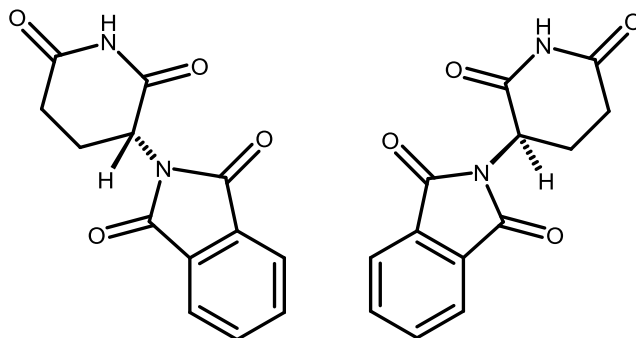


Figure 37. The S and R isomers of Thalidomide, which are effective, and dangerous, respectively.

Herein, we describe the investigation of the S and R enantiomers of chiral imidazobenzodiazepines that bind the GABA_A receptor in the brain. As a pentameric receptor, the GABA_A receptor contains five subunits, typically two α , two β , and a fifth, often γ subunit.¹⁰ This assembly has multiple variations for each of these receptor subunits. GABA_A receptors contain $\alpha 1$, $\alpha 2$, $\alpha 3$ or $\alpha 5$ subunits together with a neighboring $\gamma 2$ subunit, which is where benzodiazepines act as positive allosteric modulators. However, less than 5% of all GABA_A receptors in the brain have $\alpha 5$ subunits however $\alpha 5\beta 3\gamma 2$ GABA_ARs are common in the spinal cord.⁴⁰ Therefore, this receptor has been targeted by the Cook group and other as a therapeutic strategy for neuropathic pain.⁴¹ Through pharmacokinetic studies of a particular compounds of interest, SH-053-2'F-R/S-CH₃ was identified as lead compound and differences were seen *in vivo* with regard to concentrations of its enantiomers in rat brain. To investigate the hypothesis that

the enantiomers have different stability in the brain, an *in vitro* metabolic assay was developed to investigate the differences between the R and S stereoisomers.

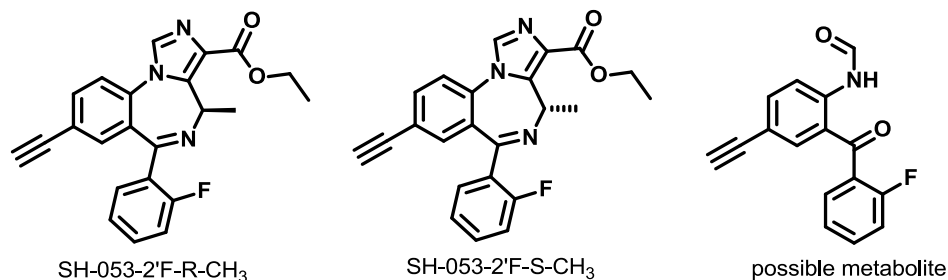


Figure 38. Structures of chiral $\alpha_5\beta_3\gamma_2$ selective GABA_AR ligands and a proposed metabolite of both isomers identified *in vivo*.

We have shown in previous assays such as the liver microsome assay and the hepatocyte assay that the activity of cytochrome P450 enzymes plays a crucial role in Phase I xenobiotic metabolism. Although it is well known that these enzymes are present in large quantities in the liver, recently it has been demonstrated that many of these enzymes are also present in the brain.⁴² Examples of CYP450s that have been identified in both tissues are displayed in Figure 39.

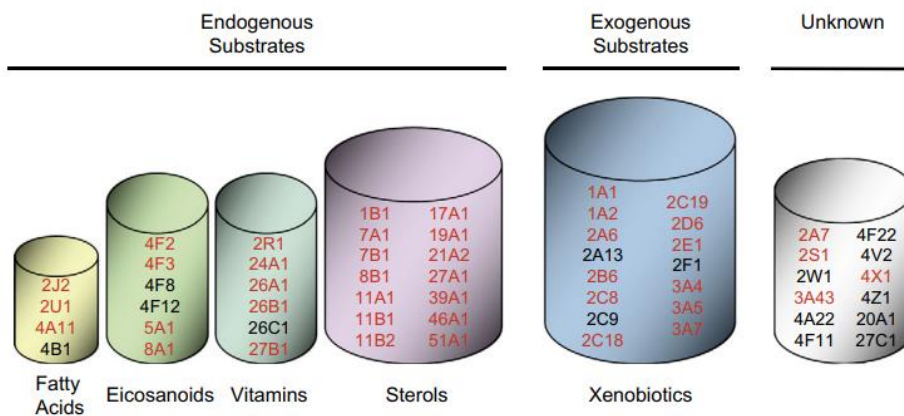


Figure 39. Known cytochrome enzymes and their identified substrates.⁴²

Therefore, the brain metabolism assay aims to gain information regarding drug-metabolizing enzymes in the brain and enable later comparison with the in vivo PK results.

4.2 Materials & Methods

Male Wistar rats (250-350 g.) were housed in pairs and kept on a 12h dark/light cycle (lights on at 7:00 am) with food and water provided *ad libitum*. For testing, a single rat was euthanized (asphyxiated via CO₂ chamber) in accordance with IACUC, and decapitated with a small animal guillotine. The brain was extracted and weighed by difference into a 15 mL conical tube. One equivalent of pre-heated PBS (37°C) was added by mass and the mixture was homogenized with a LabGen T2 homogenizer. Individual centrifuge vials (1.5 mL) were prepared (100 µL PBS, 20 µL of a 100 µM stock solution of test compound, 80 µL brain homogenate) for eight (0, 10, 30, 60, 120, 240, 480, 1440 min) time points and placed in an oscillating heat-block (37°C, 300 rpm). At each time point, the reaction vial was quenched with double the volume of cold acetonitrile (400 µL) containing a 10 µM internal standard (HZ-166) and placed on ice. The vials were vortexed and centrifuged (10,000 rpm) for three minutes and the supernatant was pipetted into a spin filter centrifuge tube (0.22 micron nylon) for filtration. Samples were diluted 20x into Optima LC-MS grade methanol (Fisher Scientific) by pipetting 25 µL of supernatant solution into 475 µL methanol in a glass autosampler vial. Samples were analyzed using a Shimadzu LCMS-8040. Three independent experiments were performed (n = 4 for each independent experiment).

4.3 Results

The graphs shown in Figure 40 were created by the Savic group following a pharmacokinetic study of both the R and S isomers of the SH-053-2'F-R/S-CH₃ compound in Wistar rats.³³ The concentrations found for both isomers in the brain were comparable, however the concentrations seen for the S isomer in plasma were an order of magnitude below that of the R isomer.

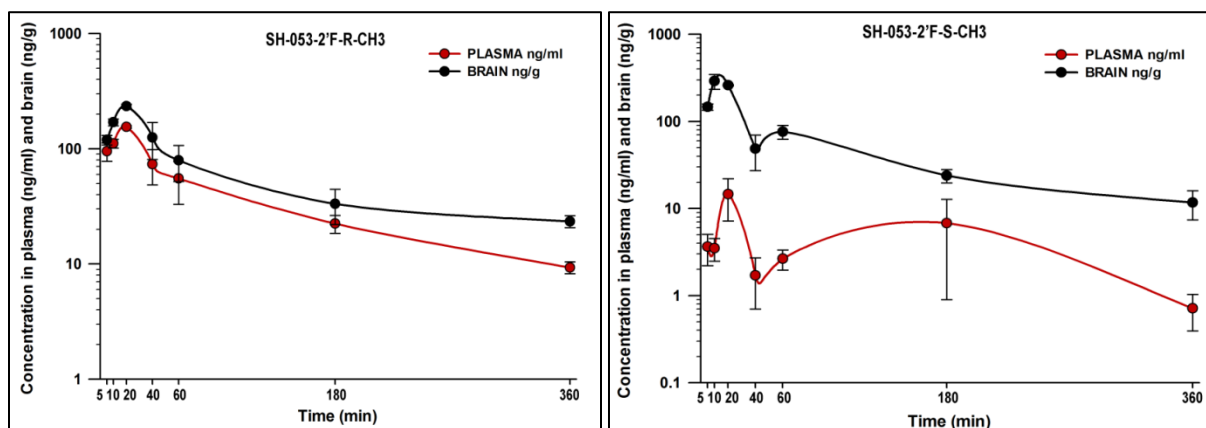


Figure 40. Pharmacokinetic profiles of the R and S isomers of the SH-053-2'F-R/S-CH₃ compound.

The pharmacokinetic profiles displayed above show a discrepancy between the plasma concentrations of SH-053-2'F-S-CH₃ and SH-053-2'F-R-CH₃. One hypothesis is that both SH-053-2'F-R/S-CH₃ undergo active transport into the brain thus even at a low blood concentration for SH-053-2'F-S-CH₃ a high brain concentrations can be reached. The clearance of SH-053-2'F-S-CH₃ is fast, which has been confirmed by human liver microsome stability assays that indicated that the S enantiomer is degraded at a faster rate than the R enantiomer. In addition, comparing the concentrations of both stereoisomers in the brain, we observed a faster clearance of SH-053-2'F-S-CH₃ than SH-053-2'F-R-CH₃ in the brain.

Thus, to investigate if transport or brain metabolism are the underlying processes a brain metabolism assay is carried out. This *ex vivo* assay utilizes fresh brain homogenates and compounds are incubated at 37°C. The compounds are quantified at different time points and the results are summarized in Figure 411.

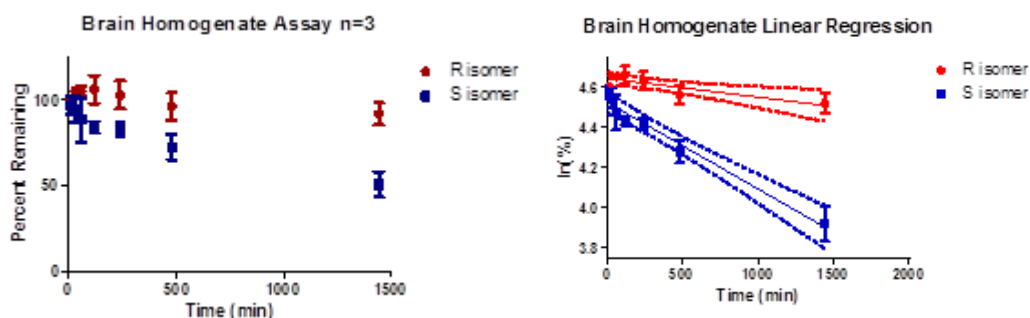


Figure 41. Results of the brain homogenate assay displayed as a percentage remaining as well as the linear regression (and the 95% confidence interval).

SH053-2'F-R-CH₃ compounds were incubated with rat brain homogenate and quantified by LC-MS/MS. The results are presented as a percentage remaining over the course of 24 hours (three independent assays with an N=4 replicates for each assay). The results of this assay are fitted with a linear regression to calculate metabolic half life, as with the microsomal stability and hepatocyte assays. Based on the linear regression the slope was used the calculated the half-life and other pharmacokinetic parameters summarized in Table 44.

Table 4. Estimated metabolic parameters for the R and S isomers in brain tissue homogenates.

Compound	Half Life, min	Internal Clearance, uL/min/mg	R square	Sy.x	Deviation from linearity
SH-053-2'F R CH3	7369.2024	0.0188	0.3426	0.0570	Not significant
SH-053-2'F S CH3	1607.8571	0.0862	0.8419	0.0931	Not significant

The results of the brain stability assay show that the *S*-isomer (50% remaining after 24 hours) was degraded at a faster rate than the *R*-isomer (84%). The half-life of SH-053-2'*F*-*R*-CH₃ in the brain is 4.5 times longer than SH-053-2'*F*-*S*-CH₃.

4.4 Discussion

In addition to the pharmacokinetic data presented above, the Savic group identified a potential metabolite of mass 267.25 g/mol at a ratio of 10:1 when derived from the *S* isomer (ratio of metabolite:parent), whereas the *R* isomer yielded the same metabolite at a ratio of 1:10. Although the data regarding this proposed metabolite is consistent with the idea that the *S* isomer is more readily metabolized than is the *R* isomer, this metabolite was not seen in the brain homogenates assay, and therefore cannot be quantified at this time.

These results show a clear trend in the difference between *R* and *S* isomers when exposed to metabolic enzymes in the brain. The *P* value for the comparison of these slopes is $P < 0.0001$, meaning that if the overall slopes were identical, there would be less than a 0.01% chance of randomly choosing data points with slopes as different as those presented above. Therefore we can conclude that the differences seen between the slopes in this assay are extremely significant. This brain metabolism assay is a relatively low-cost method with rapid analysis times to view the degradation of drug compounds in fresh brain homogenates. If this assay is to be continued in the future, one could investigate the viability of freezing brain homogenates at -80°C for a quicker sample preparation setup, or isolating the drug metabolizing enzymes within sub-cellular fractions as is done for the liver microsome stability

assay. These future directions have not yet been tested, leaving room for additional *in vitro* development with regard to brain metabolism of drug compounds.

CHAPTER 5. Quantification of GABA with a novel HILIC based method

5.1 Introduction

Ion channels are transmembrane proteins that contain a central pore to establish and control voltage potentials across cell membranes. They do this by controlling the active flow of ions between the intracellular and extracellular environments. This family of proteins is involved in a diverse array of physiological functions, therefore ion channels are popular therapeutic targets in drug discovery today.⁴³ The lead compounds for the drug development projects outlined in this work are modulators of the GABA_A receptor. This receptor is a ligand-gated ion channel, where gamma amino butyric acid is the endogenous ligand, and binding of this ligand controls the flow of chloride ions through the channel. Typically, the flow of chloride ions through this receptor is governed by GABA. The binding of a GABA_A receptor agonist (such as a drug compound) to the receptor will modify the flow of chloride ions. This flow of ions can be measured to test compound effects on the receptor, using ion channel screening assays (e.g. ligand binding, patch clamp, fluorescence and luminescence based assays, and electrophysiology). These assays are conducted *in vitro* thus it is paramount to understand the circumstances and conditions in the organism itself to recapitulate similar conditions *in vitro*. In the case of GABA, it has been well documented that T cells in addition to neurons produce endogenous GABA *in vivo* and in culture.⁴⁴ Important for the biosynthesis of GABA is the expression of glutamic acid decarboxylase, which catalyzes the decarboxylation of glutamate to GABA, therefore producing the endogenous ligand. A cartoon of the existing components within a T cell is shown in Figure 42.

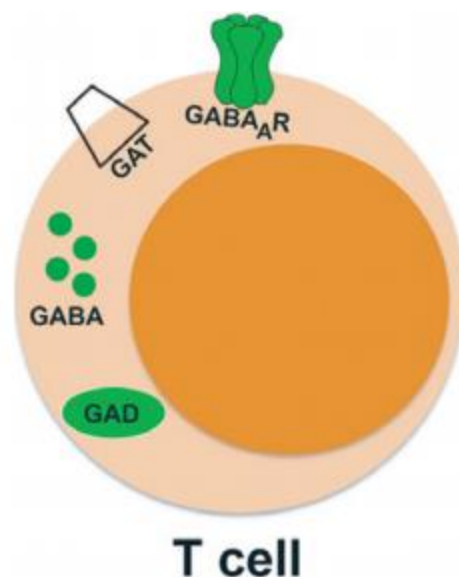


Figure 42. Cartoon image of the coexisting GABA, GABA_A receptor, glutamic acid decarboxylase (GAD), and the GABA transporter 1 (GAT).

Interleukin 2 (IL-2) is a protein that is known to play an important role in inflammation.⁴⁵ The lead compounds investigated in this work are seeking to treat diseases that result from inflammation, for example airway inflammation is a main symptom of asthma. Neuropathic pain is also closely tied to inflammation⁴⁶ and is being investigated by MIDD researchers as a therapeutic target for benzodiazepines. It is of interest to know if a drug molecule can decrease inflammation therefore our research group employs an IL-2 ELISA assay to assess the protein expression in cell culture. Similarly, a calcium detection assay is employed to look at the aforementioned ion transport (as the GABA_A receptor is an ion channel). The IL-2 ELISA assay is performed using a leukemia T cell line (Jurkat cells) and like the calcium assay GABA in addition to positive GABA_AR modulators has an influence on the outcome of the assay. For this reason a method was developed to quantify the amount of GABA present in cell culture media. The cell culture media consists of among others of salts, amino acids, sugars and most importantly fetal

bovine serum. An efficient LC-MS method was developed to inject a sample with minimal front end preparation. However, GABA is a very small analyte with a limited hydrophobic character, which presents analytical challenges in the aforementioned LC-MS methods, which employ reversed phase separation by HPLC.

The assays mentioned previously produced samples that could be analyzed with conventional reversed-phase material as stationary phases (for example, C18). These stationary phases contain hydrophobic groups, thus the analytes must display adequate hydrophobicity in order to interact with the stationary phase. For benzodiazepine-like GABA_A receptor modulators of interest in this work, the majority of the compounds are of sufficient hydrophobic for this separation technique (as is typical for most drug compounds). However, analytes that are very polar are not compatible with conventional reversed-phase analyses because they cannot be retained on a reversed-phase analytical column. GABA for instance is not retained on a reversed phase column, making quantitation by LC-MS a challenge. One approach employed to quantify amino acids and other polar analytes include a front-end derivatization technique prior to LC-MS analysis. However, these strategies complicate the sample preparation, add extra cost for chemicals needed to create a derivative, and can result in non-specific derivatization of other compounds within the complex biological matrix to be analyzed. Therefore, when separation of more polar analytes is required, a different separation strategy called hydrophilic interaction liquid chromatography, or HILIC, can be employed. The advantage of this approach is the ability to maintain a simple sample preparation and direct sample analysis. Herein, we show that GABA is retained and quantifiable by HILIC chromatography.

For HILIC chromatography, the silica stationary phase particles are coated with a functional group designed to draw and retain water on the surface of the silica. One such example, which is employed in these analyses, is cross-linked diol groups for polar selectivity. This water layer facilitates the transfer of polar compounds from the mobile phase to the stationary phase, increasing the retention factor, whereas on a reversed phase column polar analytes would elute around the void time, making separations difficult. A representation of the stationary phase coated with an adsorbed water layer is shown in Figure 43. The water layer shifts the retention mechanism from being primarily hydrophobic interactions (as in a C18 column) or π - π interactions (as in a biphenyl column) to partitioning, rather, between the adsorbed water layer and the analyte in mobile phase. The mobile phase for HILIC separations is typically very similar to what is seen in reversed phase separations, largely organic with a small percentage of water (3-15%) to hydrate the stationary phase and adequately dissolve the polar analytes.

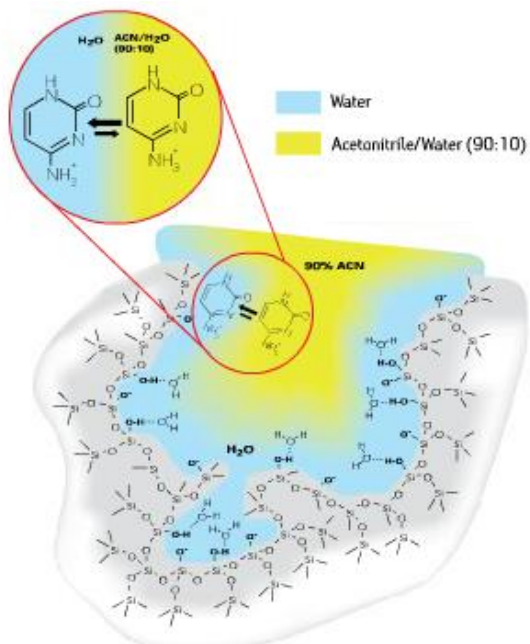


Figure 43. Cartoon representation of the polar stationary phase, the adsorbed water layer, and the partitioning mechanism of retention seen in HILIC separations (Image: Waters).

5.2 Materials & Methods

Jurkat cells were maintained in suspension in RPMI 1640 medium with L-glutamine (Thermo Fisher Scientific Inc., Rockford, IL) supplemented with 10% (v/v) fetal bovine serum. The cells were maintained in 5% CO₂, 95% humidified air at 37 °C at an approximate density of 10⁶ cells/mL. Typically for the calcium assay, the Fluo-4 NW calcium assay kit (Life Technologies, Rockford, IL) is used for intracellular calcium measurements. Jurkat cells are collected, pelleted, and resuspended in Fluo-4 NW assay buffer at a final concentration of 5 × 10⁶ cells/mL and dispensed into a 384 well plate. The plate is then analyzed as described previously. One microliter of test compound in DMSO or GABA in water is added to each well and incubated, to illustrate a dose response for either the compound, the endogenous ligand, or both.

Separation was performed on a Phenomenex Luna HILIC column (50 x 2.1 mm, 3 μ m). The mobile phase was isocratic at 85% acetonitrile and 15% water. The mobile phase contained 5 mM ammonium formate buffer, to control pH and aid in the ionization of analytes. Uracil was employed as an internal standard for the method because although it is not retained on a reversed phase column, and is generally used in RPLC to calculate void time. However, uracil is retained on a HILIC column.

5.3 Results

Previous assay results had illustrated an anomaly in the typical dose response curves of positive allosteric GABA_AR modulators, in that GABA did not need to be added to the assay to activate the receptor. Ideally, this is a parameter of the assay which needs to be controlled, in order to generate an accurate dose response curve for comparison with other drug compounds of interest. Figure 44 shows the results of this assay with this anomaly, showing extremely similar dose response curves for the compound with or without the presence of GABA.

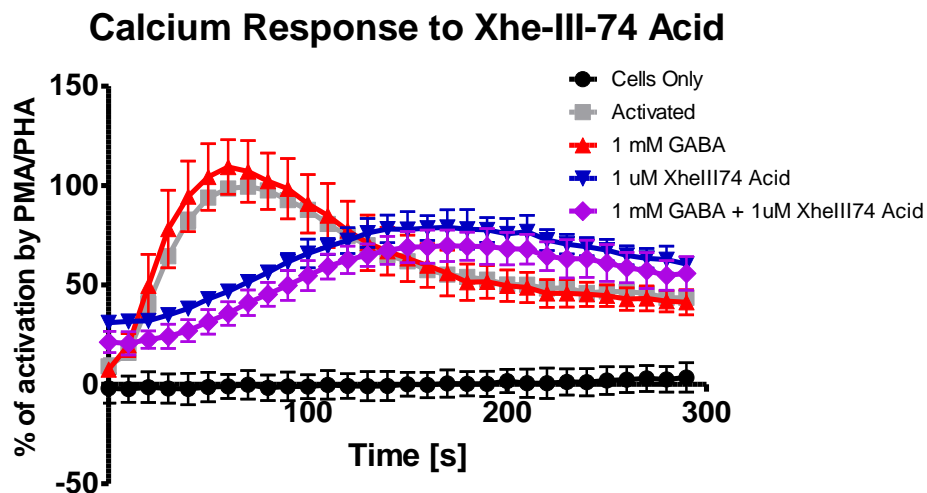


Figure 44. Calcium assay response of the lead asthma compound Xhe-III-74 acid in the presence of Jurkat cells illustrating the similarity of results with or without the addition of [1 mM] GABA. Data: Amanda Nieman.

The assay shows a response difference between GABA and GABA dosed with compound, thus Xhe-III-74 acid is modulating $[Ca]_i$. However, the addition of additional GABA did not change the response significantly, which can only be explained by endogenous GABA already present. Similar results were observed quantifying IL-2 protein by ELISA assay (Figure 455).

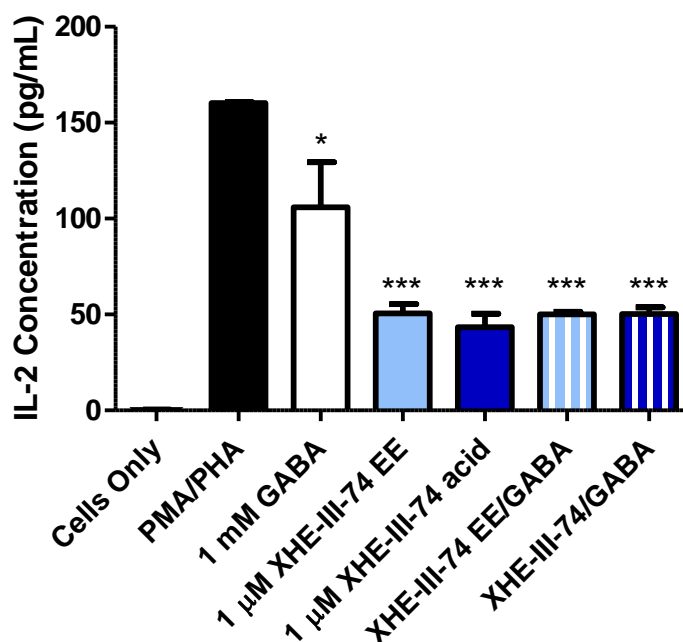


Figure 45. Results from the IL-2 ELISA assay from Jurkat cell extract showed a reduction of IL-2 in the presence of GABA and in XHE-III-74 acid and XHE-III-74 EE. However, no significant differences between the both compounds in the presence and absence of GABA were identified. (Data: Gloria Forkuo.)

Thus, the amount of GABA in Jurkat cell media was quantified by HILIC-MS/MS. The cell density was 3×10^5 cells/ml and the cell media analyzed directly with a triple quadrupole LC-MS/MS instrument. Standards of GABA were prepared in triplicate and diluted serially to generate the calibration curve.

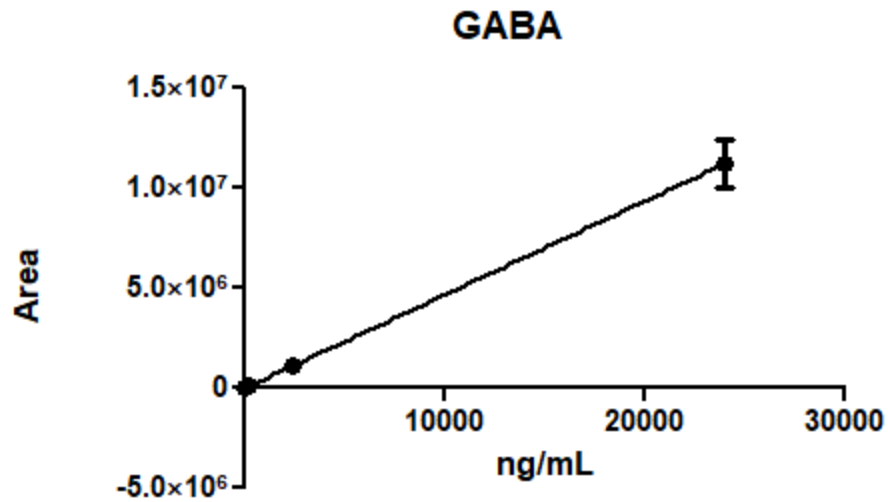


Figure 46. Calibration curve for GABA determined by HILIC/MSMS. R square = 0.9902.

The average of three aliquots of Jurkat media was found to have 87.385 ppb GABA (or [0.847 μ M]), with a relative standard deviation of 6.419%. The limit of quantification for this method was defined determined to be 24 ppb, which is consistent with other recently published articles quantifying the amount of GABA by HILIC methods.⁴⁷ Although this method was a brief component within this presented work, it illustrates the importance of multidisciplinary knowledge within the drug discovery group.

CHAPTER 6. Pharmacokinetic Studies

6.1 Introduction

Pharmacokinetic (PK) assays are used in drug development to study the absorption, distribution, and elimination of a lead compound *in vivo*. This is done by quantifying the amount of drug in biological samples at sequential time points, and using that data to generate a pharmacokinetic curve. A plot of the general shape of a pharmacokinetic curve is shown in Figure 477.¹ In this generic representation, samples would be taken at each arbitrary time unit and quantified using an analytical method, most commonly LC-MS/MS.

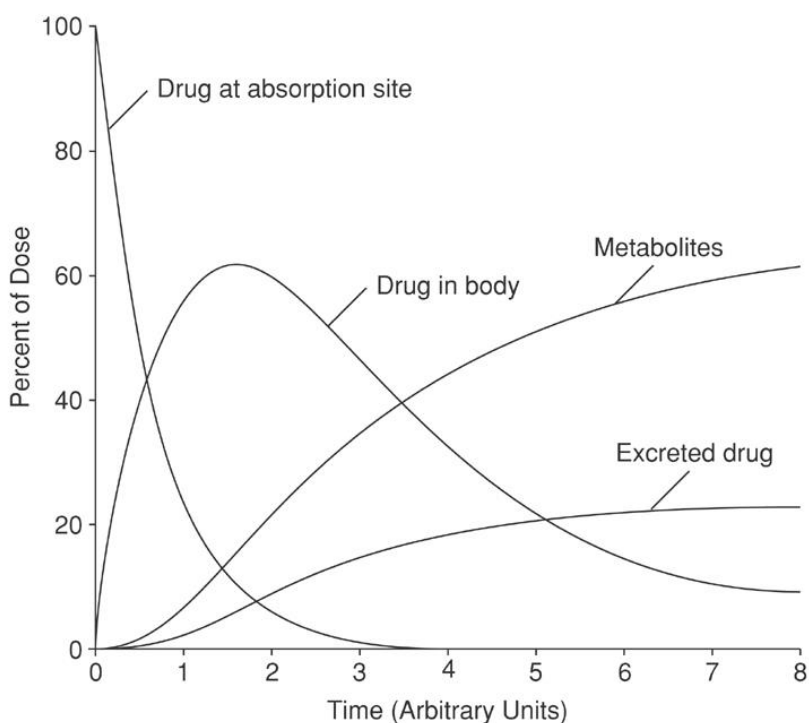


Figure 47. General representation of a pharmacokinetic curve.

Although PK data is traditionally generated from blood draws, the above curves can also be generated from quantified amounts of compounds extracted from target organs. For example, imidazobenzodiazepines in these studies are of interest to treat asthma, therefore it was

important to quantify the amount of compound in the lung, as the lung is the target organ.⁴⁸ In addition, these compounds target GABA_A receptors which are expressed in the brain, thus quantification of compound in brain tissue was important to estimate adverse side effects by the central nervous system. There are many known benzodiazepine compounds currently on the market (such as the 1,4-benzodiazepine drugs alprazolam, diazepam, and many others) for which the brain is the target organ. The primary difference between these known drugs and the lead compounds presented in this work (which contain the same core benzodiazepine structure) is the presence of key functional groups, attached to the core benzodiazepine scaffold. The functional groups determine whether or not the compound can cross the blood brain barrier and subsequently bind to GABA_A receptors in the brain. In an effort to avoid any cognitive side effects for the asthma compounds, low amounts of compound are desired in the brain. Potential cognitive side effects are monitored using separate *in vivo* biological studies, both here at UWM as well as with collaborators at Columbia University. One such assay, for example, is the rotarod assay, in which mice are dosed with lead compound and tasked to run on a cylindrical rod. If the compound acts as a sedative, the mice will fall off of the rod. To avoid cognitive side effects which may have a negative impact, like sedation, it is important to quantify the amount of compound in the brain.

Benzodiazepines are known to be well absorbed by the GI tract after oral administration. They are highly protein bound and widely distributed in the body, typically accumulating in lipid-rich areas (such as the CNS and adipose tissue). The more lipophilic the compound, the higher the absorption rate and therefore the fastest the onset of clinical effects. There are several parameters of merit that are of importance in pharmacokinetic studies, including the

area under the pharmacokinetic curve (AUC), the time at which maximum compound is present in the blood or target organ (Tmax), the maximum concentration reached at that time (Cmax), and the rates at which the compound is both absorbed and eliminated. Similar to the microsome stability and brain homogenate assays a first-order elimination is assumed that enables the calculation of half-life based on the quantified amounts of drug in various tissue types. The half-life is the time interval required for the concentration of the drug to decrease by a factor of 0.5. As a general rule, a drug is said to be completely eliminated from the body after a period of five half-lives.² The half-life expression is showed in Equation 10.

$$t_{1/2} = \frac{0.693}{k_{el}}$$

Equation 10. The natural log of 2 divided by the elimination rate yields the elimination half-life.

With regard to the concentration of compound in the blood, the compound can be bound to protein and therefore carried to the target organ, or it can be on the road to excretion. Therefore we are interested in the concentration as it relates to the protein bound drug. The rate of elimination as a function of time can be used to express the protein-bound concentration in a given sample as it relates to the initial protein-bound drug concentration, C_p^0 as shown in Equation 11. The non-protein bound fraction of the drug will not reach the target organ and generally will undergo excretion.

$$C_p = C_p^0 e^{-k_{el}t}$$

Equation 11.

From these data, the rate of elimination can be shown as a first-order function of C_p . Clearance is determined from a concentration vs. time plot, which allows for the direct calculation of the area under the curve (AUC) with Equation 13.

$$\text{rate of elimination} = \frac{dC_p}{dt} = -k_{el}C_p \quad \text{Equation 12.}$$

$$AUC = \frac{C_p^0}{k_{el}} \quad \text{Equation 13.}$$

From the AUC, the clearance can be calculated from the original dose and the area under the curve, as shown in Equation 14.

$$CL = \frac{D_o}{AUC} \quad \text{Equation 14.}$$

In addition to clearance, the volume of distribution is used to describe how a drug disperses throughout the body. An assessment of the total volume in which a drug will be distributed is a property of that drug, and is directly related to the elimination rate, the half-life, and the clearance for the drug.

$$k_{el} = \frac{CL}{V_d} = \frac{0.693}{t_{1/2}} \quad \text{Equation 15.}$$

For the studies in this work, single-dose pharmacokinetic curves are generated by quantifying the amount of compound present in samples by LC-MS/MS. A generic representation of this curve is shown in Figure 48.

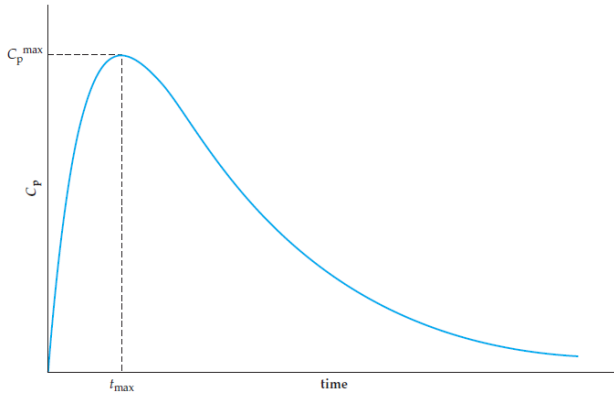


Figure 48. General image of a pharmacokinetic curve resulting from oral or i.p. dosing schedule.

However, orally delivered drugs must be absorbed from the digestive system first before they can enter the bloodstream (which is where C_p is determined).³⁷ Therefore, from these curves we show both an absorption phase and an elimination phase. These relationships can also be described by Equation 17.

$$C_p = \frac{FD_o}{V_d} \frac{k_{ab}}{(k_{ab} - k_{el})} (e^{-k_{el}t} - e^{-k_{ab}t})$$

Equation 17.

The variable F in the above equation is for bioavailability, which for an oral drug, depends on the resistance to first pass metabolism in the liver. The variable E_H in Equation 18 refers to the hepatic extraction, therefore drugs with a high E_H value have poor bioavailability.

$$F_{\text{oral}} = 1 - E_{\text{H}}$$

Equation 18.

In order to effectively plot all data points and calculate the parameters of particular interest, we have implemented a software program called PK Solutions from Summit Research Services.

The analysis of bioanalytical samples presents challenges with regard to the elimination of matrix effects and species that interfere with analysis. These assays require highly sensitive analytical methods capable of achieving very low limits of detection for quantification. Obtaining low LOD and LOQ values can be achieved by increasing analyte signal, decreasing background noise, or both. One of the challenges in pharmacokinetics studies can result from the fact that complex biological matrices can create ion suppression issues in the mass spectrometer, due to many endogenous compounds that co-elute with analytes of interest. This is an inherently problematic shortcoming in LC-MS/MS analysis. Therefore, one of the method development goals is to maximize the amount of analyte available for analysis, as well as clean up the sample as much as possible to minimize matrix effects. PK studies require efficient chromatographic and sample preparation strategies, not only for the reasons listed above but also to facilitate the analysis of a large number of samples. The most commonly used sample preparation techniques are protein precipitation (with an organic solvent, essentially liquid-liquid extraction, or LLE) and solid phase extraction (SPE). Typically, extraction solvents for LLE are non-polar organic solvents that are different from the starting mobile phase of an LC method. Unfortunately, this disparity in polarity can lead to band broadening during

chromatographic separations. It can also create unpredicted changes in retention times. The most common way to remedy this issue in LLE sample preparation techniques is by evaporation of the extraction solvent followed by reconstitution in mobile phase. This reconstitution step allows for the flexibility to extract with any solvent desired rather than exclusively LC-MS friendly solvents.

The other sample preparation approach, SPE, employs trapping the analytes in a hydrophobic sorbent (such as a C18) on a separate “trap” column. The samples are injected with an aqueous mobile phase to ensure that all of the hydrophobic analytes partition into the hydrophobic trap. Provided that the analytes are hydrophobic as well (as is the case with the imidazobenzodiazepines in these studies) they will partition preferentially into the trap column. Meanwhile, any water soluble proteins, peptides, salts, and contaminants will be flushed to waste. The analytes are then eluted from the SPE trap column with percentage of organic LC solvents and carried to the traditional analytical column. This process yields significantly cleaner chromatography given the absence of water-soluble interferences, which are endogenous to complex biological matrices. Herein, methods for both sample preparation strategies are presented, and results for several GABA_A receptor modulators are presented.

6.2 Experimental Procedure

5-10 weeks old female Swiss Webster mice (Charles River Laboratory, WIL, MA) were used for the experiments. Mice were housed under pathogen-free conditions, under standard conditions of humidity, temperature and a controlled 12 hour light and dark cycle and had free access to food and water. All animal experiments conformed to the rules and regulations of the

University of Wisconsin, Milwaukee Institutional Animal Care and Use Committee (IACUC). Female Swiss Webster Mice were dosed by interperoniteal (i.p.) injection with vehicle or test compound formulated in DMSO/ propylene glycol/ PBS, 10:40:50, (v/v/v) and injected at a dose of 5 mg/kg. At 3, 10, 15, 20, 40 60, 90 and 120 minutes groups of mice were euthanized and blood (collected into heparinized tubes, 50 μ L of 1 mg/mL heparin), lungs, and brain were harvested and the sample were stored in liquid nitrogen until analysis.

Blood samples were thawed on wet ice, vortexed for 10 seconds, and a 100 μ L aliquot was taken and added to 400 μ L cold acetonitrile containing [20 nM] internal standard (HZ-166), which was of similar structure and had similar chemical properties. Samples were vortexed for 30 seconds and centrifuged at 13,000 RPM for 3 minutes. The supernatant layer was then transferred to clean tubes and evaporated overnight. The residue was reconstituted with 300 μ L of mobile phase and spin-filtered through 0.22 μ m nylon centrifugal filter units (Costar). After reconstitution, verapamil was added as a second internal standard to all samples as well as calibration standards. 5 μ L of the sample was injected to the LC-MS/MS 8040.

Brain and lung tissue samples were stored in liquid nitrogen prior to homogenization and extraction. Whole organs were thawed over ice, weighed, and homogenized directly into 500 μ L ACN containing an internal standard using either a Benchmark Scientific BeadBug Homogenizer with three 3.2mm stainless steel beads, or a handheld LabGen T2 homogenizer. Samples were homogenized for 30 seconds, centrifuged for 3 minutes at 13,000 RPM. This process was repeated for a total of three extractions. The supernatants were combined and prepared in the same manner as the blood samples for LC-MS/MS analysis.

High performance liquid chromatography (HPLC) was performed with Shimadzu Nexera X2 LC30AD series pumps (Shimadzu, Kyoto, Japan) that include a 20A5R degassing unit, SIL 30AC autosampler and a 20A column oven. Analytes were separated by a Restek Ultra Biphenyl II column (2.1 mm × 50 mm, 5 μm particle size, Restek, California, US) under gradient elution at a flow rate of 0.6 mL/min. The mobile phase consisted of acetonitrile for the organic 'B' solvent and water for the aqueous 'A' solvent (both containing 0.1% formic acid). Time program: 10% B → 99% B (3 min), hold at 99% B (3.75 min), return to 10% B (4 min), hold (4.5 min). Column Temperature: 50°C.

Analytes were monitored under positive mode by Shimadzu 8040 triple quadrupole mass analyzer (Shimadzu, Kyoto, Japan) electrospray (ESI) and atmospheric pressure ionization (APCI) run in dual (DUIS) mode. The fragmentation transitions are monitored in multiple reaction monitoring (MRM) mode. Ion transition pairs for all analytes and collision energies are listed in Appendix A. Collision energy is optimized for each transition to obtain optimal sensitivity. The mass spectrometer was operated with the heat block temperature of 400°C, drying gas flow of 15 L/min, desolvation line temperature of 250°C, nebulizing gas flow of 1.5 L/min, and both needle and interface voltages of 4.5 kV. The response acquisition was performed using LabSolutions software.

HZ-166 was chosen as an internal standard for the extraction method because it has similar chemical structure than the analyte and was therefore used to account for sample dilution, evaporation, and matrix effects. Verapamil was used as a second standard to monitor instrumental variations, both intra- and inter-batch. Stock solutions of all analytes were

prepared at concentration of 2 mg/mL separately in ACN and stored in a -20°C freezer, with the exception of carboxylic acid compounds, which were prepared in 80:20 ACN:water due to a lack of solubility in pure organic solvent. Intermediate working solutions of each were prepared by serial dilution with mobile phase (80:20, ACN:water with 0.1% formic acid). Calibration curve solutions were prepared at concentrations of 1, 5, 10, 15, 25, 50, 75, 100, and 150 nM on the same day as the analysis was performed.

The intra-run/within-run validation was performed for concentrations of 10, 25 and 75 nM with three replicates for each concentration. For separate validations, separate standard curves were newly prepared. The standard curves were fit by a linear regression and the validation samples were calculated back by the calibration curve of that day. The mean and the coefficient of variance (CV) were calculated accordingly. Accuracy was calculated by comparing calculated concentrations to corresponding nominal concentrations.

Quantified concentrations were then analyzed by a separate software program to calculate pharmacokinetic parameter of merit. These parameters were calculated with PK solutions software 2.0 and fitted to the following equation: $c = A \cdot e^{-at} + B \cdot e^{-bt} + C \cdot e^{-ct}$. Due to the rapid absorption, two phases $C = A \cdot e^{-at} + B \cdot e^{-bt}$ were sufficient to describe the pharmacokinetic curve: distribution/absorption phase and elimination phase.

In an effort to increase throughput and decrease sample handling time, blood samples were analyzed in parallel using an on-line solid phase extraction setup. Whole blood samples were diluted 4x into acetonitrile and filtered with push filter vials (Thompson Instrument Company, Oceanside CA) and placed directly into the autosampler for analysis by LC-MS/MS.

Analytes were loaded onto a 'trap' column (Strata-X column, Phenomenex, Torrence CA) with water at a flow rate of 0.1 mL/min. This is done using a third pump that is separate from the two traditional binary HPLC pumps. The instrument is plumbed using two valves to change the direction of the flow, which enables the binary pumps to elute the analytes from the trap column to the analytical column (as shown in Figure 49). Polar compounds from the blood samples such as small proteins or peptides will not be retained on the trap, and therefore will stay in the water phase during the loading process. The HPLC mobile phase begins the gradient method described above after the analytes have been given 3 minutes to load onto the trap column, and then conventional reversed phase LC-MS/MS analysis occurs as described above. Although the on-line SPE method requires additional analysis time on the instrument, it allows for a great decrease in sample handling time, as there is no need for manual protein precipitation with acetonitrile followed by evaporation and reconstitution in mobile phase.

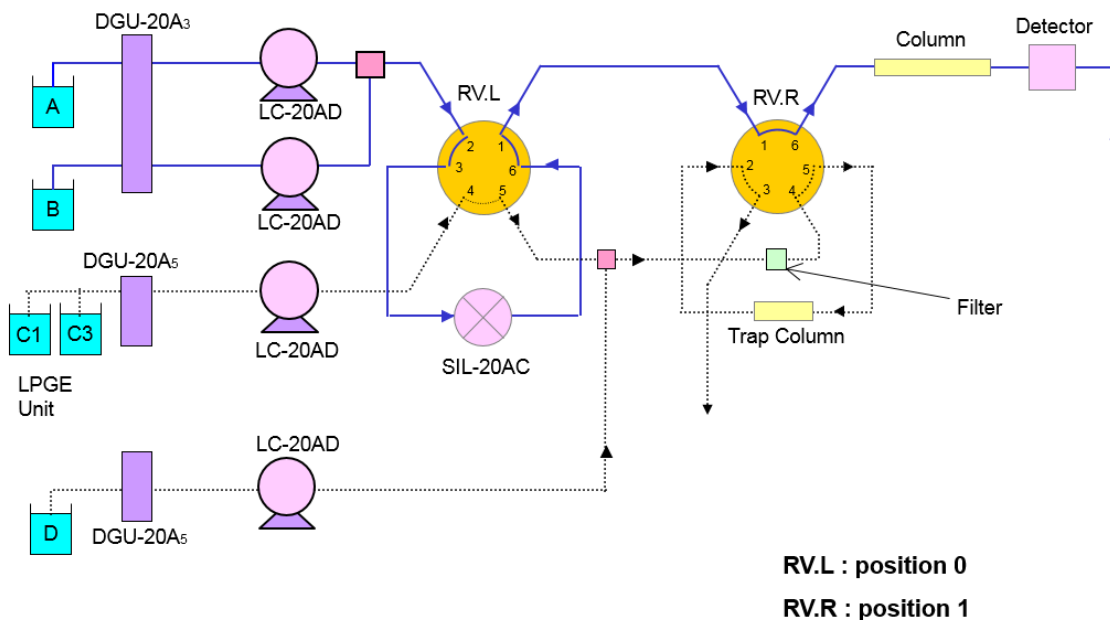


Figure 49. Schematic of the on-line solid phase extraction and HPLC system, featuring four pumps, three degassing units, two rotation valves, and an autosampler. Pumps A and B are typical gradient pumps for HPLC, pump C is an HPLC pump for loading the trap column, and pump D is an extra pump for flushing lines to waste. The directionality pictured above illustrates the valves in load position. This directionality is reversed to send the eluate from the trap column to the analytical column.

6.3 Results

The initial development for the homogenization and extraction methods were applied for the extraction of analyte from biological samples sent from the Emala group at Columbia University. The initial lead compound, Xhe-III-74, was dosed via nebulized treatment to twelve C57/BL6 mice using a 12.5 mM solution of lead compound with 12.5 mM diazepam in 50:50 ethanol:water. This initial distribution study aimed to identify whether or not the lead compound was seen in various tissue types: lung, liver, brain, and also blood plasma. Before attempting a full pharmacokinetic assessment, a method was needed to quantify these compounds in various biological samples.

Samples were weighed by difference into a 50 mL plastic conical tube. The tissue samples were homogenized with twice the amount of water. The homogenizer barrel was rinsed with two 650 μ L portions of water, and the rinses were added to the mixture. The total solution was extracted four times with 6 mL of diethyl ether (this volume was chosen because it was approximately double the volume of the homogenate mixture). The ether layers were combined and evaporated to dryness in a round bottom flask. The analyte was reconstituted in 5 mL methanol and sonicated to ensure all compound was dissolved. 1 mL of the analyte solution in methanol was spiked with HZ-166 as an internal standard at [20 μ g/mL] and quantified on the triple quadrupole LC-MS 8040. Samples were ionized in DUIS mode, with 1.5 L/min nebulizing gas, 250° C desolvation line temperature, 400° C heat block. Drying gas flow was 15 L/min. Analysis was completed with a method run time of 4.5 minutes with a methanol/water gradient containing 0.1% formic acid in the mobile phase. Gradient parameters: 10% B to 99% B (3 min), hold at 99% B (3.75 min), return to 10% (4 min), hold for 30 seconds; flow rate of 0.6 mL/min. Column was a Restek Ultra biphenyl column, 3 μ m, 100 x 2.1 mm (with a 10 x 2.1 mm guard column). Retention times seen in this method were 2.8 minutes for HZ-166, 3.1 minutes for Xhe-III-74, and 2.9 minutes for Diazepam. Results for this quantification are seen below in Figure 500.

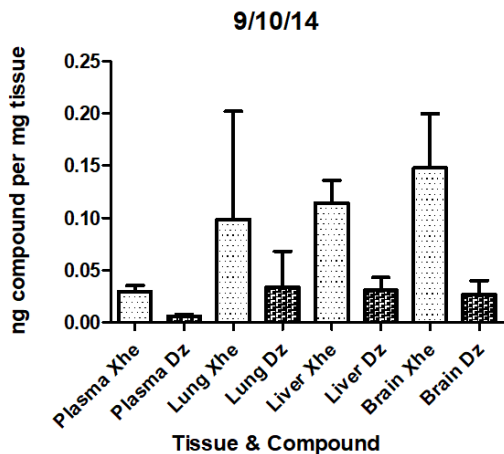


Figure 50. Results of initial compound extraction study.

Although the standard deviation bars for this experiment were much higher than desired, the main conclusion that can be drawn from this distribution study is that Xhe-III-74 is better absorbed than diazepam, especially in the brain. This is interesting because diazepam is known to cross the BBB and act upon GABA_A receptors in the brain (the antidepressant Valium). However, it is also well known that diazepam is actually a pro-drug and is metabolized to nordiazepam, an active metabolite that is also able to pass the BBB. This metabolism is shown in Figure 511.

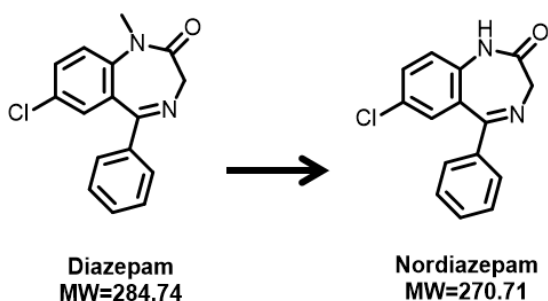


Figure 51. Diazepam and its active metabolite, nordiazepam.

Because the triple quad detects compounds by mass it was necessary to develop an additional LC-MS/MS method to detect nordiazepam. Thus, the concentrations of nordiazepam were quantified and combined with the concentrations for diazepam to create Figure 52.

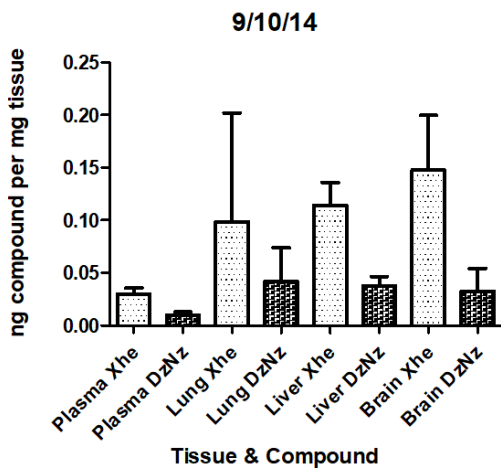


Figure 52. Modified graph including the quantification of diazepam and nordiazepam (denoted DzNz for both compounds together).

The comparison between Figure 50 and Figure 52 showed a small increase of the identified amounts of diazepam and nordiazepam. However, the distribution of XHE-III-74 is still superior to that that of diazepam.

Although this method was very thorough and was able to yield over 90% recovery via liquid-liquid extraction, the volume of organic solvent consumed was considerable. In addition to the cost of the solvent, this procedure must be performed in a fume hood due to the fumes of diethyl ether. Therefore, this method was not appropriate for high-throughput quantification for a large number of samples.

In an effort to miniaturize this method, tissue samples were transferred to flat bottom 2 mL tubes as opposed to 50 mL conical tubes. The tissue samples were then homogenized directly with organic solvent, as opposed to being homogenized in water and then extracted with organic solvent. This in essence creates a form of solid-liquid extraction, as the solid organ is homogenized with the liquid organic solvent. An internal standard of similar structure was spiked into the organic solvent prior to homogenization (e.g. HZ-166 in acetonitrile). These procedural changes allow for a significant decrease in solvent usage as well as a decrease in use of consumable materials (50 mL plastic tubes). The transfer of these samples from large conical tubes to smaller Eppendorf tubes also allows for the use of multichannel pipettes, which is helpful when preparing a large number of samples, to dispense the homogenization solvent with internal standard. It is also noteworthy that the large surface area of the 50 mL conical tube creates room for transfer error, as there is more solvent being transferred which requires multiple aspirations with a pipette.

The first *in vivo* study completed with the miniaturized procedure was Xhe-III-74 Ethyl Ester. The compound was dosed by IP injection as described above. Xhe-III-74 Ethyl Ester was quantified in brain, lung, and blood samples, as shown in Figure 533.

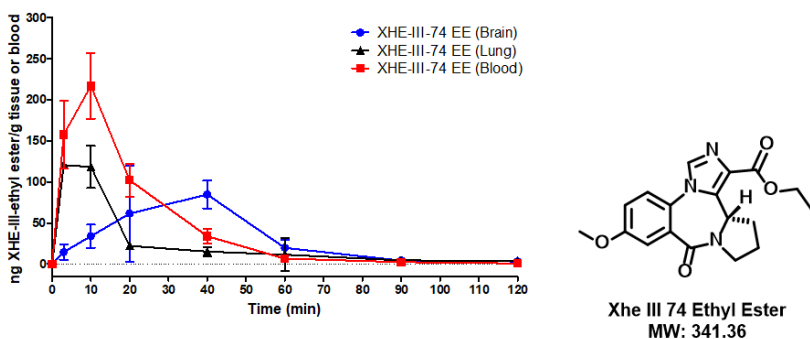


Figure 53. Pharmacokinetic analysis of Xhe-III-74 Ethyl Ester.

Table 5. Pharmacokinetic parameters of interest for the PK study of the Xhe-III-74 Ethyl Ester.

Figure of Merit	Blood	Lung	Brain
C_{max} (ng/ml)	216.9	120.7	84.8
T_{max} (min)	10	3	40
AUC (ng*min/ml)	5737.0	3358.0	4516.0
$T_{1/2,E}$ (min)	16.3	17.6	22.9
$T_{1/2,D}$ (min)	26.6	2.2	36.7

Although Xhe-III-74 Ethyl Ester is rapidly absorbed and distributed, the concentrations seen in the brain are higher than desired for an asthma lead compound. Because hydrolyzed products are commonly seen in first pass metabolism, a carboxylic acid product was hypothesized to be created *in vivo* for this compound, as seen in Figure 544. The original samples that were dosed with the Xhe-III-74 Ethyl Ester compound were then re-quantified in search of the acid analog.

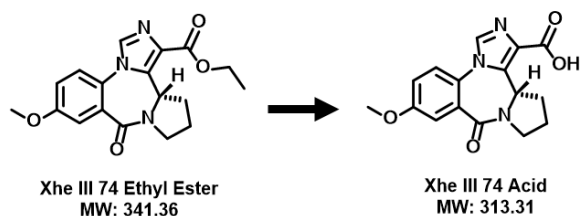


Figure 54. Conversion of Xhe-III-74 Ethyl Ester to the Xhe-III-74 Acid by hydrolysis *in vivo*.

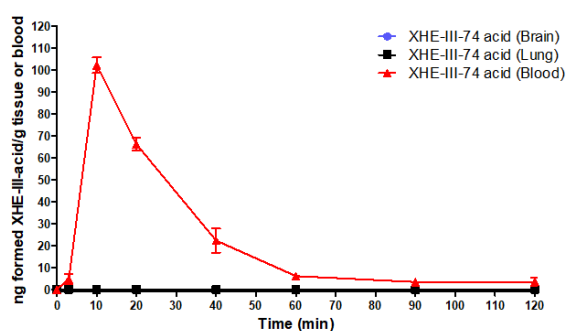


Figure 55. Pharmacokinetic curve for the Xhe-III-74 Acid in brain, lung, and blood samples. The animals were originally dosed with the Xhe-III-74 Ethyl Ester, therefore this acid compound is a metabolite.

Table 6. Pharmacokinetic data for the acid metabolite of the Xhe-III-74 Ethyl Ester. *nd* indicates not determined due to the compound concentration being less than the lower limit of quantification.

PK Parameters	Blood	Lung	Brain
C_{max} (ng/ml)	102.3	<LLOQ	<LLOQ
T_{max} (min)	10	<i>nd</i>	<i>nd</i>
AUC (ng*min/ml)	4282.3	<i>nd</i>	<i>nd</i>
$T_{1/2,E}$ (min)	11.6	<i>nd</i>	<i>nd</i>
$T_{1/2,D}$ (min)	2.8	<i>nd</i>	<i>nd</i>

As the PK curve shows, the acid compound is not seen in the lung or the brain in any appreciable amount. It is also noteworthy that the AUC for the acid metabolite is very similar to the AUC for the Ethyl Ester compound, illustrating an equally effective distribution. Therefore,

the next logical step was to dose the mice directly with Xhe-III-74 acid, as opposed to rely on *in vivo* metabolism. This data is presented in Figure 566.

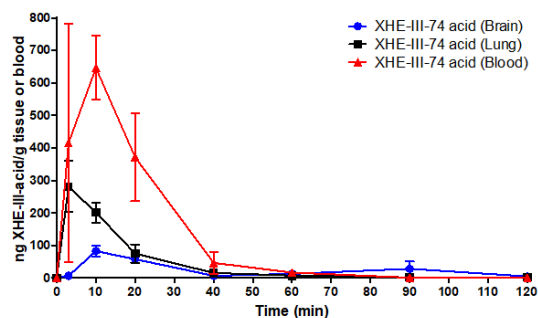


Figure 56. Pharmacokinetic study for the Xhe-III-74 acid analog, dosed in the same manner as the Xhe-III-74 Ethyl Ester.

Xhe-III-74 Ethyl Ester acid displayed good distribution in the blood and lung, as well as a lack of absorption in the brain. However, the compound was cleared or metabolized very rapidly from both the blood and the lung, so although it appears to have a fast onset the clearance is too rapid for a good asthma drug. The goal following this PK study was to screen additional compounds to identify a compound that does not cross the BBB and is cleared slowly.

An inherent challenge presented by thorough *in vivo* studies is the immense time it takes to procure samples and the number of mice. Therefore it is difficult to screen many compounds with this method. In addition, the sample preparation as described above is time-consuming. Although the miniaturization of this method was helpful for the throughput of samples as compared to LLE with diethyl ether, the manual homogenization step with the hand-held homogenizer is a bottleneck step in and of itself, as the barrel must be thoroughly cleaned

between samples to avoid cross contamination. To eliminate this bottleneck issue and eliminate the risk of cross contamination between samples, several automated bead-based homogenizers were tested to investigate if the manual homogenizer could be eliminated.

The Omni BeadRuptor is a beadmill that uses ceramic, metal, glass, garnet, or carbide beads for homogenizing 24 samples simultaneously. The BeadBug is a much lower power tool that uses zirconium or steel beads to homogenize 3 samples simultaneously. Several bead types were tested first with the BeadBug, as this was a relatively inexpensive tool (Figures 57 and 58).

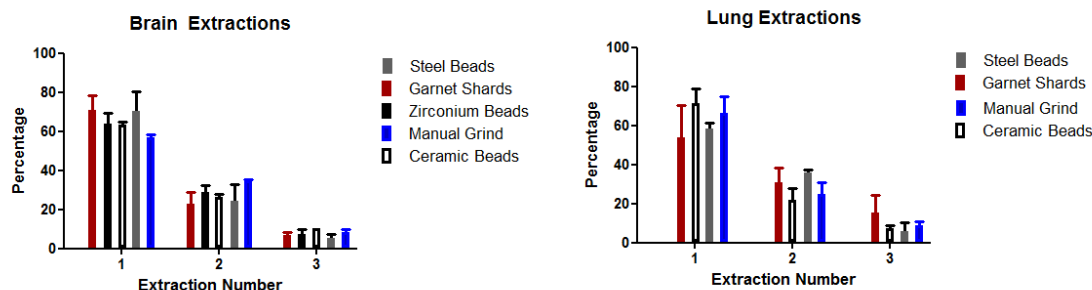


Figure 57. Brain extractions using the BeadBug tool. Figure 58. Lung extractions using the BeadBug.

The zirconium beads were not strong enough to homogenize the lung tissue, therefore they were excluded as an option. Although the garnet and ceramic beads were able to homogenize the lung and brain tissue, the stainless steel beads were found to have a greater percentage of compound extracted within the first extraction. Therefore the stainless steel beads were chosen for future investigation. The Omni BeadRuptor was borrowed from Thermo Fisher Scientific for testing, with stainless steel beads used as the homogenization medium. The BeadRuptor yielded similar results to the BeadBug.

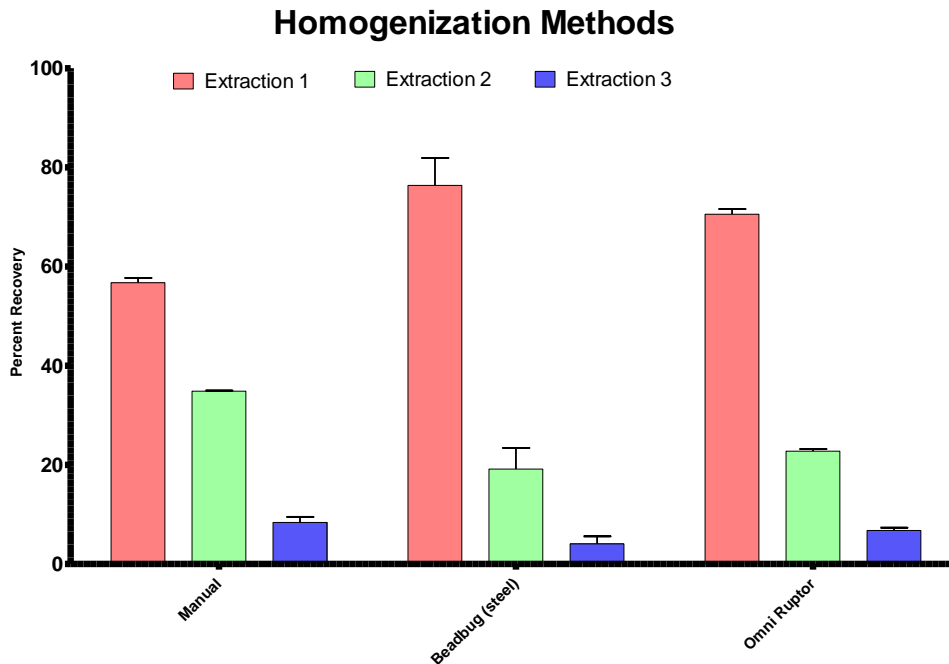
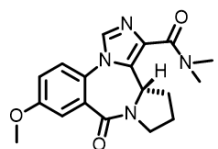


Figure 59. Homogenization methods overall comparison.

Although the bead homogenization tools appeared to yield higher extraction results in the first extraction, ultimately a second extraction is still required to achieve greater than 90% extraction efficiency. Therefore, there is no significant difference between the bead-based homogenizers and the manual homogenizer. The main advantage that the bead tools provide is that they eliminate cross contamination between samples. However, the time to load the tubes and beads, and then recover the beads, does not actually decrease the sample preparation time. This added time would be worth it if this method was able to yield close to 100% recovery in one extraction, but this is not this case. In addition, these tools create an added cost in the beads, the specialized tubes, and the instruments themselves. Therefore we proceeded with hand-held homogenization at this time.

The liquid-liquid extraction method as listed previously is an inexpensive, robust, and uncomplicated method that is being used by several MIDD members. However, for the analysis of blood samples, an on-line solid phase extraction method was also tested. The advantage of this method for blood samples is the “dilute and shoot” capability provided. The method utilized the reversed phase cartridge to trap the analytes, and then they were eluted from the trap with the HPLC mobile phase. Figure 61 illustrates the comparison between both methods using samples for a PK study with MRS-01-66 (Figure 60).



MRS-01-66
Molecular Weight: 340.38

Figure 60. Structure for MRS-01-66, the dimethyl amide analog to Xhe-III-74.

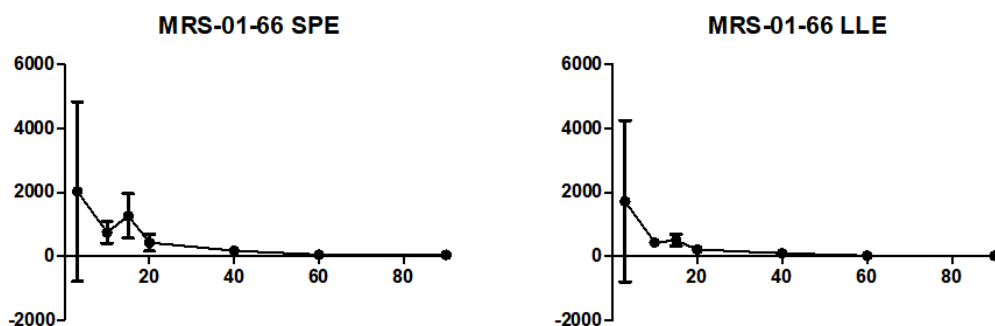


Figure 61 SPE vs. LLE data for blood samples, from the PK study of MRS-01-66. The variances seen are not statistically different. The means are only statistically different at the end time points (60, 90, 240 minutes), which are at quantities <LLOQ.

That the two methods (SPE vs. LLE) are not statistically different and either method is acceptable for the analysis of whole blood samples on the triple quadrupole LC-MS/MS instrument. Quantified amounts were compared at each time point first with the two-tailed t test, and then with the f test, to illustrate no significant differences in both the means as well as the variances for the measurements. Thus, SPE and LLE methods yield very similar results. However, the SPE cannot be used for whole tissue samples because the samples cannot be injected, as solids, onto the LC-MS instrument.

Our collaborators in the Cook group have synthesized the dimethyl amide compound MRS-I-66 to explore the differences between esters and amides for the imidazobenzodiazepine scaffold. As it is the case with the Xhe-III-74 Ethyl Ester, such compounds might hydrolyze to the corresponding acid. We observed in the microsome stability assay that esters and amides with longer and more branched carbon chains are metabolically less stable than their short carbon chain analogs. The result of the PK analysis for MRS-I-66 is depicted in Figure 622.

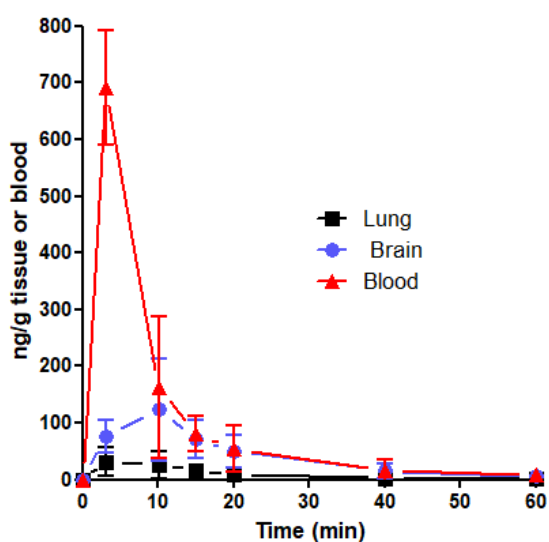


Figure 62. PK graph for the dimethyl amide compound.³²

Table 7. PK results for MRS-01-66

Figure of Merit	Blood	Brain	Lung
C_{max} (ng/g)	691	123	30
T_{max} (min)	3	10	3
AUC (ng*min/ml)	6205	2701	764
$T_{1/2,E}$ (min)	8.8	10.3	11.7
E_{rate} (min ⁻¹)	0.078	0.067	0.059

Interestingly, MRS-01-66 displayed a rapid onset and also a rapid clearance. The amount of compound found in the lung, however, was far less at 30 ng/g. For these reasons, the MRS-01-66 compound was not pursued as the primary lead compound for the asthma project.

3.2 Results for GLO1 Inhibitors

Methylglyoxal is a non-enzymatic side product of glycolysis, catalyzed by a cytosolic enzyme, GLO1.⁴⁹ The compound is inversely proportional to the enzymatic activity of GLO1, and has been shown in primary neuronal cultures to act as a competitive partial agonist for the GABA_A receptor.⁵⁰ An overexpression of this enzyme in mice has been shown previously to increase symptoms of anxiety and depression, but when dosed with methylglyoxal or a direct inhibitor to GLO1, these symptoms were decreased.^{49a} Therefore, we investigated the potential of GLO1 inhibitors as antidepressants.⁵¹ Mice were dosed with i.p. injection as described above, and the samples prepared in the same manner as the compounds for the asthma project (LLE for the blood samples and manual homogenization for the tissues).

Initially, the analyte pursued for detection in this study was the original GLO1 inhibitor pBBG, shown in Figure 633. However, the compound was not found in the blood samples by LC-MS/MS analysis. Employing a similar strategy as above, we searched for a metabolite. Although the parent compound was not identified in the samples, the diacid metabolite was identified and quantified. The structure for this metabolic transition is illustrated in Figure 633. This metabolite was produced *in vivo* by hydrolysis.

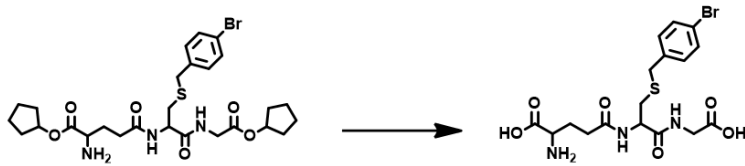


Figure 63. Transition of pBBG compound into the diacid analog, proposed to occur *in vivo*.

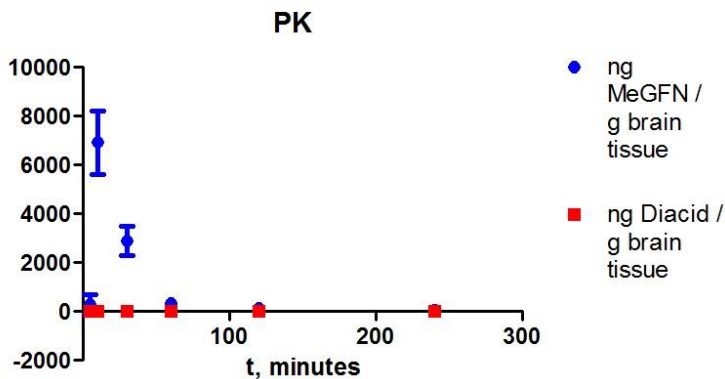


Figure 64. PK graphs for pBBG diacid and MeGFN in the brain.

Table 8. Calculated PK parameters for two GLO1 inhibitor in the brain.

	pbbg diacid	MeGFN
AUC	846 ng min/ml	191580 ng min/ml
E rate	0.003 1/min	0.008 1/min
E 1/2	254.182	90.882 min
t max	5 min	10 min
c max	7.8 ng/ml	6922.2 ng/ml
A rate	n/a	0.181 1/min
A 1/2	n/a	3.835 min

The published results for the GLO1 project show the potential to produce fast acting antidepressant effects. The most straightforward explanation for the observed antidepressant-like effects is that GLO1 inhibition increases MG concentrations. MG is a competitive partial agonist at GABA_A receptors, and depression is associated with reductions in cerebrospinal fluid GABA levels as well as the number of GABA_A receptors in cortical regions. In addition, chronic

antidepressant treatment correlates with an increase in GABA, supporting a potential role for GABAergic signaling in depression. The effects of GLO1 inhibitors on GABAergic signaling is distinct from any other GABA_AR-acting compounds (such as benzodiazepines like alprazolam). MG acts as a competitive partial agonist at GABA_A receptors, thus modulation of MG concentrations by GLO1 inhibitors may have different effects as compared to other GABA_AR-acting compounds.

Previous studies have shown that genetic and pharmacological GLO1 inhibition, as well as MG administration, are anxiolytic, have anti-seizure effects and reduce ethanol consumption. The current results show that GLO1 inhibition might provide a unique strategy for treating depression with comorbid anxiety, epilepsy or alcohol use disorders, which would constitute a unique class of therapeutic compounds and would address an urgent need, given the high comorbidity of these disorders. Our findings suggest that modulation of GABA_AR signaling may be a promising approach for the development of fast-acting antidepressants.

6.4 Conclusions

The importance of high-throughput analyses in drug discovery cannot be overstated. In an effort to speed up the sample preparation process as well as increase reproducibility, several homogenization methods were compared, several extraction methods were tested, and every opportunity to exploit rapid analyses was taken advantage of for these studies. Although the stainless steel bed homogenization method was able to yield comparable results to the manual homogenizer, the added cost of materials and equivalent sample preparation time did not

make this an advantageous option. However, the miniaturized extraction method with acetonitrile or methanol employed as the extraction solvent is sufficient for our analyses, as the analytes quantified in this work are all soluble in one or both of those solvents. Thus, the need for diethyl ether is eliminated. In addition, the on-line solid phase extraction continues to be implemented for studies within the MIDD due to increased purity of the sample and decreased sample preparation time for liquid matrices. We have created the capability for the MIDD to establish a full pharmacokinetic profile for any lead compound of interest, and this assay has been repeated multiple times for various compounds to qualify drug candidates for further testing. If additional funding becomes available in the future, the Omni Bead Ruptor 24 could be re-visited as an option for tissue homogenates, including tissues other than brain and lung such as liver, kidney, small intestine, or any other pertinent organs important to drug discovery projects. The utility of solid-phase extraction can also be employed in an off-line manner, with 96 or 384 well plates. This could be employed for metabolomics studies on the IT-TOF, which does not have an on-line solid phase extraction setup. It would be interesting not only to quantify the parent compound from drugs dosed in pharmacokinetic studies, but also to identify new metabolites in various tissue types.

CHAPTER 7. MALDI imaging mass spectrometry (MALDI IMS)

7.1 Introduction

Matrix assisted laser desorption ionization (MALDI) mass spectrometry had been widely implemented as a method to investigate large biomolecules, notably proteins and peptides that are too large to be analyzed with conventional LC-MS instruments. For example, a protein with a mass of tens of kilodaltons is far too large to be analyzed by a quadrupole mass analyzer (which typically has a maximum around 5,000 m/z with a reasonable scanning speed) without first being digested into small peptides by an enzyme such as trypsin. In the last decade, MALDI-MS has come to the forefront in small molecule analyses, particularly as a method to analyze drugs or other small molecules in complex biological samples, such as whole cells and tissue sections without using extraction procedures. MALDI-MS also shows promise in diagnostic imaging (MALDI IMS), potentially identifying and localizing markers for diseases like cancer.⁵² One distinct advantage of MALDI IMS as an imaging tool is that it is a label-free all-encompassing technique, which doesn't require antibodies or expensive and hazardous radiolabels. MALDI IMS has diverse application to many different analyte types and research areas, including but not limited to the study of new and existing proteins, peptides, nucleic acids, small molecules, and even polymers.⁵³ Herein, we present a method developed to image drug compounds in tissue slices, employing collision induced dissociation to identify compounds of interest based on known fragmentation patterns. The mass detector employed for MALDI IMS is a Dual Time of Flight (TOF) analyzer with a collision cell that enables increased specificity with the generation of daughter ions (Figure 65).

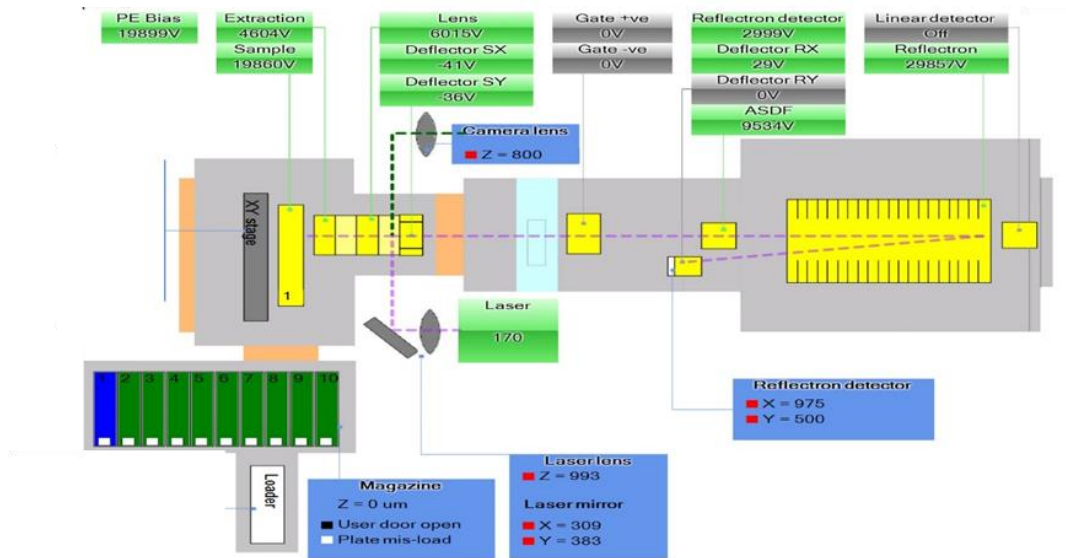
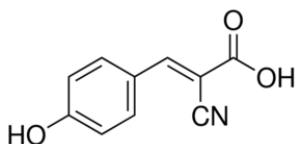


Figure 65. Shimadzu 7090 MALDI-TOF/TOF instrument schematic.

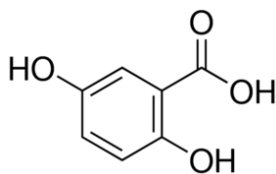
The instrument used in this work employs a 2kHz UV laser (355 nm) for ionization. The instrument is also equipped with a dual wire-grid ion gate, to gate species that may be close ion nominal mass, and produce distinct fragment ion spectra. High mass resolutions (10,000 FWHM) are achieved by a combination of pulsed extraction, the ion optics, and axial spatial distribution focusing. When employing MSMS mode, the ions enter a collision cell at 20keV, which is a high-energy collision induced dissociation method with helium as the collision gas. The instrument is also capable of fragmenting ions in a low-energy manner. In this variation, the collision gas is not used, and so the ions detected are the result of spontaneous metastable decay of the precursor. The two differing fragmentation methods generate different fragments which can garner useful information about the analytes (for example, peptide side-chain and lipid backbone fragments will only be generated by high-energy CID).

In Matrix-Assisted Laser Desorption Ionization (MALDI), a low molecular weight matrix is mixed with the sample and allowed to crystallize. The crystalline matrix absorbs UV energy from the laser, and also aids to ionize the analytes (hence the term, matrix-assisted). There are many matrix options commercially available, however, the matrix selections chosen for this work are common for small molecule analyses.

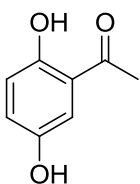
Matrix selections:



CHCA (α -cyano-4-hydroxycinnamic acid)



DHB (2,5-dihydroxybenzoic acid)



DHA (2,5-dihydroxyacetophenone)

The MALDI technique is based on laser irradiation, which induces desorption and ionization of the analyte of interest as a molecular species ($[M+1]$ or $[M-1]$).

MALDI IMS generates an ion density map or “heat map” in which more brightly appearing areas indicate a higher abundance of a specific ion at that particular location.

Therefore, the technology gives us valuable information regarding the spatial distribution e.g. a drug distribution in a particular tissue. The spatial resolution in MALDI IMS is dependent on the laser beam focus (including diameter and space between laser shots), the size of the crystal matrix, and the diffusion or delocalization of analytes during the sample preparation process.⁵⁴ The localization of compounds in a specific target tissue has valuable information in regards to the interaction of drug and protein target.⁵⁵ Pharmacokinetic studies have shown that imidazobenzodiazepines distribute in the lungs (which is the target organ for our asthma project) by quantification of lung homogenates using LC-MS/MS. Herein, a method is presented to image the localization of imidazobenzodiazepines in mouse lung tissue slices.

Although the ion density map generates valuable information regarding localization of ions of interest, the information can be enhanced when combining it with histological stains. Sections can be taken in serial fashion, thereby making the differences between the sections equivalent only to the thickness of the tissue section (for example, 12 micrometers). The histological stain gives morphological information about the tissue, which can aid in the explanation of why certain areas of the MALDI image may show high or low ion density. For example, if there is a large gap in the ion density map of the lung, the histological stain might show the absence of tissue such as a large airway or blood vessel. The hematoxylin and eosin stain will show the nuclear contents as blue-purple, and red blood cells, non-nuclei, and extracellular material will be pink. An example of the H&E stain is presented in Figure 66, showing an airway for mouse lung tissue sliced at 12 μm thickness.

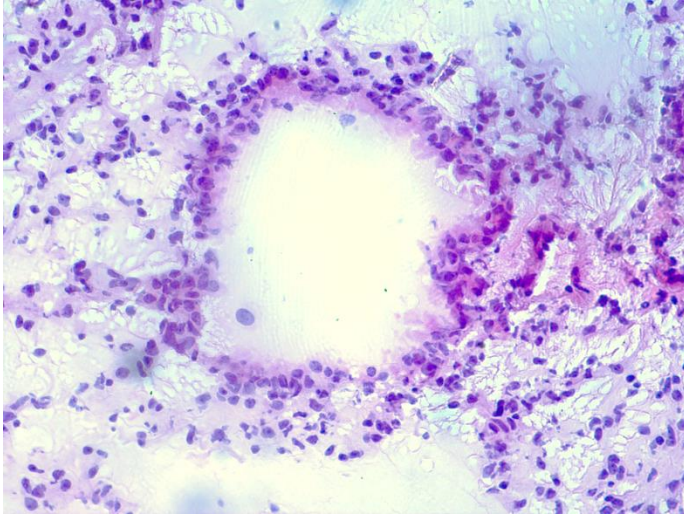


Figure 66. H&E stain of mouse lung, showing the airway morphology.

In order to visualize the target protein of a small molecule, immunohistochemistry can be employed using specific antibodies in conjunction with enzymatic or fluorescent detection. Indirect immunohistochemistry methods employ an unlabeled primary antibody to bind to the target antigen, in this case the $\alpha 5$ subunit of the GABA_A receptor. A labeled secondary antibody interacts specifically with the primary antibody and enables detection of the receptor. Two labels were used to image the alpha 5 subunit of the GABA_A receptor. Firstly, horseradish peroxidase protein (HRP), which is an enzyme that catalyzes the oxidation of specific substrates in the presence of hydrogen peroxide, resulting in a colored product. The substrate used for HRP was 3,3'-diaminobenzidine (DAB). DAB reacts with HRP in the presence of peroxide to yield an insoluble brown-colored phenazine polymer at locations where peroxidase-conjugated antibodies are bound to the tissue.

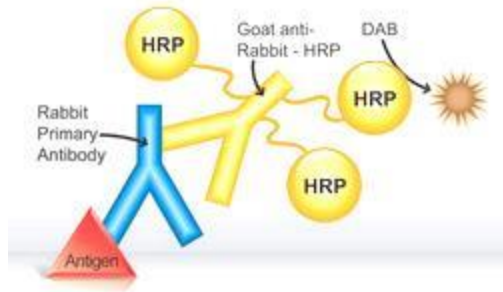


Figure 67. Cartoon of the reaction of horseradish peroxidase and DAB substrate to produce brown coloration in tissue stains. (Image: AbCam.)

Secondly, a fluorescent small molecule can be attached to the secondary antibody, and its fluorescence signal measured rather than visualizing the product on an enzymatic reaction. Fluorescein and Cy5, both very common fluorescent dyes used for the immunohistochemistry, were attempted for the immunofluorescence stain of the $\alpha 5$ receptor.

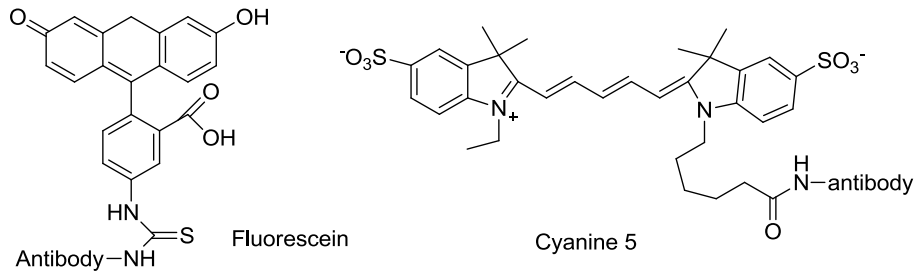


Figure 68. Dyes used for immunofluorescence. FITC shows excitation and emission at 495 nm and 519 nm, respectively, and Cy5 Ex: 650nm, Em: 667nm.

4,6-Diamidino-2-phenylindole (DAPI) was used to stain the nuclei of all cell Figure 69.

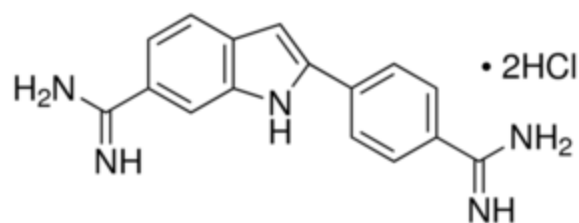


Figure 69. 4,6-Diamidino-2-phenylindole DAPI Ex: 358 nm, Em: 461 nm.

DAPI is a di-cation at physiological pH and becomes strongly fluorescent when bound to double-stranded DNA in the nucleus. The interaction with RNA is weaker thus the resulting fluorescence is less pronounced for RNA.

The combination of MALDI-MS, H&E stain and immunohistochemistry can illustrate valuable information of how a compound is distributed *in vivo*. MALDI IMS can also be used to investigate metabolites generated through xenobiotic metabolic processes in the animal, as well as adducts generated by the mass spectrometer itself. Investigative results will be presented herein.

7.2 Materials and Methods

7.2.1 MALDI IMS

MALDI matrices were purchased from Sigma Aldrich (St. Louis, MO, USA): α -Cyano-4-hydroxycinnamic acid #70990; 2,5-dihydroxybenzoic acid #85707, 2,6-Dihydroxyacetophenone, #37468. MALDI calibration kit was also purchased from Sigma Aldrich (ProteoMass™ Peptide and Protein MALDI-MS Calibration Kit, MSCAL) and used for calibrations according to the package insert. Metal slides were purchased from Shimadzu Scientific (Japan).

Swiss Webster female mice were dosed with 25 mg/kg compound via oral gavage and sacrificed as according to the T_{max} determined in previous PK studies. Mice were sacrificed by CO₂ and spinal cord dislocation (IACUC protocol 16-17 #25). Tissues were procured immediately and exposed to dry ice vapor for five seconds followed by dry ice to freeze. Lungs were stored at -80°C until cryosectioning with a Leica cryostat. Just before cryosectioning, lungs were allowed to equilibrate to -20°C for 30 minutes. Lungs were sectioned at 20 micron thickness and thaw-mounted to metal slides. Slides were allowed to come to room temperature in a desiccator for 5 minutes, gently rinsed with water containing 0.1% TFA to remove salts, and allowed to dry again at room temperature before matrix application. Matrix was applied using a manual spray coating method with a TLC sprayer. 10 mL of matrix solution at 50 mg/mL was passed at 3 psi using nitrogen gas. Matrix was allowed to dry fully between passes. The spray is wet enough to extract analytes from the solid sample into the matrix, but dry enough to rapidly crystallize and prevent delocalization of the analytes' spatial locations. The TLC sprayer is slowly passed approximately 12 inches in front of the sample plate, which hangs vertically in the fume hood. Each pass applies a small amount of matrix, therefore the passes are repeated until all of the solution is used up and the samples are sufficiently coated.

7.2.2 H&E stain

Fresh frozen tissue sections were taken in serial fashion (to the sections used for MALDI IMS) at 12 µm thickness and stored at -80°C prior to staining. Sections were rehydrated in the following sequence: 30s in 95% ethanol, 30s in 70% ethanol, 30s in Milli-Q water. Slides were stained in hematoxylin stain (VWR, 95057-844) for 1 minute, followed by rinsing in Milli-Q water for 3 minutes, and again 30s in 70% EtOH and 30s in 95% EtOH. Sections were then stained for 30s in

eosin stain (VWR 95057-848), and subsequently cleared for 30s in 95% EtOH, 30s in 100% EtOH, and 2.5 min in histoclear clearing solution (VWR 64110-04), which is a substitute for the traditional clearing reagent xylene. After drying, 1 drop of Permount adhesive (VWR 100496-550) was placed on each section and covered with a glass cover slip. Slides were allowed to dry overnight before viewing under light microscopy.

7.2.3 Immunohistochemistry:

Mouse lung sections were taken at 12 micron thickness in serial fashion to the slides for the MALDI and for H&E staining, and placed on glass microscope slides. Frozen section slides were stored at -80°C in a sealed slide box. Just before staining, slides were allowed to equilibrate to -20°C. Slides were fixed for 10 minutes in cold 4% paraformaldehyde solution and allowed to warm to room temperature. Antigen retrieval was performed by placing the slides in 10 mM sodium citrate buffer at pH = 6.0 in a pressure cooker at 15 psi for 10 minutes. Slides were then rinsed with PBS and a PAP Pen was used to create wells for the liquid on the surface of the glass slides. Slides were subsequently washed with TBS Tween for 5 min, peroxidase suppressor (Thermo Fisher Scientific, 35000) for 15 min, and twice more with TBST for 5 minutes. The peroxidase suppressor reduces the background signals generated from endogenous horseradish peroxidase in the tissue. Slides were then washed with background sniper for 10 minutes to block nonspecific staining resulting from the antibodies binding to proteins other than GABA_ARs. Slides were washed twice more with TBST before incubation with the primary antibody. Antibodies were diluted 1:100 and 1:250 with superbloc T20 buffer as the diluent. The slides were incubated overnight in the 4 degree. Wet paper towels were placed inside the slide holder to retain moisture and prevent the glass slides from drying overnight.

Following overnight incubation, slides were washed three times with TBS Tween for 6 minutes. The secondary antibody was diluted in the same manner as the primary antibody and was applied to the slides at room temperature and allowed to incubate for 40 minutes. Slides were again washed three times with TBST for 6 minutes. Following the washes the chromogen DAB substrate, which was diluted 10-fold into peroxidase substrate buffer and applied to the slides for 6 minutes. Slides were washed with ddH₂O for 5 min and counterstained with Hemotoxylin solution for 1.5 min to stain the nuclei. Slides were rinsed with ddH₂O and dehydrated through 4 changes of alcohol solutions (95%, 95%, 100% and 100%). Finally, slides were cleared in 3 changes of histoclear and coverslipped using permount mounting solution.

For the fluorescent immunohistochemistry stains, the same procedure was followed, except rather than fixing the tissue and performing antigen retrieval, which is necessary to preserve the tissue for an overnight incubation step, this step was omitted and the tissue was incubated rather for 1 hour at room temperature (with the primary antibody). Silane coated microscope slides (NC9968319, Fisher Scientific) were also implemented to improve the adherence of the tissue to the slides. The simplified procedure consisted of rehydration in PBS for ten minutes, PAP pen to create wells, blocking non-specific background staining with background sniper or 5% animal serum, washing with PBS, application of the primary antibody with 60 minutes incubation, washing, application of the secondary antibody with 30 minutes incubation, washing, application of 1.5 µg/mL DAPI for 10 minutes, two final washes with TBST and coverslipping with Prolong Gold anti-fade reagent.

7.3 Results & Discussion

The method development process for MALDI IMS is very involved, including optimization steps required at several stages: the *in-vivo* dosing of the animal, the sample preparation of the tissue, the matrix selection and deposition, instrument conditions, and finally, image resolution. The ADME property of a drug determines how a test animal processes a compound and which concentrations can be found in biological sample at a particular time point. For MALDI IMS, high tissue compound concentrations are necessary due to its desorption process, which is significantly less sensitive than quantification of tissue extracts by triple quadrupole LC-MS/MS. The matrix application plays an important role in this. Typical matrix concentrations are 20-100 mg/mL, which by far exceeds the expected concentration of the analyte. The large matrix concentrations in turn cause interferences in the TOF analyzer. Purification of the sample is challenging and often not seen in MALDI IMS, especially with small molecule imaging. Samples used for small molecule imaging experiments cannot undergo extensive washing steps, because the analytes can delocalize from their original location or be washed away completely. The introduction of high levels of matrix also presents challenges regarding signal suppression, which are enhanced as compared to typical LC-MS analysis. For the MALDI IMS experiments presented herein, a full pharmacokinetic profile of each compound was established first by LC-MS/MS to determine the T_{max} . In a separate experiment, dosed animals were sacrificed at that specific time point to ensure high compound concentrations.

The matrix deposition process is, in and of itself, a broad field of study in MALDI IMS. The most common methods employed are sublimation, spotting via micropipette or an automated liquid distribution system, and spray coating, which can be automated with a spray

instrument, or performed manually using a TLC sprayer or an artistic sprayer. The most rapid and cost effective option was determined to be manual spray coating.

Matrix selection for each compound presents another unique challenge for MALDI IMS because although one can easily optimize a matrix for pure compound by spotting the compound directly with various matrixes followed by analysis, the results may not translate to imaging experiments with tissue samples. One reason for this is that the matrix interferences presented by a complicated sample like a tissue slice cannot be predicted or adequately assessed beforehand. Therefore, the optimization of matrix selection needs to take place using actual tissue. It is ideal to take one tissue and serial section it so that the comparison of matrix choices are under comparable experimental conditions. An image of the workflow for the sample preparation prior to MALDI ISMS is shown in Figure 70.

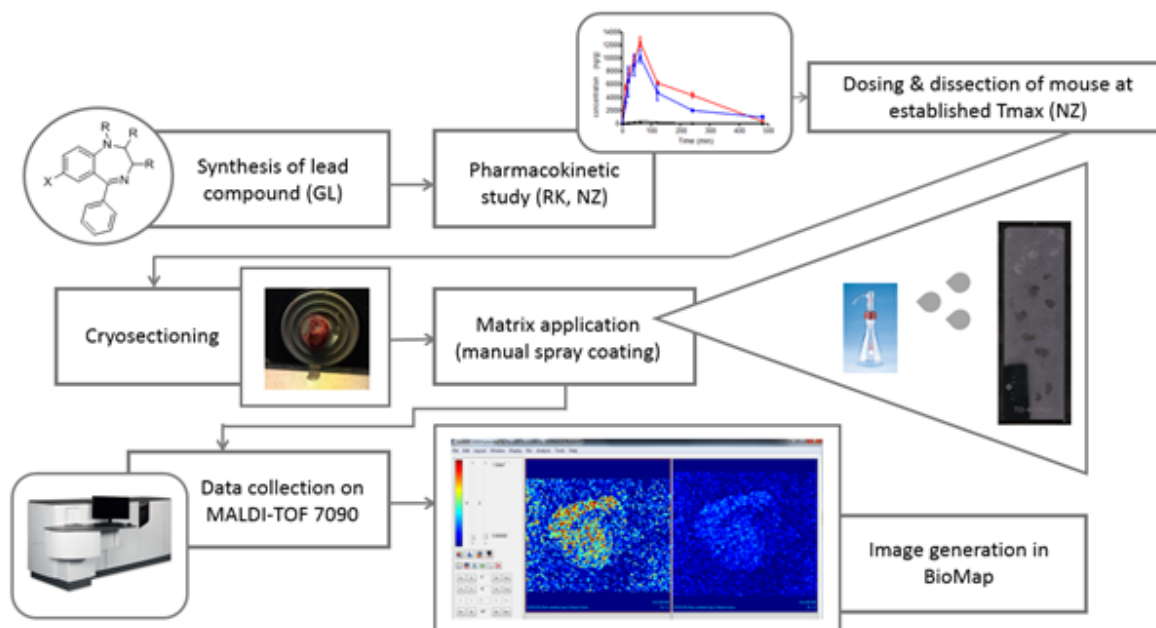


Figure 70. MALDI IMS workflow. Images presented in this chapter were generated from a compound synthesized by Guanguan Li of the Cook research group. Pharmacokinetic study was performed previously by Revathi Kodali and Nick Zahn, as published previously.⁵⁶

7.3.1 MALDI IMS results using MS/MS mode

Initial method development was performed on a manual spot of the analyte, for verification that the analyte is in fact ionized by MALDI. Manual spotting also allows us to ascertain the masses of fragments generated in MS/MS mode (similar to the method development process on LC-MS/MS instruments) prior to actual sample analysis. A table of fragments generated via both ionization methods is listed in appendix a. Figure 71 shows a typical spectrum for the MALDI in MS/MS mode for the SH-053-2'F-R-CH₃ acid compound.

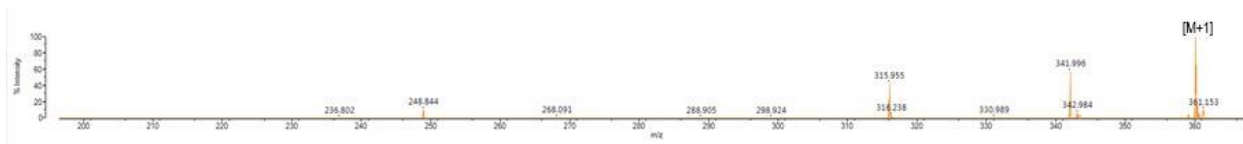


Figure 71. MALDI-MS/MS spectrum of the SH-053-2'F-R-CH₃ acid spotted with DHB as the matrix.

Although generally speaking many of the same fragments are generated by collision induced dissociation in both MALDI-TOF/TOF and ESI-MS/MS, there can certainly be differences in fragmentation patterns. Initial lung section images were generated based on the transition of m/z 360 [M+1] to m/z 316 fragment common to both ionization methods (Figure 72).

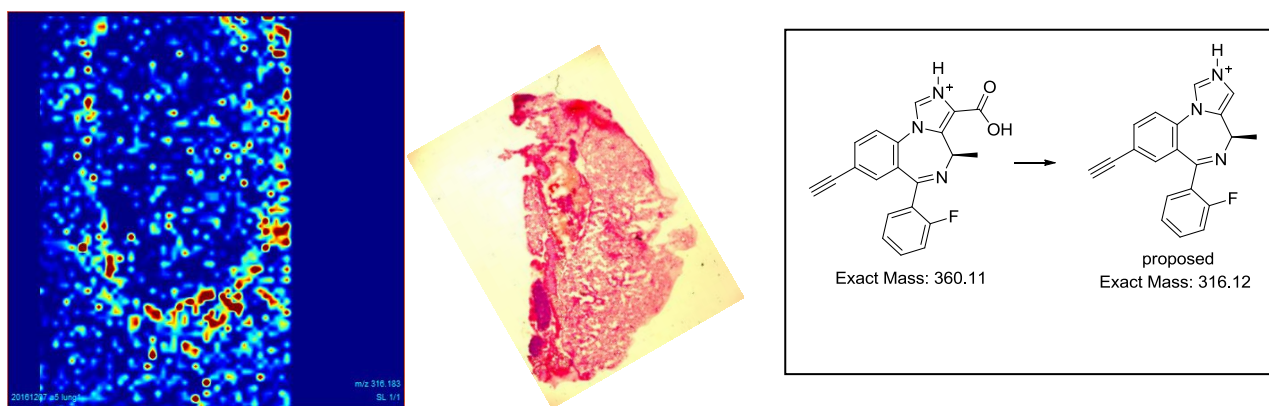


Figure 72. Lung section imaged for the 360>316 transition in MALDI-MS/MS. MSI import 200-400 bin size 3, 5905 data points, 54.1843 MB, 62x74x51500 dpi and H&E stained serial tissue section.

The initial MALDI IMS image produced an unexpected result, showing what appears to be an outline of the lung tissue section. This raises concerns of validity for this experiment because we know this compound is localized in the lung and binds GABA_AR alpha 5 receptors, which are believed to be located in the airway of the lung.⁴⁸ Thus, the image above must be the product of either wrong sample preparation or wrong analysis.

Another important sample preparation consideration is the limited options for purifying the sample. One such option is washing the tissue, in an attempt to de-salt the sample and

eliminate interferences. Without this step, the analyte was only detected around the edges of a tissue section of interest. However, with the addition of a gentle washing step, the analyte then appears throughout the tissue section, which more closely correlates with the target receptor in the tissue (Figure 73).

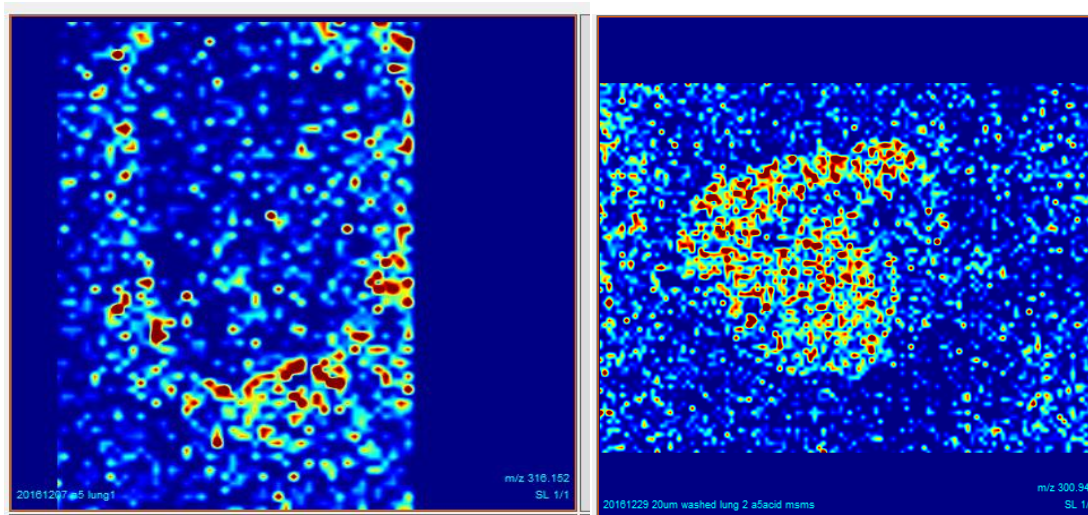


Figure 73. Comparison of unwashed vs. washed lung tissue sections in MALDI IMS using the 360>316 transition.

The washing step improved the signal for SH-053-2'F-R-CH₃ acid not only due to the removal of potential interferences, but also by removing SH-053-2'F-R-CH₃ acid from the edge of the slice that may have been delocalized during the sample preparation process. The cryosectioning for the lung tissue sections was performed at -20°C. However, the matrix application was performed at room temperature. Therefore, before application of the matrix, it was necessary to equilibrate the slides from -20°C to RT. The issue presented is that taking a metal slide from a freezer and bringing it to room temperature results in condensation across the entire slide. As a water layer forms, the small droplets have the ability to move the analytes of interest from their original location, potentially leeching out of the tissue sample and onto

the slide. This coupled with fact that the tissue slice is a slightly raised on a rough surface compared to a smooth, flat metal slide, resulted in the formation of a ring of condensation around the edges of the tissue section. In attempts to avoid this condensation issue, slides are placed in a desiccator to equilibrate to temperature. This alone, however, did not solve the edging issue. Adding a washing step to uniformly remove all of the condensation prior to matrix application appears to solve the issue of the compound appearing only along the edges of the tissue section. Using this methods to other transitions of SH-053-2'F-R-CH₃ acid were analyzed using serial tissue slices (Figure 74)

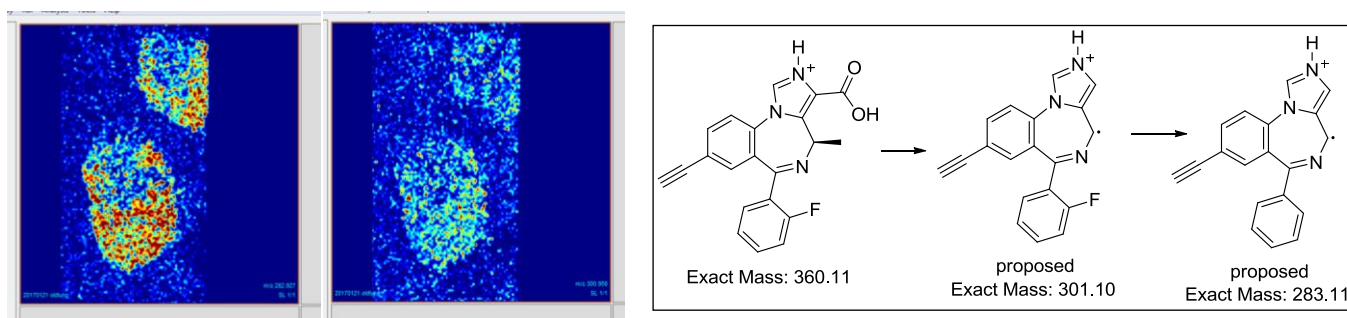


Figure 74. Images of two lung tissue sections of SH-053-2'F-R-CH₃ acid dosed mice at 360>283 m/z and 360>301 m/z transition, respectively.

The fragments imaged in Figure 74 are reproducible in imaging the SH-053-2'F-R-CH₃ acid, and are seen in every dosed tissue section. It is important to note that these masses are not present in tissue section prepared from vehicle dosed animals under the same experimental conditions, as illustrated in Figure 75.

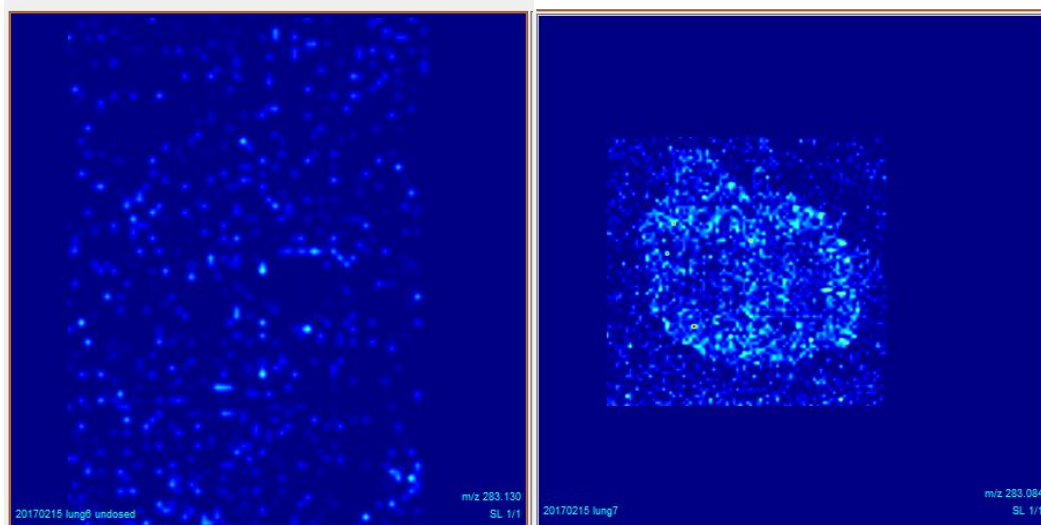


Figure 75. Comparison of lung tissue from vehicle and SH-053-2'F-R-CH₃ acid dosed mice. These sections were taken using the same MS/MS method 360>283 m/z. Both samples were prepared on the same day with the same matrix solution and application.

Compared with the tissue from non-treated mice, SH-053-2'F-R-CH₃ acid was present in the lungs and distributed throughout the tissue.

For any MS/MS technique, it is imperative that the method utilize reproducible fragmentation of the analyte, to ensure that the compound is identified correctly. This high level of specificity holds true for MALDI IMS, with the ability to distinguish the analyte from other compounds. The Shimadzu 7090 instrument also employs a reflectron after the flight tube, which is useful for the detection of low molecular weight analytes, as they can be difficult to separate in TOF analysis. These compounds travel very quickly down the flight tube impeding separation by time limited by the flight path. The reflectron enables additional separation by increasing the flight path. The instrument tuning varies when employing the reflectron in MS1 mode vs. MS/MS mode. For larger masses, the tuning is set in linear mode. For small masses

with no fragmentation, the tuning is set in reflectron mode. For small masses with fragmentation, the tuning is set in reflectron MS/MS mode. The parameters for each instrument mode are shown in Figure 77, linear mode, reflectron mode, and reflectron MS/MS mode. Although the parent compound can be detected using MS1 mode, the MS/MS capabilities increase this specificity and therefore yield a better spatial resolution for the location of the analyte (Figure 76).

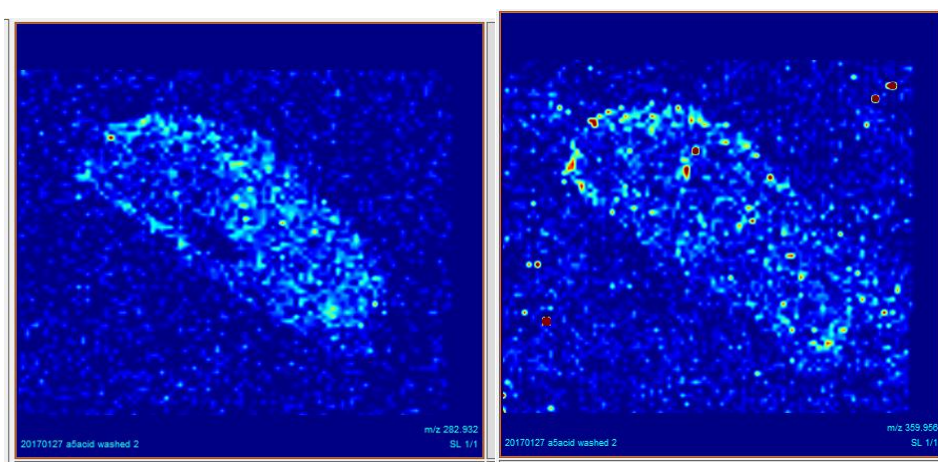


Figure 76. [M+1] ion image for the lead compound (SH-053-2'F-R-CH₃ acid) in reflectron mode and fragmentation 360>282.932 m/z in reflectron MS/MS mode.

	Axial Spatial Distribution Focusing		Axial Spatial Distribution Focusing	
Axial Spatial Distribution Focusing				
ASDF enabled	False	False	ASDF enabled	True
ASDF polarity	Positive	Positive	ASDF polarity	Positive
ASDF scaling factor	5	5	ASDF scaling factor	2.7708
ASDF switch offset	100	100	ASDF switch offset	-77.6
Voltage ASDf (2000Hz).	0	0	Voltage ASDf (2000Hz).	9650
Voltage ASDf (200Hz).	0	0	Voltage ASDf (200Hz).	9450
Baseline			Baseline	
Linear baseline	164	163	Linear baseline	163
Neutral baseline	0	0	Neutral baseline	0
Reflectron baseline	0	154	Reflectron baseline	153
Camera			Camera	
Camera lamp power.	40	40	Camera lamp power.	40
Deflectors			Deflectors	
Reflectron X deflector voltage	0	20	Reflectron X deflector voltage	30
Reflectron Y deflector voltage	0	-5	Reflectron Y deflector voltage	0
Source X deflector voltage	-55	-35	Source X deflector voltage	-40
Source Y deflector voltage	-95	-40	Source Y deflector voltage	-35
Einzel Lens			Einzel Lens	
Einzel lens enabled	True	True	Einzel lens enabled	True
Einzel lens polarity	Positive	Positive	Einzel lens polarity	Positive
Einzel lens voltage	6000	6000	Einzel lens voltage	6000
High mass			High mass	
High mass mode	False	False	High mass mode	False
Ion Gate			Ion Gate	
Ion gate end offset	-100	202.7392	Ion gate end offset	405
Ion gate end scaling factor	2.5	4.136	Ion gate end scaling factor	4.136
Ion gate start offset	-100	194.8274	Ion gate start offset	378
Ion gate start scaling factor	2.6	4.1592	Ion gate start scaling factor	4.156
Laser			Laser	
Laser 10 second density wheel position	160	160	Laser 10 second density wheel position	160
Laser 10 X offset	323	311	Laser 10 X offset	311
Laser 10 Y offset	394	382	Laser 10 Y offset	382
Laser 100 second density wheel position	180	160	Laser 100 second density wheel position	160
Laser 100 X offset	304	309	Laser 100 X offset	309
Laser 100 Y offset	384	383	Laser 100 Y offset	383
Laser 20 second density wheel position	160	160	Laser 20 second density wheel position	160
Laser 20 X offset	323	300	Laser 20 X offset	323
Laser 20 Y offset	394	384	Laser 20 Y offset	394
Laser 200 second density wheel position	160	160	Laser 200 second density wheel position	160
Laser 200 X offset	323	323	Laser 200 X offset	323
Laser 200 Y offset	394	394	Laser 200 Y offset	394
Laser 300 second density wheel position	160	160	Laser 300 second density wheel position	160
Laser 300 X offset	323	323	Laser 300 X offset	323
Laser 300 Y offset	394	394	Laser 300 Y offset	394
Laser 400 second density wheel position	160	160	Laser 400 second density wheel position	160
Laser 400 X offset	323	323	Laser 400 X offset	323
Laser 400 Y offset	394	394	Laser 400 Y offset	394
Laser 50 second density wheel position	160	160	Laser 50 second density wheel position	160
Laser 50 X offset	323	323	Laser 50 X offset	323
Laser 50 Y offset	394	394	Laser 50 Y offset	394
Laser min focus	1040	1103	Laser min focus	1100
Linear			Linear	
Linear detector enabled	True	False	Linear detector enabled	False
Linear detector voltage	3250	2800	Linear detector voltage	2750
Low Mass Zoom			Low Mass Zoom	
LMZ gradient	0	0	LMZ gradient	0
LMZ intersect	1	1	LMZ intersect	1
Motor			Motor	
Motor viewing focus	800	800	Motor viewing focus	800
MSMS calibration			MSMS calibration	
MSMS over parent time constant	0.00042	0.00035	MSMS over parent time constant	0.00035
MSMS parent time offset	0	0	MSMS parent time offset	0
MSMS parent time scaling	1	0.997565	MSMS parent time scaling	0.998255
Pulsed Extraction			Pulsed Extraction	
Pulsed extraction bias enabled	True	True	Pulsed extraction bias enabled	True
Pulsed extraction bias voltage	19910	19910	Pulsed extraction bias voltage	19910
Pulsed extraction enabled	True	True	Pulsed extraction enabled	True
Pulsed extraction scaling factor	720	875	Pulsed extraction scaling factor	800
Pulsed extraction switch offset	263	233	Pulsed extraction switch offset	233
Pulsed extraction switch on time.	13000	13000	Pulsed extraction switch on time.	13000
Voltage PE (2000Hz).	4500	5000	Voltage PE (2000Hz).	4750
Voltage PE (200Hz).	4265	4740	Voltage PE (200Hz).	4490
Reflectron			Reflectron	
Reflectron detector enabled	False	True	Reflectron detector enabled	True
Reflectron detector voltage	0	2850	Reflectron detector voltage	3000
Reflectron enabled	False	True	Reflectron enabled	True
Reflectron polarity	Positive	Positive	Reflectron polarity	Positive
Reflectron voltage	0	30000	Reflectron voltage	30000
Reflectron X detector motor offset	500	975	Reflectron X detector motor offset	975
Reflectron Y detector motor offset	500	500	Reflectron Y detector motor offset	500
Source			Source	
Source enabled	True	True	Source enabled	True
Source polarity	Positive	Positive	Source polarity	Positive
Source voltage	19930	19955	Source voltage	19930

Figure 77. Tuning settings for the linear, reflectron, and reflectron MSMS modes of the MALDI-7090.

When the ion density map is compared with microscope images of stained tissue, the morphological information yielded by H&E stain allows for rationalization of patterns within the ion density map. In Figure 78 below, it can be seen that any sparse areas within ion density map, or “holes” where the compound is not present are actually a result of the serial section lacking tissue in that particular area. When viewing the ion density map alone, it may appear that the compound is not evenly distributed in the lung. However, when viewing the H&E stain in parallel, it is clear that this is not the case.

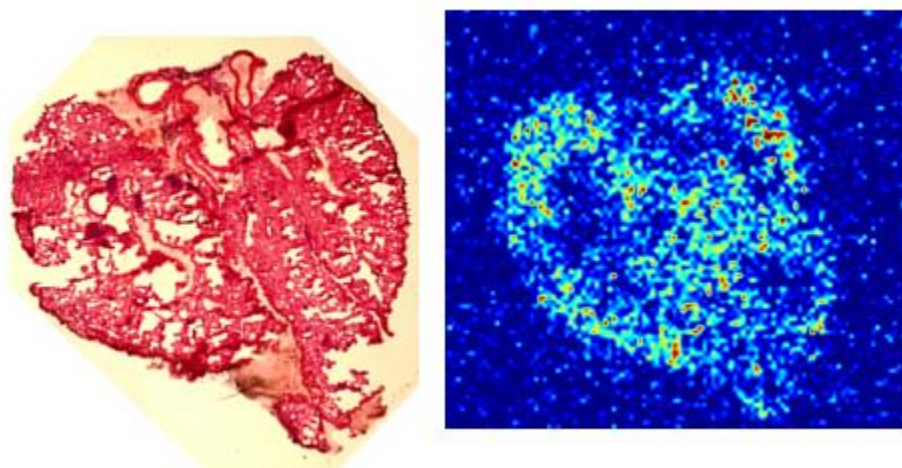


Figure 78. Light microscope image of lung tissue stained with H&E (4x magnification) and MALDI IMS image of the daughter ion in a serial tissue section (transition 360>282.930).

MALDI IMS presents an additional unique challenge in that the sample preparation strategy employed for one analyte may not necessarily translate to another analyte. One example is compound GL-II-93. Initial images acquired presented the same challenges as SH-053-2’F-R-CH₃ acid, showing what appeared to be an outline of the tissue section, as opposed to consistent distribution throughout the lung section.

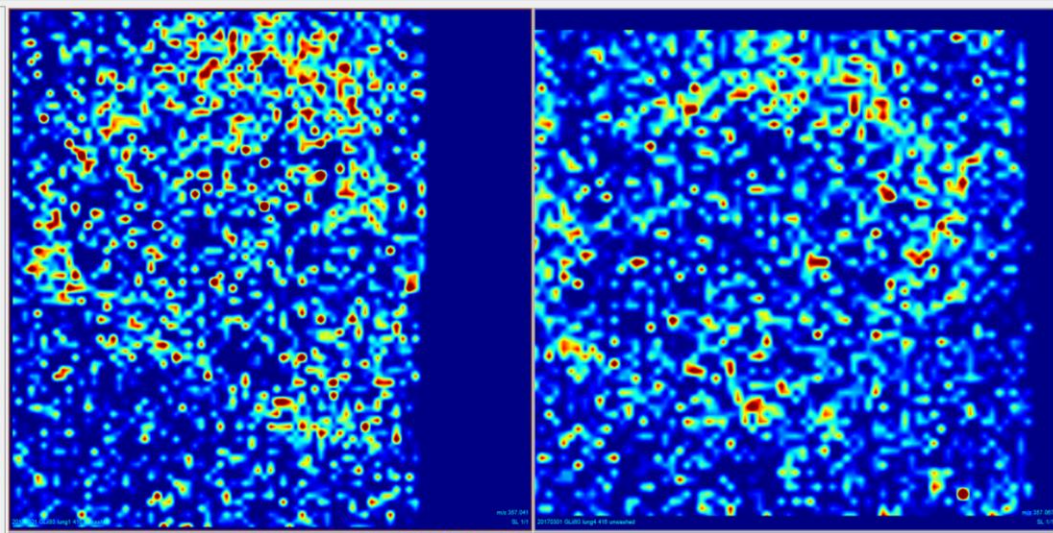


Figure 79. Two separate lung tissue sections imaged for GL-II-93 in reflectron MSMS mode, for the transition of the parent 416>357.

The GL-II-93 is structurally similar to SH-053-2'F-R-CH₃ acid, having the same core imidazobenzodiazepine scaffold and pendant phenyl ring (Figure 80). However, there is a difference in electron density due to the variance in the functional groups present. GL-II-93 has a bromine instead of an acetylene substituent. Unfortunately, a simple washing step did not prove effective for GL-II-93 to remove interferences and generate better images.

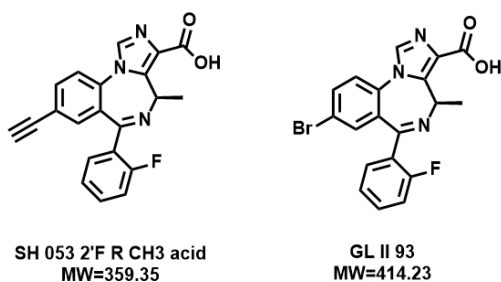


Figure 80. Structure of GL-II-93 and SH-053-2'F-R-CH₃ acid.

The solution for this particular sample preparation challenge lied in the selection of matrix. Although many application work with DHB, each analyte can cocrystallize and ionize

better or worse depending on the matrix selected. Shifting from DHB to DHAP showed a significant improvement in the image for GL-II-93 as seen in Figure 81.

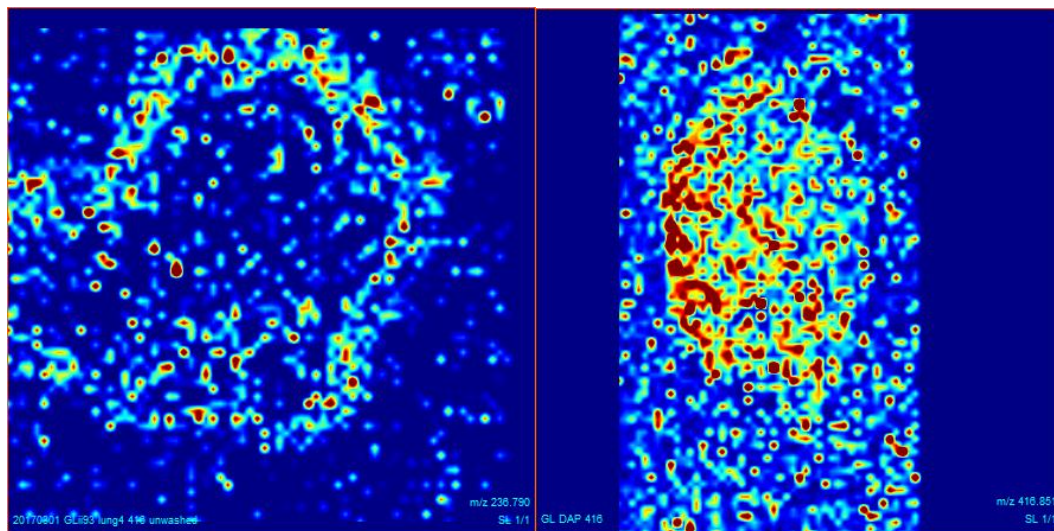


Figure 81. Images for GL-II-93 with dihydroxybenzoic acid (416>237), and with dihydroxyacetophenone (416 parent viewed in MSMS mode) as the matrix, respectively

Reproducible fragments were generated for GL-II-93 as well (Figure 82), although the ion density maps were not as strong as those seen for SH-053-2'F-R-CH₃ acid. Figure 83 illustrates a proposed fragmentation pattern seen for the analyte in both ESI-MS and MALDI-MS.

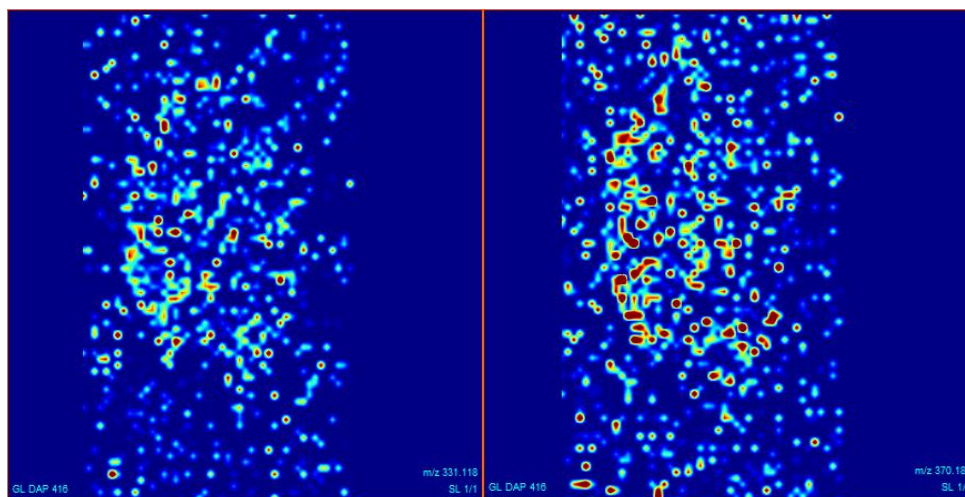


Figure 82. Fragment images for GL-II-93 for 416>331 and 416>370 transitions.

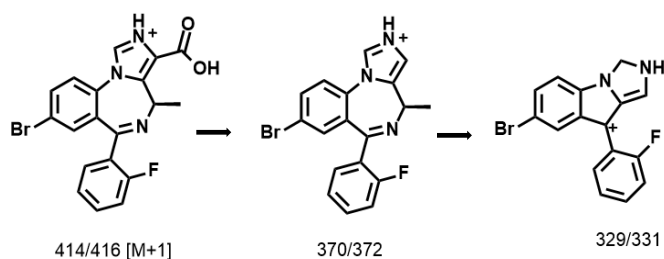


Figure 83. Proposed fragmentation pattern for the GL II 93 compound, for the fragments imaged above.

An important consideration in any analytical method development is the efficiency of a method. In MALDI-IMS, the spatial resolution of the image can be increased based on the distance between spots the laser fires upon, as well as the diameter of the laser itself. All images above were taken at a spatial resolution of 100 micron, with a laser diameter of 100 micron. However, the instrument is capable of smaller diameters for both spatial resolution and laser diameter. The image in Figure 84 shows the same experimental sample preparation as the images above, but with the spatial resolution and laser diameter both set to 50 micron instead of 100 micron.

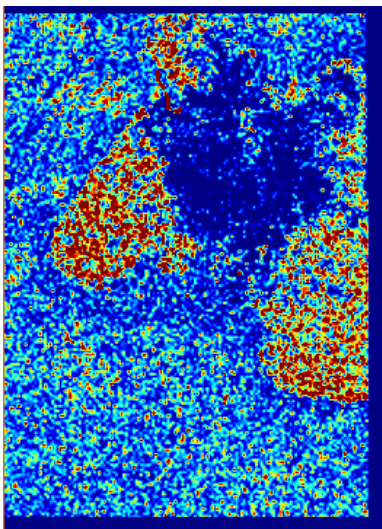


Figure 84. GL-II-93 parent compound (416 m/z) at 50 micron resolution, for two lobes of lung tissue.

The resolution is greatly improved with the 50 micron resolution and good distribution of GL-II-93 is detected throughout the tissue. However, the analysis time and data file size was also significantly larger. For the acquired image analysis above the analysis time doubled. Therefore it is important to determine if the information gained from a higher resolution (and longer lasting) experiment is really more significant than that of a lower resolution experiment. One does not necessarily need to keep the spatial resolution and laser diameter the same, however. It is possible to “oversample” and have a laser diameter larger than the diameter of the laser, therefore rastering across parts of the tissue twice and potentially ionizing even more sample. An example of this “oversampling” technique is shown with the images in Figure 85. The spatial resolution is decreased while the laser diameter is held constant.

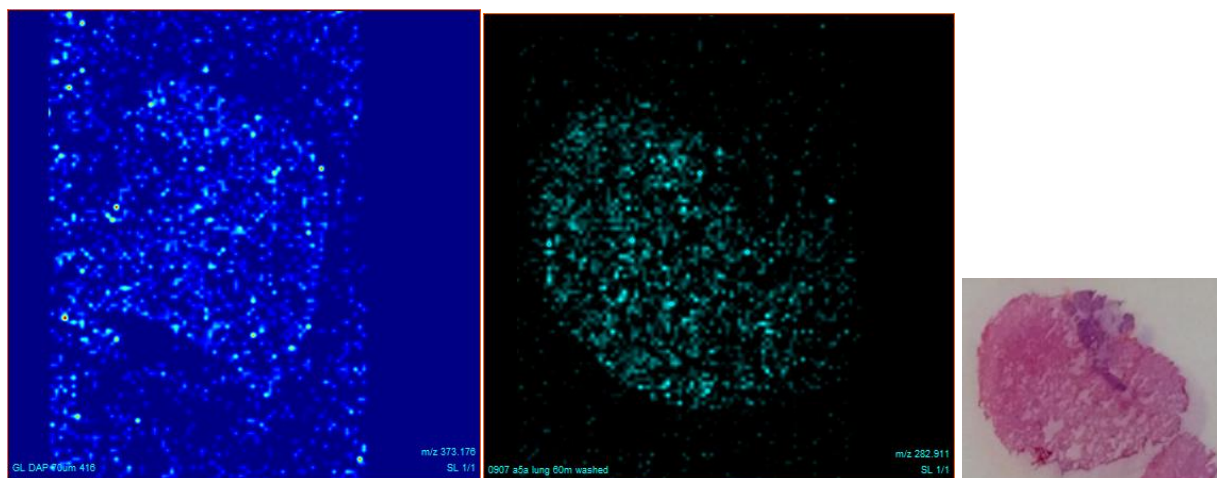


Figure 85. Samples imaged at 70 micron and 80 micron spatial resolution, respectively, with the laser diameter held at 100 micron. Left image is GL-II-93 416>373, right image is SH-053-2'F-R-CH₃ acid 360>283. H&E stain is also pictured at zero magnification, which correlates with the SH section.

By moving the sample target a distance that is less than the diameter of the laser beam, image resolution is enhanced, as more of the sample is ablated. Ideally the MALDI matrix is applied sufficiently wet so that the analyte within the sample is incorporated into the matrix, but must dry rapidly enough to minimize migration within the tissue sample. In addition to this, complete ablation of the sample is desired, to consistently acquire the maximum amount of signal possible.⁵⁷

7.3.2 MALDI results in MS1 mode

MALDI IMS can also be used as an investigative tool to gain insight into potential metabolites generated *in vivo*, since all of the samples imaged are from lungs of mice dosed with GL-II-93.

In addition, to use MALDI IMS in the reflectron MS/MS mode, which results in high specificity towards an analyte of interest, the MS1 mode (linear mode) can be used to investigate adducts generated *in vivo*, or metabolites within the tissue sample. In reflectron MS/MS mode, ion gating only allows the parent mass (defined by a specified range) to be fragmented and analysis by the second flight tube. Therefore, adducts or metabolites that have a different mass will be excluded. The MS1 mode however, will enable the quantification of distinct masses defined by a specific mass range, such as in Figure 86, which depicts the mass of 436 m/z which corresponds to GL-II-93 + Na⁺.

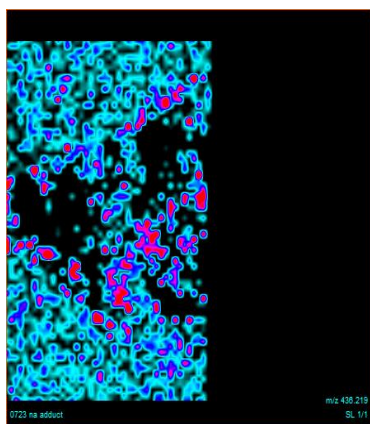


Figure 86. The GL-II-93+Na⁺ imaged in a lung tissue section.

Another strong ion 203 m/z was detected in the MS1 mode and quantified by MALDI IMS. This mass was absent in the lung tissue from non-treated mice thus it strongly suggest that it might be a metabolite of GL-II-93 (Figure 87).

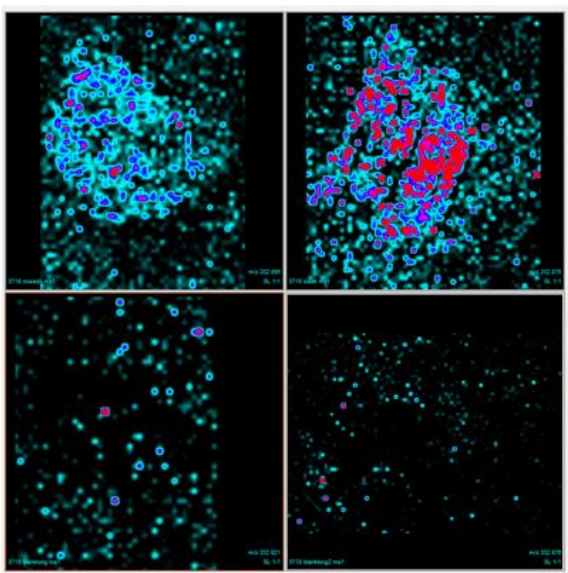


Figure 87. Unknown metabolite at m/z 203. The top sections show the lung without and with washing to remove salt interferences. The bottom sections show this mass imaged in undosed lung tissue sections.

Although the structure of the 203m/z ion is not known, it might be interesting to quantify it in PK samples to determine its occurrence in a time dependent manner. To confirm this compound as a metabolite of GL-II-93, its concentration should increase and then decrease in time similar to parent compound GL-II-93.

7.3.3 Immunohistochemistry results

The results of the immunohistochemistry experiment using a HRP conjugated secondary antibody for the $\alpha 5$ subunit or the GABA_AR are depicted in Figure 88.

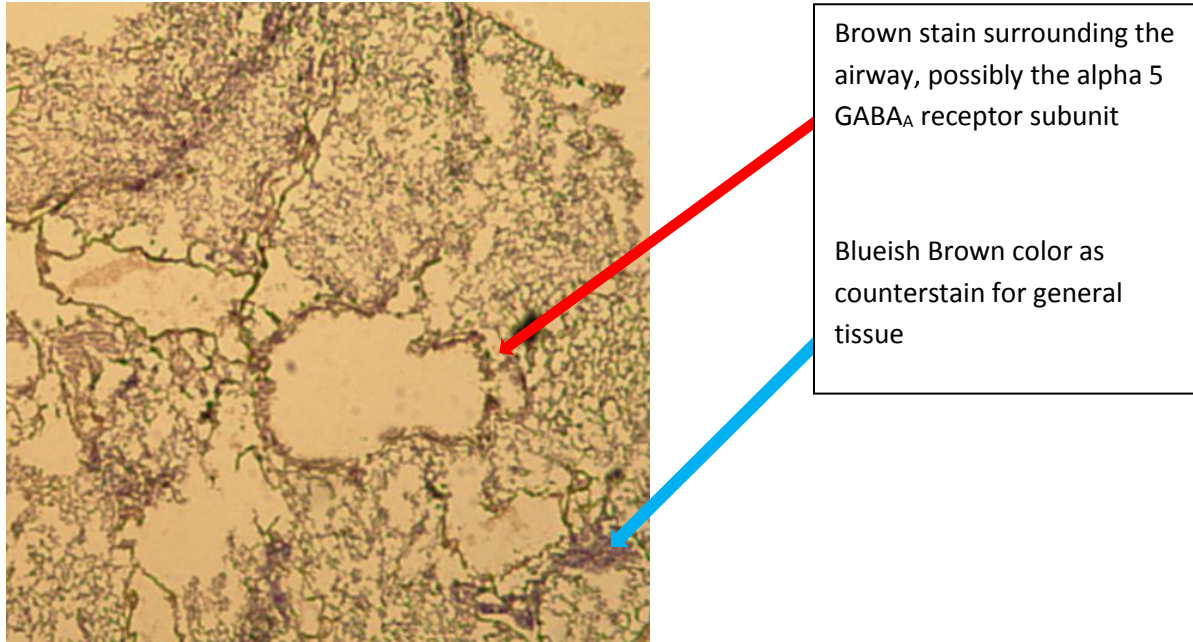


Figure 88. HRP stain of lung tissue section, with brown and blue colors.

Figure 88 shows a light brown background stain and a more intensive brown stain for some of the lung tissue areas. Unfortunately, the blue counter stain of hematoxylin was difficult to distinguish from the brown tissue stain using a standard light microscopy. Therefore, a secondary antibody with a fluorescein tag was employed to improve the quality of the immunohistochemistry picture using fluorescence microscopy rather than light microscopy, which enables the decrease of background signals (Figure 89). For immunofluorescence, the tissue counterstain is imaged in a different channel than the antibody conjugate. Therefore the overlap issue is eliminated.

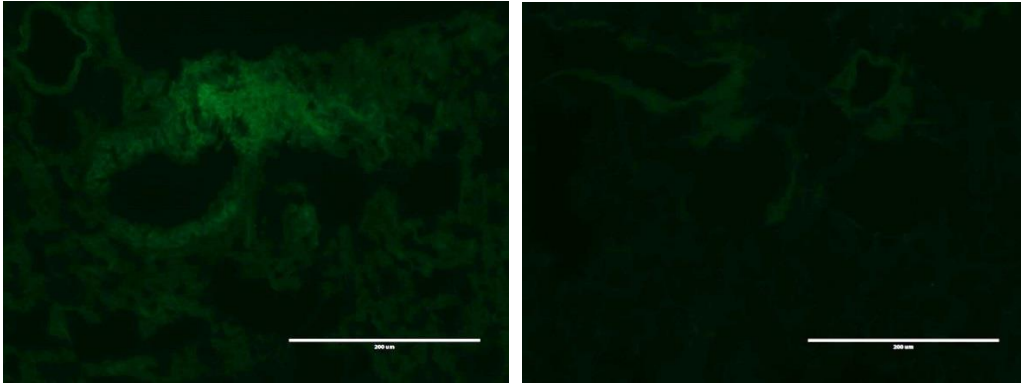


Figure 89. Positively and negatively (without primary antibody for $\alpha 5$ GABA_AR subunit) stained lung airways imaged with a FITC conjugated secondary antibody.

Although the positive image (left) appears brighter than the negative control, a better resolution is necessary to confirm staining of the $\alpha 5$ GABA_AR subunit in lung tissue. These pictures were taken with an Evos AMG fluorescence microscope (Frick lab, Department of Chemistry & Biochemistry, UWM). However, while improving this procedure the imaging was transferred to a Nikon inverted fluorescence microscope (Steeber lab, Department of Biological Sciences, UWM) which provided significantly improved image quality. We also substituted the FITC conjugated secondary antibody for a Cy5 conjugated secondary antibody. The resulting images are shown in Figure 90.

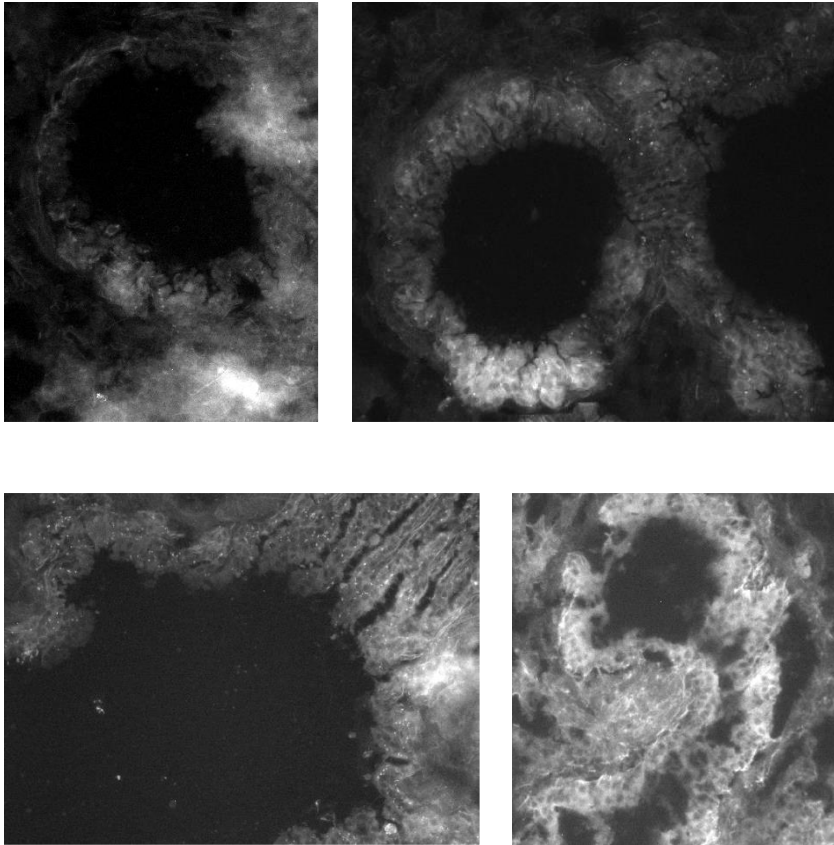


Figure 90. Positively stained mouse airway sections, imaged with Cy5 fluorescence at 200x magnification.

Staining for the $\alpha 5$ GABA_AR subunit was clearly observed with relatively intense staining around the lung airways that consist of epithelial cells and smooth muscle cells. Although the Nikon microscope produces black and white images, the level of background and signal can be matched between samples for comparison. The images can also be colored after the fact, which can aid in the overlay of multiple images if necessary. A comparison between positive and negative staining is provided in Figure 91.

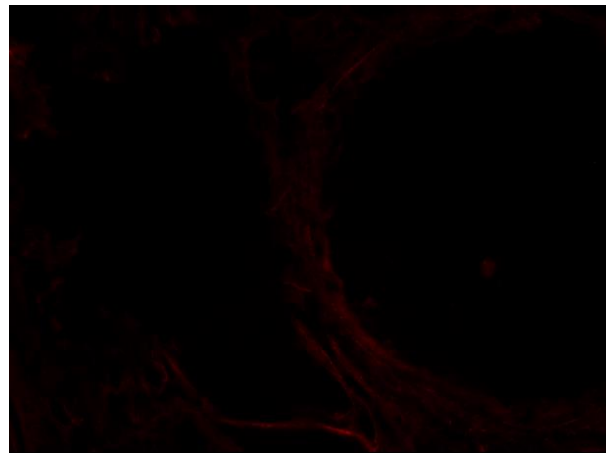
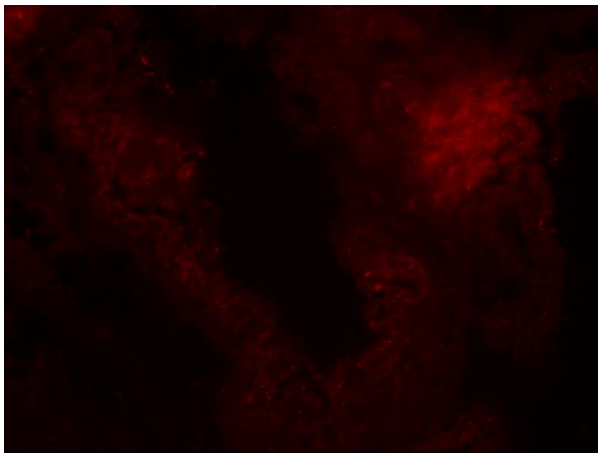
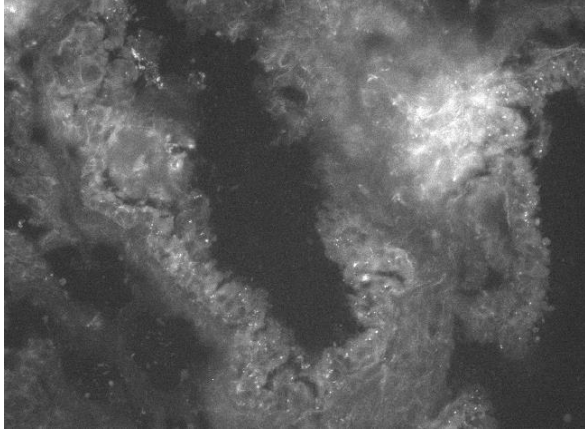


Figure 89. Mouse lung airways stained with the Cy5 probe at the alpha 5 receptor (positive staining and negative control). Image on the top represents a positive airway stain, original black and white color. The image presented on the left is the same as the previous figure, however the pseudocoloring functionality has been employed on the microscope to show the positive staining as a red color. Negative controls were conducted by omission of the primary antibody.

In order to establish a comparison between positive and negative sections, it is desirable to compare similar morphologies. In this work, the airway is the morphology of specific interest. Therefore, during the imaging process, airways were first identified using a DAPI stain, to ensure that the morphologies being compared were correct ones. An example is given in Figure 90.

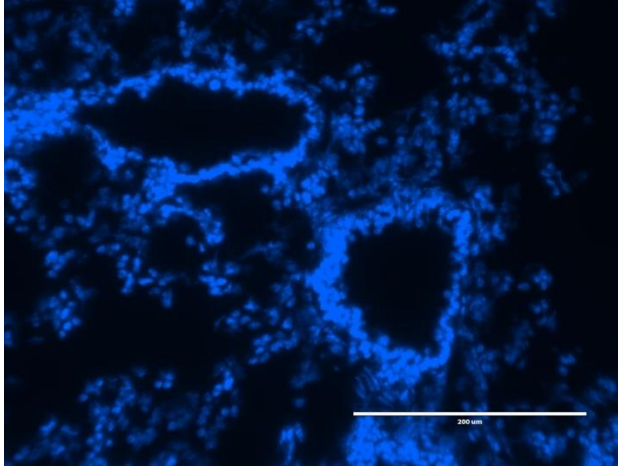


Figure 90. DAPI stain of lung tissue, showing two airways.

Once the morphology of the airway was identified, the tissue slice was imaged with fluorescent light to visualize the location of the $\alpha 5$ GABA_AR subunit. The above immunological stains were taken from serial sections to the following, which was concurrently analyzed by MALDI IMS.

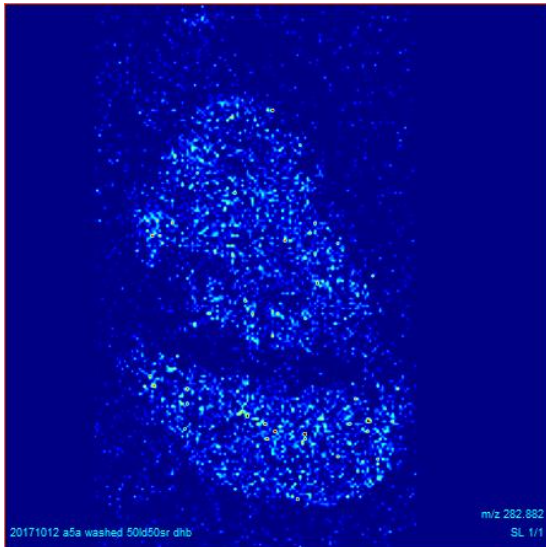


Figure 91. Serial section of lung tissue imaged for the SH-053-2'F-R-CH₃ acid. The IHC images in **Error! Reference source not found.** were taken from a serial section of this lung sample, indicating the presence of both the alpha 5 GABA_AR subunit and SH-053-2'F-R-CH₃ acid in the same lung.

In addition, brain tissue was used as a positive control for the immunohistochemistry protocol because the expression of the alpha 5 GABA_AR subunit has been reported for the brain.⁵⁸

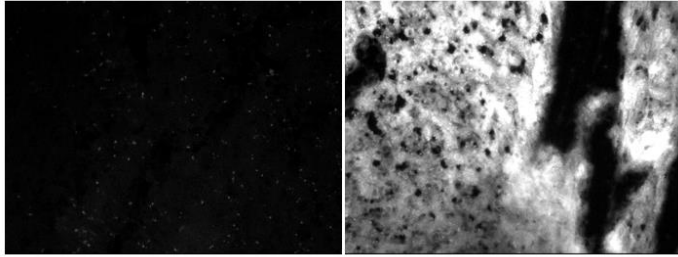


Figure 92. Mouse brain sections stained for alpha 5 GABA_AR subunit. The left section was a negative control by omission of the primary antibody. For the right image the primary antibody was added.

Finally all four imaging techniques (immunohistochemistry, MALDI IMS, H&E and confocal microscopy) were combined from four consecutive slices from a mouse lung (Figure

95).

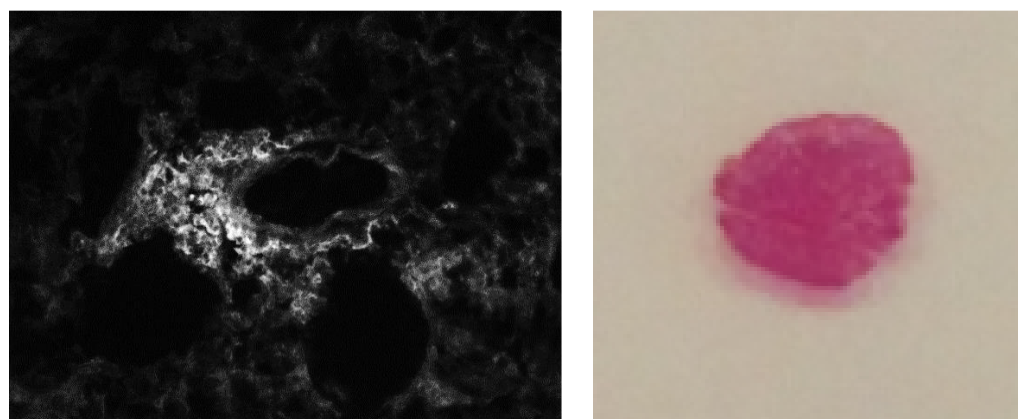
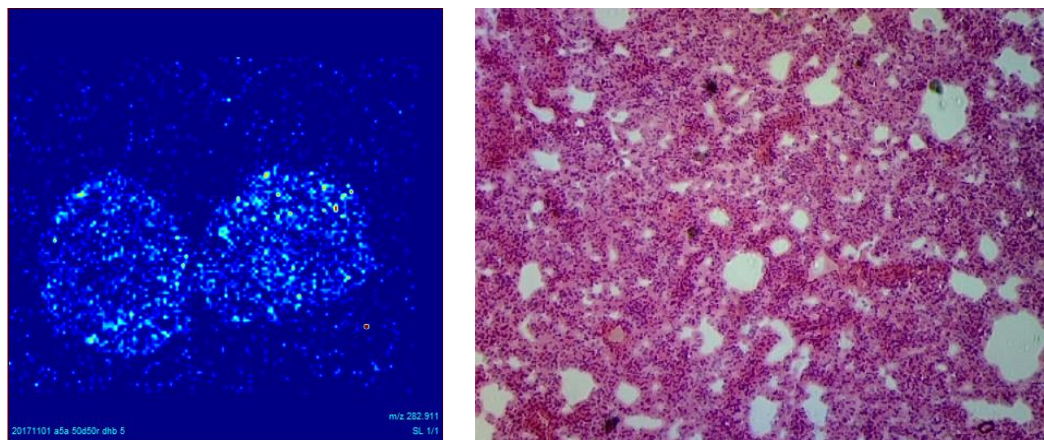


Figure 93. Mouse lung serial sections including overall ion density map, correlating H&E stain at 100x magnification, and Cy5 IHC at 200x magnification.

These images show good correlation between the location of the compound of interest in the MALDI IMS data, the IHC tissue stain, and the H&E stained tissue, all taken in serial fashion. The current obstacle with this multi-modal comparison lies in the varying magnification levels that generate optimum data for each method. While H&E stains can be viewed at any magnification, the immunofluorescence is only seen when the magnification is at 200x. The fluorescence signal can be somewhat visualized at 100x, but the resolution makes localization difficult. The MALDI IMS image resolution can be increased and therefore “zoomed in” if the images were taken with a higher spatial resolution image (the instrument can go as low as 10 μm), however

at the time of this work, the instrument was experiencing technical limitations which made imaging experiments lower than 50 μm impossible. This issue is currently being resolved by the MIDD.

7.4 Conclusions

We have shown the ability to image small molecules in different tissue samples by MALDI-MS/MS, which is a technique on the forefront of drug discovery today. The 7090 Shimadzu instrument, however, has limitations with regard to the quality of images that can be generated. Major limitations are regarding the laser diameter and spatial resolution. An important compromise was made for imaging experiments, as the more data points acquired equates to longer analysis time. The image resolution can actually be predictively increased using image fusion software, which combines the spectra from the MALDI with an image taken from a histological stain (acquired with a light microscope) and relates these images to predict, with greater resolution, where the analyte is located.⁵⁹

Closing Remarks

Metabolic assays such as liver microsome stability and brain homogenate metabolism give us an indication of about the *in vivo* stability of a drug, which enables early stage rule-outs for some drug candidates. This is no trivial task, as medicinal chemists typically synthesize dozens if not hundreds of analogs around a particular lead compound, and high throughput screening methods are necessary to hone in on the most viable drug candidates. *In vitro* assays enable us to choose the best lead compounds to move forward with *in vivo* studies. Pharmacokinetic studies are not high throughput assays, rather they are time consuming and expensive.

However, these assays are paramount to gather more information about ADME and formulation. Absolute compound quantitation verifies the presence or absence within real biological samples. Low limits of detection were achieved using a triple quad LC-MS/MS at UWM. Without the low limits of detection offered by LC-MS/MS analysis, later time points of a PK study would be challenging to quantify, which would make the calculation of PK parameter such as clearance more difficult. Prior to the development of these methods researchers at UWM were forced to hire an outside CRO for these studies (contract research organization). Based on this analysis, we were able to show by MALDI IMS where within that target tissue a compound was located. MALDI-IMS is an exciting field in mass spectrometry with new applications still emerging.

In the future, MIDD investigators can combine pharmacokinetics studies and mass spectrometry imaging. We have not yet attempted this method, and it is actually a controversial approach as MALDI is generally thought to be a semi-quantitative method. Without standards, quantification based on desorption and ionization is not reliable. In addition, complex matrix effects seen with *in vivo* samples, such as tissue slice thickness, further complicate the separation of ions and the ability to quantify. Other research groups are attempting to tackle this issue by using different internal and external standard methods.^{53, 60} This is an interesting potential future direction because it would offer the ability to combine two experiments into one, quantifying the amount of compound in the tissue and also showing the localization of this compound at the same time.

Another important future direction for the MIDD lies in high resolution mass spectrometry and its application in metabolomics. IT-TOF provides high resolution capabilities in LC-MS/MS, and compounds can be fragmented multiple times to elucidate structures. Our current approach creates metabolites *in vitro*, with the microsome assay, and *in vivo*, with PK studies. One particular metabolite, XHE-III-74 acid, has been shown specificity for the alpha 4 GABA_AR subunit and is generated *in vivo* from the precursor, XHE-III-74 ethyl ester. This metabolite was discovered using a unit resolution quadrupole instrument, which is less ideal for metabolomics. However, the IT-TOF possesses formula prediction software in addition to the MSⁿ fragmentation capabilities. Therefore it is the ideal instrument to continue investigation of both active and non-active metabolites. In addition, once robust methods for metabolite identification are established, excretion samples could be collected and investigated. Phase II metabolites would be of high interest here. Blood or other tissue samples could be further investigated to look for pro-drug possibilities. HRMS is an incredible tool for metabolite identification and we are mere steps away from exploring this field within the Arnold Group embedded in the MIDD.

References

1. Patrick, G. L., *An introduction to medicinal chemistry*. 4th ed.; Oxford University Press: New York, NY, 2009.
2. Stevens, E., *Medicinal Chemistry: The Modern Drug Discovery Process*. 1st ed.; Pearson: 2014.
3. John Keogh, B. H., Caroline Rynn, Bruno Stieger, Glynis Nicholls., *Drug Transporters: Volume 1: Role and importance in ADME and Drug Development*. 2016.
4. Mohammed S. Alavijeh, A. M. P., The pivotal role of drug metabolism and pharmacokinetics in the discovery and development of new medicines. *Idrugs* **2004**, 7 (8), 755-63.
5. Lipinski, C. A., Drug-like properties and the causes of poor solubility and permeability. *Journal of Pharmacological and Toxicological Methods* **2000**, 44, 235-249.
6. Li, A. P., Preclinical *in vitro* screening assays for drug-like properties. *Drug Discovery Today: Technologies* **2005**, 2 (2), 179-185.
7. Gad, S. C., *Preclinical Development Handbook: ADME and Biopharmaceutical Properties*. John Wiley and Sons: Hoboken, New Jersey, 2008.
8. Rogge, M. C.; Taft, D. R., *Preclinical Drug Development*. 2nd ed.; Informa Healthcare USA, Inc.: New York, NY, 2010; Vol. 187.
9. (a) Xu, R.; Manuel, M.; Cramlett, J.; Kassel, D. B., A high throughput metabolic stability screening workflow with automated assessment of data quality in pharmaceutical industry. *Journal of Chromatography A* **2010**, 1217, 1616-1625; (b) Soars, M. G.; Grime, K.; Sproston, J. L.; Webborn, P. J. H.; Riley, R. J., Use of Hepatocytes to Assess the Contribution of Hepatic Uptake to Clearance in Vivo. *Drug Metabolism and Disposition* **2007**, 35 (6), 859-865
10. Johnston, M. C. a. G. A. R., GABA-Activated Ligand Gated Ion Channels: Medicinal Chemistry and Molecular Biology. *Journal of Medicinal Chemistry* **2000**, 43 (8), 1427-1447.
11. Varagic, *British Journal of Pharmacology* **2013**, 169 (371).
12. Bruce J. Melancon, C. R. H., Michael R. Wood, Kyle A. Emmitte, Colleen M. Niswender, Arthur Christopoulos, P. Jeffrey Conn, and Craig W. Lindsley, Allosteric modulation of seven transmembrane spanning receptors: theory, practice, and opportunities for central nervous system drug discovery. *Journal of Medicinal Chemistry* **2012**, 55, 1445-1464.
13. Douglas A. Skoog, F. J. H., Stanley R. Crouch, *Principles of Instrumental Analysis*. 7th Edition ed.; Cengage Learning: Boston, MA, 2018.
14. Rouessac, F. R. a. A., *Chemical Analysis, Modern Instrumentation Methods and Techniques*. 2nd ed.; John Wiley & Sons Ltd.: West Sussex, England, 2007.
15. Martin, A. J. P.; Synge, R. L. M., A new form of chromatogram employing two liquid phases. *Biochemical Journal* **1941**, 35, 1358-1368.
16. (a) Kellner, R.; Mermet, J. M.; Otto, M.; Valcarcel, M.; Widmer, H. M., *Analytical Chemistry: A Modern Approach to Analytical Science*. 2nd ed.; Wiley-VCH: 2004; (b) Macek, K.; Deyl, Z.; Janák, J., *Liquid Column Chromatography: A Survey of Modern Techniques and Applications*. Elsevier: 1975.
17. vanDeemter, J. J.; Zuiderweg, F. J.; Klinkenberg, A., Longitudinal diffusion and resistance to mass transfer as causes of nonideality in chromatography. *Chemical Engineering Science* **1956**, 5 (6), 271-289.
18. Bhat, R., *Proceedings of the National Academy of Sciences* **2010**, 107 (6), 2580-2585.
19. Harris, D. C., *Quantitative Chemical Analysis*. 8th ed.; W. H. Freeman and Company: New York, NY, 2010.
20. Robert M. Silverstein, F. X. W., David J. Kiemle, *Spectrometric identification of organic compounds*. 7th Edition ed.; John Wiley & Sons, Inc.: Hoboken, NJ, 2005.
21. Surveyor MSQ Plus Hardware Manual. Thermo Fisher Scientific: 2007.

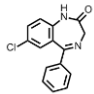
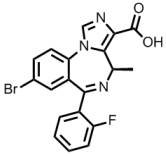
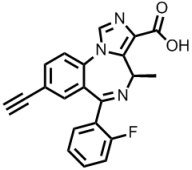
22. John B. Fenn, M. M., CK Meng, SF Wong, CM Whitehouse, Electrospray ionization for mass spectrometry of large biomolecules. *Science* **1989**, *246* (4926), 64-71.
23. Ardrey, R. E., *Liquid Chromatography-Mass Spectrometry: An Introduction*. John Wiley & Sons Ltd.: West Sussex, England, 2003.
24. O Belgacem, E. P., M E Openshaw, P J Hart, A Bowdler, G Allmaier, Axial spatial distribution focusing: improving MALDI-TOF/RTOF mass spectrometric performance for high-energy collision-induced dissociation of biomolecules. *Rapid Communications in Mass Spectrometry* **2016**, *30* (3), 343-351.
25. Sparkman, J. T. W. a. O. D., *Introduction to Mass Spectrometry: Instrumentation, Applications, and Strategies for Data Interpretation*. John Wiley & Sons: West Sussex, England, 2007.
26. Dermot F. McGinnity, M. G. S., Richard A. Urbanowicz, and Robert J. Riley, Evaluation of fresh and cryopreserved hepatocytes as in vitro drug metabolism tools for the prediction of metabolic clearance. *Drug Metabolism & Disposition* **2004**, *32* (11), 1247-1253.
27. Pallmann, T.; Jonas, U.; Wagner, M.; Thevis, M.; Kaferstein, H.; Rothschild, M. A.; Bender, K., Enzyme-assisted synthesis and structural characterization of pure benzodiazepine glucuronide epimers. *European journal of pharmaceutical sciences : official journal of the European Federation for Pharmaceutical Sciences* **2010**, *39* (4), 233-40.
28. de Paula, N. C.; Araujo Cordeiro, K. C.; de Melo Souza, P. L.; Nogueira, D. F.; da Silva e Sousa, D. B.; Costa, M. B.; Noel, F.; de Oliveira, V., Biosynthesis of human diazepam and clonazepam metabolites. *Bioorg Med Chem Lett* **2015**, *25* (5), 1026-9.
29. Ulrike Hubl, D. E. S., In vitro enzymic synthesis of mammalian liver xenobiotic metabolites catalysed by ovine liver microsomal cytochrome P450. *Enzyme and Microbial Technology* **2001**, *29*, 306-311.
30. Sevrioukova, I. F.; Poulos, T. L., Structural basis for regiospecific midazolam oxidation by human cytochrome P450 3A4. *Proceedings of the National Academy of Sciences of the United States of America* **2017**, *114* (3), 486-491.
31. Houston, J. B., Utility of in vitro drug metabolism data in predicting in vivo metabolic clearance. *Biochemical pharmacology* **1994**, *47* (9), 1469-79.
32. Rajwana Jahan, M. R. S., Gloria S. Forkuo, Revathi Kodali, Margaret L. Guthrie, Amanda N. Nieman, Nina Y. Yuan, Nicolas M. Zahn, Michael M. Poe, Guanguan Li, Olivia B. Yu, Gene T. Yocum, Charles W. Emala, Douglas C. Stafford, James M. Cook, Leggy A. Arnold, Optimization of substituted imidazobenzodiazepines as novel asthma treatments. *European Journal of Medicinal Chemistry* **2016**, *126*, 550-560.
33. Poe, M. M. Synthesis of subtype selective Bz/GABAA receptor ligands for the treatment of anxiety, epilepsy and neuropathic pain, as well as schizophrenia and asthma. University of Wisconsin-Milwaukee, Milwaukee, WI, 2016.
34. Hallifax, D.; Rawden, H. C.; Hakooz, N.; Houston, J. B., Prediction of metabolic clearance using cryopreserved human hepatocytes: kinetic characteristics for five benzodiazepines. *Drug metabolism and disposition: the biological fate of chemicals* **2005**, *33* (12), 1852-8.
35. Guillouzo, C. G., General Review on In Vitro Hepatocyte Models and Their Applications. In *Hepatocytes: methods and protocols*, Maurel, P., Ed. Springer Science 2010.
36. Hallifax, D.; Galetin, A.; Houston, J. B., Prediction of metabolic clearance using fresh human hepatocytes: comparison with cryopreserved hepatocytes and hepatic microsomes for five benzodiazepines. *Xenobiotica; the fate of foreign compounds in biological systems* **2008**, *38* (4), 353-67.
37. Thomas L. Lemke, D. A. W., Victoria F. Roche, S. William Zito, *Foye's Principles of Medicinal Chemistry*. 6th Edition ed.; Lippincott Williams & Wilkins: Baltimore, MD, 2008.
38. Vargesson, N., Thalidomide-induced teratogenesis: history and mechanisms. *Birth defects research. Part C, Embryo today : reviews* **2015**, *105* (2), 140-56.

39. D'Amato, R. J.; Loughnan, M. S.; Flynn, E.; Folkman, J., Thalidomide is an inhibitor of angiogenesis. *Proceedings of the National Academy of Sciences of the United States of America* **1994**, *91* (9), 4082-5.
40. Castro, A.; Aguilar, J.; Gonzalez-Ramirez, R.; Loeza-Alcocer, E.; Canto-Bustos, M.; Felix, R.; Delgado-Lezama, R., Tonic inhibition in spinal ventral horn interneurons mediated by alpha5 subunit-containing GABA(A) receptors. *Biochemical and biophysical research communications* **2011**, *412* (1), 26-31.
41. Tamara Timic Stamenic, M. M. P., Sabah Rehman, Anja Santrac, Branka Divovic, Petra Scholze, Margot Ernst, James M. Cook, Miroslav M. Savic, Ester to amide substitution improves selectivity, efficacy and kinetic behavior of a benzodiazepine positive modulator of GABAA receptors containing the alpha 5 subunit. *European Journal of Pharmacology* **2016**, *791*, 433-443.
42. Fabien Dutheil, P. B., Marie-Anne Lorient, Xenobiotic metabolizing enzymes in the central nervous system: Contribution of cytochrome P450 enzymes in normal and pathological human brain. *Biochimie* **2008**, *90*, 426-436.
43. Bagal, S. K.; Brown, A. D.; Cox, P. J.; Omoto, K.; Owen, R. M.; Pryde, D. C.; Sidders, B.; Skerratt, S. E.; Stevens, E. B.; Storer, R. I.; Swain, N. A., Ion channels as therapeutic targets: a drug discovery perspective. *J Med Chem* **2013**, *56* (3), 593-624.
44. Barragan, A.; Weidner, J. M.; Jin, Z.; Korpi, E. R.; Birnir, B., GABAergic signalling in the immune system. *Acta physiologica* **2015**, *213* (4), 819-27.
45. Liao, W.; Lin, J. X.; Leonard, W. J., IL-2 family cytokines: new insights into the complex roles of IL-2 as a broad regulator of T helper cell differentiation. *Current opinion in immunology* **2011**, *23* (5), 598-604.
46. Tsuda, M.; Masuda, T.; Tozaki-Saitoh, H.; Inoue, K., Microglial regulation of neuropathic pain. *Journal of pharmacological sciences* **2013**, *121* (2), 89-94.
47. Rong Yi, S. Z., Noel Kong, Julia Zhang, Devan Loganathan, Sandrine Merette, Barbara Morrissey., Quantitation of gamma-aminobutyric acid in equine plasma by hydrophilic interaction liquid chromatography with tandem mass spectrometry. *Journal of Separation Science* **2017**, 1-9.
48. Gloria S. Forkuo, M. L. G., Nina Y. Yuan, Amanda N. Nieman, Revathi Kodali, Rajwana Jahan, Michael R. Stephen, Gene T. Yocum, Marco Treven, Michael M. Poe, Guanguan Li., Olivia B. Yu, Benjamin D. Hartzler, Nicolas M. Zahn, Margot Ernst, Charles W. Emala, Douglas Stafford, James M. Cook, Leggy A. Arnold, Development of GABAA receptor subtype selective imidazobenzodiazepines as novel asthma treatments. *Molecular Pharmaceutics* **2016**, *13* (6), 2026-2038.
49. (a) Williams, R. t.; Lim, J. E.; Harr, B.; Wing, C.; Walters, R.; Distler, M. G.; Teschke, M.; Wu, C.; Wiltshire, T.; Su, A. I.; Sokoloff, G.; Tarantino, L. M.; Borevitz, J. O.; Palmer, A. A., A common and unstable copy number variant is associated with differences in Glo1 expression and anxiety-like behavior. *PLOS one* **2009**, *4* (3), e4649; (b) McMurray, K. M.; Distler, M. G.; Sidhu, P. S.; Cook, J. M.; Arnold, L. A.; Palmer, A. A.; Plant, L. D., Glo1 inhibitors for neuropsychiatric and anti-epileptic drug development. *Biochemical Society transactions* **2014**, *42* (2), 461-7.
50. Distler, M. G.; Palmer, A. A., Role of Glyoxalase 1 (Glo1) and methylglyoxal (MG) in behavior: recent advances and mechanistic insights. *Frontiers in genetics* **2012**, *3*, 250.
51. McMurray, K. M.; Ramaker, M. J.; Barkley-Levenson, A. M.; Sidhu, P. S.; Elkin, P. K.; Reddy, M. K.; Guthrie, M. L.; Cook, J. M.; Rawal, V. H.; Arnold, L. A.; Dulawa, S. C.; Palmer, A. A., Identification of a novel, fast-acting GABAergic antidepressant. *Molecular psychiatry* **2017**.
52. Caprioli, M. L. R. a. R. M., MALDI-MS-based imaging of small molecules and proteins in tissues. *Current opinion in chemical biology* **2007**, *11*, 29-35.
53. Chad W. Chumbley, M. L. R., Jamie L. Allen, Gwendolyn A. Marriner, Laura E. Via, Clifton E. Barry III, Richard M. Caprioli, Absolute quantitative MALDI imaging mass spectrometry: a case of rifampicin in liver tissues. *Analytical Chemistry* **2016**, *88*, 2392-2398.

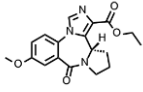
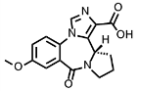
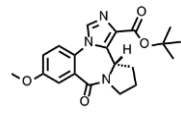
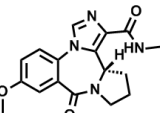
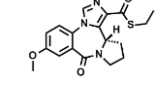
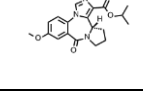
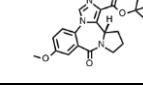
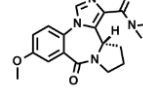
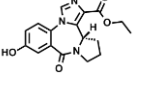
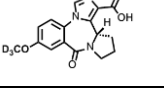
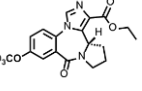
54. Karlsson, O.; Hanrieder, J., Imaging mass spectrometry in drug development and toxicology. *Archives of toxicology* **2017**, *91* (6), 2283-2294.
55. Reyzer, M. L.; Hsieh, Y.; Ng, K.; Korfmacher, W. A.; Caprioli, R. M., Direct analysis of drug candidates in tissue by matrix-assisted laser desorption/ionization mass spectrometry. *Journal of mass spectrometry : JMS* **2003**, *38* (10), 1081-92.
56. Forkuo, G. S.; Nieman, A. N.; Yuan, N. Y.; Kodali, R.; Yu, O. B.; Zahn, N. M.; Jahan, R.; Li, G.; Stephen, M. R.; Guthrie, M. L.; Poe, M. M.; Hartzler, B. D.; Harris, T. W.; Yocum, G. T.; Emala, C. W.; Steeber, D. A.; Stafford, D. C.; Cook, J. M.; Arnold, L. A., Alleviation of Multiple Asthmatic Pathologic Features with Orally Available and Subtype Selective GABAA Receptor Modulators. *Mol Pharm* **2017**, *14* (6), 2088-2098.
57. Jurchen, J. C.; Rubakhin, S. S.; Sweedler, J. V., MALDI-MS imaging of features smaller than the size of the laser beam. *Journal of the American Society for Mass Spectrometry* **2005**, *16* (10), 1654-9.
58. Hevers, W.; Luddens, H., The diversity of GABAA receptors. Pharmacological and electrophysiological properties of GABAA channel subtypes. *Molecular neurobiology* **1998**, *18* (1), 35-86.
59. Van de Plas, R.; Yang, J.; Spraggins, J.; Caprioli, M., *Nature Methods* **2015**, *12*, 366-372.
60. (a) Rao, T.; Shen, B.; Zhu, Z.; Shao, Y.; Kang, D.; Li, X.; Yin, X.; Li, H.; Xie, L.; Wang, G.; Liang, Y., Optimization and evaluation of MALDI TOF mass spectrometric imaging for quantification of orally dosed octreotide in mouse tissues. *Talanta* **2017**, *165*, 128-135; (b) Rzagalinski, I.; Volmer, D. A., Quantification of low molecular weight compounds by MALDI imaging mass spectrometry - A tutorial review. *Biochimica et biophysica acta* **2017**, *1865* (7), 726-739.

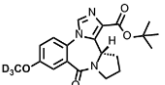
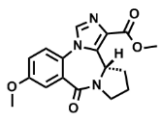
Appendix A: MRM parameters for $\alpha_5\beta_3\gamma_2$ selective ligands

Compound Name	Precursor m/z	Product m/z	Dwell time	Q1 pre bias (V)	Collision Energy	Q3 Pre Bias (V)	Structure
MP II 069	383.20	339.20	20.0	-13.0	-13.0	-21.0	
		329.30	20.0	-23.0	-16.0	-30.0	
		311.20	20.0	-24.0	-22.0	-10.0	
MP II 068	371.20	329.00	20.0	-23	-15	-21	
		311.00	20.0	-23	-23.0	-30.0	
		285.10	20.0	-23	-21.0	-30.0	
		232.10	20.0	-23	-29	-23	
HZ 166	356.90	311.15	35.0	-17	-20	-30	
		283.15	35.0	-17	-31	-18	
		282.15	35.0	-17	-39	-28	
MP III 024	343.20	311.00	20.0	-21	-20	-30	
		283.00	20.0	-22	-30	-12	
		256.00	20.0	-17	-37	-26	
Diazepam	285.20	241.00	30.0	-18	-37	-22	
		222.10	30.0	-19	-27	-22	
		193.10	30.0	-19	-33	-29	
		154.10	30.0	-18	-27	-25	
MP III 004	373.95	342.05	30.0	-25	-18	-22	
		314.25	30.0	-25	-30	-29	
		273.00	30.0	-25	-40	-26	
MP IV 004	397.9	340.10	100.0	-26	-23	-36	
		356.85	100.0	-26	-9	-40	
		220.70	100.0	-26	-30	-34	
MP024 HZ acid	328.9	297.05	30.0	-22	-8	-30	
		99.10	30.0	-22	-21	-21	
		265.00	30.0	-22	-7	-28	
SH-053 2'F	373.9	327.95	30.0	-18	-20	-30	
		299.95	30.0	-18	-34	-29	
		273.05	30.0	-18	-40	-27	
MP IV 062	267.95	240.10	30.0	-29	-11	-24	
		144.05	30.0	-29	-20	-28	
		123.05	30.0	-29	-24	-20	
SH053 RS CH3	388	342.05	100.0	-19	-20	-21	
		249.10	30.0	-19	-35	-20	
		315.00	30.0	-19	-35	-20	
		301.00	100.0	-19	-30	-19	
Nordiazepam	276.05	213.00	10.0	-19	-30	-22	

		139.95	10.0	-19	-30	-22	
		164.90	10.0	-19	-35	-22	
GL-II-93	413.9	396	100	-20	-18	-24	
		368	100	-30	-35	-20	
		355.05	100	-30	-29	-36	
		302.95	100	-28	-30	-32	
		326.8	100	-30	-44	-32	
		276.05	100	-30	-34	-28	
		248.2	100	-30	-41	-26	
		168.1	100	-38	-43	-28	
SH-053 2'F R/S							
CH3	360	342.1	100	-24	-16	-22	
Acid		316	100	-24	-17	-34	
		301.1	100	-24	-29	-30	
		249.05	100	-24	-28	-26	
		219.9	100	-24	-41	-40	

Appendix B: MRM parameters for $\alpha_4\beta_3\gamma_2$ selective ligands

Compound Name	Precursor m/z	Product m/z	Dwell time	Q1 pre bias (V)	Collision Energy	Q3 Pre Bias (V)	Structure
Xhe III 74 EE	342.00	296.15	30.0	-16.0	-19.0	-30.0	
		278.15			-28.0	-29.0	
		268.15			-31.0	-28.0	
Xhe III 74 Acid	313.90	296.05	100.0	-23	-16	-30	
		278.00	100.0	-23	-26	-28	
		108.95	100.0	-23	-40	-25	
Xhe III 74 (TBE)	370.00	338.45	35.0	-18	-9	-15	
		314.20	35.0	-18	-13	-20	
		296.15	35.0	-18	-22	-30	
		149.30	30.0	-17	-30	-20	
MRS-01-64	326.8	100.4	100	-36	-38	-40	
		296	100	-36	-19	-30	
		278.1	100	-38	-27	-28	
		268.2	100	-36	-29	-26	
		227.1	100	-36	-36	-40	
MRS-01-67	357.7	296.2	30	-17	-15	-30	
		278.2	30	-17	-27	-29	
		290.4	30	-17	-32	-21	
MRS-01-36	355.7	296.15	30	-17	-21	-30	
		216.5	30	-17	-35	-12	
		120.8	30	-17	-30	-18	
CMD-45	356	300.15	35	-17	-11	-30	
		282.1	35	-17	-22	-28	
		227.4	35	-17	-40	-15	
MRS-01-66	340.85	296.05	100	-40	-20	-30	
		277.95	100	-40	-20	-30	
		268.1	100	-40	-20	-30	
		227.15	100	-40	-20	-30	
RJ-02-50	328.05	282.05	100	-16	-20	-18	
		192.9	100	-16	-19	-25	
		264.1	100	-16	-30	-16	
Xhe Acid OCD3	316.9	299.05	100	-20	-16	-20	
		281	100	-20	-26	-20	
		111.95	100	-20	-40	-20	
Xhe EE OCD3	345.05	298.55	100	-22	-18	-28	
RJ-02-46	281.15	100	-22	-28	-28		

		271.15	100	-22	-31	-26	
Xhe TBE OCD3	299.15	299.15	100	-24	-22	-30	
RJ-02-52	281.1	281.1	100	-20	-34	-28	
	271.1	271.1	100	-20	-36	-26	
MRS 01 68	328	296.1	100	-22	-18	-30	
	328	277.95	100	-36	-29	-28	
	328	268.05	100	-36	-31	-26	
	328	250.95	100	-36	-37	-40	
	328	227.1	100	-36	-36	-36	

Appendix C: MRMs for non-benzodiazepine compounds

Compound Name	Precursor m/z	Product m/z	Dwell time	Q1 pre bias (V)	Collision Energy	Q3 Pre Bias (V)	Structure
GABA	104.10	87.10	100.0	-22.0	-15.0	-26.0	
		86.10	100.0	-22.0	-15.0	-28.0	
		69.20	100.0	-22.0	-10.0	-26.0	
4,6-diphenyl N OH pyridone	264	218.15	30	-30	-22	-21	
		247.05	30	-13	-21	-14	
		218.95	30	-19	-31	-21	
pBBG	614	416.80	30	-32	-19	-27	
		331.90	30	-32	-26	-21	
		245.90	30	-32	-34	-24	
		170.80	30	-32	-48	-27	
pBBG Diacid	477.95	170.95	30	-34	-37	-30	
		348.95	30	-34	-15	-38	
		332.00	30	-34	-18	-34	
Verapamil	454.7	165.15	100	-22	-30	-28	
		150.20	100	-22	-29	-30	
		303.30	100	-22	-43	-26	
MeGFN	302.9	271.05	100	19	15	27	

Curriculum Vitae

EDUCATION

University of Wisconsin – Milwaukee
Ph.D. Analytical Chemistry
Final defense date: December 1, 2017
GPA: 3.88

Graduate Research Project

Development of preclinical assays based on tandem mass spectrometry to investigate GABA_A receptor modulators

Research Advisor: Alexander Arnold, PhD

- Developed *in-vitro* metabolic assay for assessment of drug degradation via CYP340 enzymes
- Absolute quantitation performed on triple quadrupole LC-MS/MS instrument (Shimadzu 8040) using reversed-phase and HILIC methods
- Performed *in-vivo* pharmacokinetic studies followed by quantitation in mouse brain, lung, and blood samples (liquid-liquid extraction and solid-phase extraction sample preparation)
- Developed methods for small molecule imaging mass spectrometry on MALDI-TOF/TOF instrument (Shimadzu 7090)

Laboratory Techniques: IR, NMR, UV-Vis and fluorescence spectroscopy, cell culture, aseptic technique, light and fluorescence microscopy, wet chemistry techniques (titrations, extractions, distillation, recrystallization), gel and capillary electrophoresis, RT-PCR, HPLC, LC-MS, LC-MS/MS, MALDI-MS

Undergraduate Research Project

January 2012 – December 2012

Undergraduate Research Advisor: Mark Dietz, PhD

Determination of octanol-water partition coefficients for imidazolium-based ionic liquids

PUBLICATIONS

Alleviation of Multiple Asthmatic Pathologic Features with Orally Available and Subtype Selective GABA_A Receptor Modulators

Mol. Pharmaceutics, (2017), 14(6), 2088-2098.

Forkuo, Gloria S.; Nieman, Amanda N.; Yuan, Nina Y.; Kodali, Revathi; Yu, Olivia B.; Zahn, Nicolas M.; Jahan, Rajwana; Li, Guanguan; Stephen, Michael Rajesh; Guthrie, Margaret L.; Poe, Michael M.; Hartzler, Benjamin D.; Harris, Ted W.; Yocum, Gene T.; Emala, Charles W.; Steeber, Douglas A.; Stafford, Douglas C.; Cook, James M.; Arnold, Leggy A.

Identification of a novel, fast-acting GABAergic antidepressant

Molecular Psychiatry, Ahead of Print, 2017

DOI:10.1038/mp.2017.14

McMurray, K. M. J.; Ramaker, M. J.; Barkley-Levenson, A. M.; Sidhu, P. S.; Elkin, P. K.; Reddy, M. K.; Guthrie, M. L.; Cook, J. M.; Rawal, V. H.; Arnold, L. A.; Dulawa, S. C.; Palmer, A. A.

Development of GABA_A Receptor Subtype-Selective Imidazobenzodiazepines as Novel Asthma Treatments

Mol. Pharmaceutics, 2016, 13 (6), pp 2026–2038

DOI: 10.1021/acs.molpharmaceut.6b00159

Forkuo, Gloria S.; Guthrie, Margaret L.; Yuan, Nina Y.; Nieman, Amanda N.; Kodali, Revathi; Jahan, Rajwana; Stephen, Michael R.; Yocum, Gene T.; Treven, Marco; Poe, Michael M.; Li, Guanguan; Yu, Olivia B.; Hartzler, Benjamin D.; Zahn, Nicolas M.; Ernst, Margot; Emala, Charles W.; Stafford, Douglas C.; Cook, James M.; Arnold, Leggy A

Antitumor Activity of 3-Indolylmethanamines 31B and PS121912

Anticancer Research, Volume 35, Issue 11, Pages 6001-7

Guthrie Margaret L.; Sidhu Preetpal S; Nandhikonda Premchendar; Teske Kelly A; Yuan Nina Y; Sidorko Marina; Rodali Revathi; Cook James M; Han Lanlan; Silvaggi Nicholas R; Arnold Leggy A; Hill Emily K; Horan Timothy C; Moore Richard G; Singh Rakesh K; Bikle Daniel D

Rapid quantification of imidazolium-based ionic liquids by hydrophilic interaction liquid chromatography: Methodology and an investigation of the retention mechanisms

Journal of Chromatography A, Volume 1400, Pages 54-64

<http://dx.doi.org/10.1016/j.chroma.2015.04.047>

Hawkins, Cory A.; Rud, Anna; Guthrie, Margaret L.; Dietz, Mark L.

Anticancer activity of VDR-coregulator inhibitor PS121912

Cancer Chemotherapy and Pharmacology, Volume 74, Issue 4, Pages 787-798

Sidhu, Preetpal S.; Teske, Kelly; Feleke, Belaynesh; Yuan, Nina Y.; Guthrie, Margaret L.; Han, Lanlan; Preston, Joshua; Bogart, Jonathan W.; Silvaggi, Nicholas R.; Cook, James M.; Singh, Rakesh K.; Bikle, Daniel D.; Arnold, Leggy A.

WORK EXPERIENCE

Eurofins SF Analytical

New Berlin, WI

August 2017 – Present

Mass Spectrometry Method Development Sr. Scientist

- Development of quantitative and qualitative methods on GC-MS and LC-MS/MS instrumentation

Gen-Probe Incorporated

Waukesha, WI

June 2012 – August 2013

Research Associate I

Limit of detection and sensitivity studies for human rhinovirus on novel instrumentation

Optimization and development of existing and new in-vitro diagnostics products

Performed RT-PCR, nucleic acid extractions and serial dilutions on a regular basis

Note: Gen-Probe was acquired by Hologic in August 2012

Lab Support, a division of On Assignment

West Allis, WI

November 2009 – June 2012

Associate Recruiter

Interviewed applicants for positions in Chemical, Biotechnology, Pharmaceutical, Food, and Environmental testing positions

Communicated with clients on a regular basis regarding needs

Prepared marketing campaigns by industry and location

Ensured compliance with state employment laws and Department of Homeland Security work eligibility

API Healthcare

Hartford, WI

July 2007 – November 2009

Training Specialist

Traveled to 32 clients across 22 states for software implementation, consulting and training (80-100% travel)

Made both training and software recommendations based upon client needs

Prepared training materials and documentation for individual client visits

Made minor database modifications on an as-needed basis (via Microsoft SQL Server 2005)

TEACHING EXPERIENCE

Chemistry 221 (Elementary Quantitative Analysis)

Spring 2016, Fall 2016, Fall 2017

Instructed students for laboratory experiments in introductory analytical chemistry, including titrations, absorbance spectroscopy, fluorescence spectroscopy, and cyclic voltammetry.

Chemistry 105 (General Chemistry for Engineering Majors)

Fall 2013, Spring 2014

Led discussion and laboratory sections for introductory general chemistry.

AWARDS

Keulks Award for Graduate Research – 2nd place poster, May 2017

ACS Milwaukee section travel award – April 2017

UWM Graduate School travel award – April 2017

UWM Chemistry & Biochemistry department travel award – April 2017

UWM Chemistry & Biochemistry 3rd place undergraduate research award – April 2012

PROFESSIONAL PRESENTATIONS

American Society for Mass Spectrometry meeting, June 2017

Indianapolis, IN

Shimadzu breakfast talk invited speaker

"Imaging the distribution of selective GABAA receptor modulators in the asthmatic lung using MALDI imaging mass spectrometry"

American Chemical Society meeting, April 2017

253rd ACS National Meeting, San Francisco, CA

Poster presenter, Analytical division

"Imaging the distribution of selective GABAA receptor modulators in the asthmatic lung using MALDI assisted mass spectrometry."

250th American Chemical Society National Meeting & Exposition, August 2015

Boston, MA

Poster presenter, Analytical division & Sci-Mix

"Development of a liquid chromatography-tandem mass spectrometry (LC-MS/MS) method for quantification of subtype-selective GABAA receptor ligands following liquid-liquid extraction (LLE) and on-line solid-phase extraction (SPE)"